THESE

Pour l'obtention du Grade de

DOCTEUR DE L'UNIVERSITE DE POITIERS

(Faculté des Sciences Fondamentales et Appliquées)
(Diplôme National - Arrêté du 25 mai 2016)

Ecole Doctorale : Sciences et Ingénierie en Matériaux, Mécanique, Energétique et Aéronautique

Secteur de Recherche : Sciences pour l'ingénieur

Spécialité : Mécanique des solides, des matériaux, des structures et des surfaces

Présentée par :

Yopa Eka PRAWATYA

****

MULTIVARIATE OPTIMISATION AND STATISTICAL PROCESS CONTROL OF POLYMER TRIBOELECTRIC CHARGING

****

Directeur de thèse : **Lucien DASCALESCU**
Co-directeur : **Thami ZEGHLOUL**

****

Soutenue le 17 avril 2018 devant la Commission d'Examen

****

JURY

Mme	**Sylvie DESCARTES**	IR-HDR	INSA de Lyon	Rapporteur
M	**Alain SYLVESTRE**	PU	Université de Grenoble - Alpes	Rapporteur
M.	**Sorin CANANAU**	PU	Université Politehnica de Bucarest	Examinateur
Mme	**Khouira SENOUCI**	MCU-HDR	Université de Sidi-Bel-Abbes	Examinateur
M.	**Thierry PAILLAT**	PU	Université de Poitiers	Examinateur
M.	**Hamid ZAIDI**	PU	Université de Poitiers	Examinateur
M.	**Thami ZEGHLOUL**	MCU	Université de Poitiers	Examinateur
M.	**Lucien DASCALESCU**	PU	Université de Poitiers	Examinateur

AKNOWLEDGEMENTS

First of all I would like to express my sincere gratitude to my advisors, M. **Lucian DASCALESCU** and M. **Thami ZEGHLOUL** for all their help. I am delighted to have worked with them because of the scientific support, patience, motivation, knowledge, and precious time they offered to me.

This study was carried out in two departments of the Institut Pprime « **Fluide Thermique Combustion** » and « **Génie Mécanique et Systèmes Complexes** » and was financially supported by a scholarship of **Directorate General of Resources for Science Technology and Higher Education, Ministry of Research Technology and Higher Education of The Republic of Indonesia**, and a grant under the **LABEX INTERACTIVES** program. The author also appreciates the support provided by the Institut Pprime for the registration fees, the accommodation and travel expenses related to the participation in several international scientific conferences.

I would like to express my sincere appreciation to Mme **Sylvie DESCARTES** and M. **Alain SYLVESTRE** for agreeing to judge this study as “rapporteurs” and for the time spent reading this document.

I extend my respectful thanks to M. **Sorin CANANAU**, Mme **Khouira SENOUCI**, M **Thierry PAILLAT** and M. **Hamid ZAIDI** for agreeing to examine the thesis.

I would like to thank M **Karim MEDLES** very much for the many excellent scientific and non-scientific advice and exchanges.

I express my gratitude to M. **Horia Nicolai TEODORESCU** of the Technical University of Iasi 'Georghe Asachi' for his enlightenment about the effects of anisotropy on the triboelectric charging processes.

My grateful thanks also go to my colleague M. **Marian Bogdan NEAGOE** with whom I shared the test benches, science and the good time.

I want to thank in a general way all the researchers of Institut Pprime in Angoulême and Futuroscope who helped me with their advice and fruitful discussions throughout the thesis.

My thanks are also extended to all doctoral students, young doctors and trainees, colleagues and also good friends. Thanks to **Bogdan, Sara**, **Gontran**, **Ali**, **Sergei**, **Alex**, **Catalin**, **Jalil**, **Kader**, **Fethi**, **Hanane**, **Bhanu**, **Mohamed**, **Abdu**, **Arthur**, **Ana**, **Florin**, **Nabil**, **Hamza**, **Imed**, **Alin**, **Ahlem**.

I would like to warmly thank the administrative, technical, teaching and research staff of IUT Angoulême for their availability and support.

I would like to express my special thanks to M. **Thamrin USMAN,** Rector of **Tanjungpura University**, and M **R.M. RUSTAMAJI,** Dean of Engineering Faculty, who motivated me to study in France and support further collaboration with the Université de Poitiers. I am also grateful to the former chiefs of Industrial Engineering Department: Mme **Silvia USLIANTI,** M. **Ivan SUJANA,** M. **Tri WAHYUDI** and M. **Mohamad SOFITRA** for their support to the development of my career as a lecturer and researcher.

I would like to express my special thanks to M **Gérard MAUCO**, who gave me the golden opportunity to prepare this Ph.D. thesis at Université de Poitiers.

Finally, I thank my **mother**, my **father** and my **sister** with all my affection for supporting me and helping me to continue my studies. Special thanks to my **wife** who gave me the power and courage to complete this thesis.

Table of Contents

INTRODUCTION

The components and systems that engineers design for various sectors, from household appliances to the aerospace industry, depend on the properties of the available materials and the existing manufacturing techniques. The evolution of engineering materials is shown in the **Figure 1**. Currently, plastics can successfully replace metals and ceramics in many industrial applications [1,2]. This tendency is related in part to the fact that environmental protection and sustainability are major concerns for the engineers. The concept of eco-design reflects these concerns. Thus, the designer has to take into consideration a multitude of economic and ecological factors, more specifically the environmental impact of the use of a material, as well as its cost, long-term viability and fulfilling human needs [3,4]. In a concurrent engineering or simultaneous engineering approach, the designer must also integrate the end-of-life management of materials for reuse after recycling.

Polymers are more and more employed in the design of mechanical parts as they have many favorable characteristics: resistance to chemical agents, corrosion and mechanical impact, dry running capability, ease of processing, high strength-to-weight ratio, low cost. They are good insulators and only slightly affected by moisture, have a low coefficient of friction and some are weld-able or easy to bond. The electrical insulator properties allow the polymer material to be used in components for high-voltage engineering applications[5,6].

The choice of polymers as materials for mechanical parts is also related to the recent advances in tribology, a field of science and technology related to the study of the mechanical contact between two solid surfaces that can be in relative motion. Optimizing friction, lubrication and wear are key issues of successful machine design. These interfacial phenomena significantly depend on the surface characteristic, on the chemical, physical, thermal, and mechanical properties of the contact bodies as well as on the operational conditions such as applied normal load, sliding velocities, ambient humidity and temperature [7,8].

. Tribological applications of polymers include gears, a wide range of bearings and bearing cages, such as artificial human joint bearing surfaces, as well as bearing materials for space applications [9]. Polymers also serve for coatings, tires, shoe soles, automobile brake pads, non-stick frying pans, floorings [10]. One good reason for using polymers is their low coefficient of friction (between 0.1 and 0.5), which facilitates the sliding contact between two surfaces. Thus, their characteristics make them excellent solutions for utilization where

friction is a concern. In addition, they have interesting self-lubricating capabilities under dry running conditions, because of the thin film generated on the surfaces in contact. This is a consequence of the transfer of microscopic amounts of material between the pairing surfaces. Thus, this self-lubricating property makes polymers commonly used as materials of choice in light-duty applications [11,12].

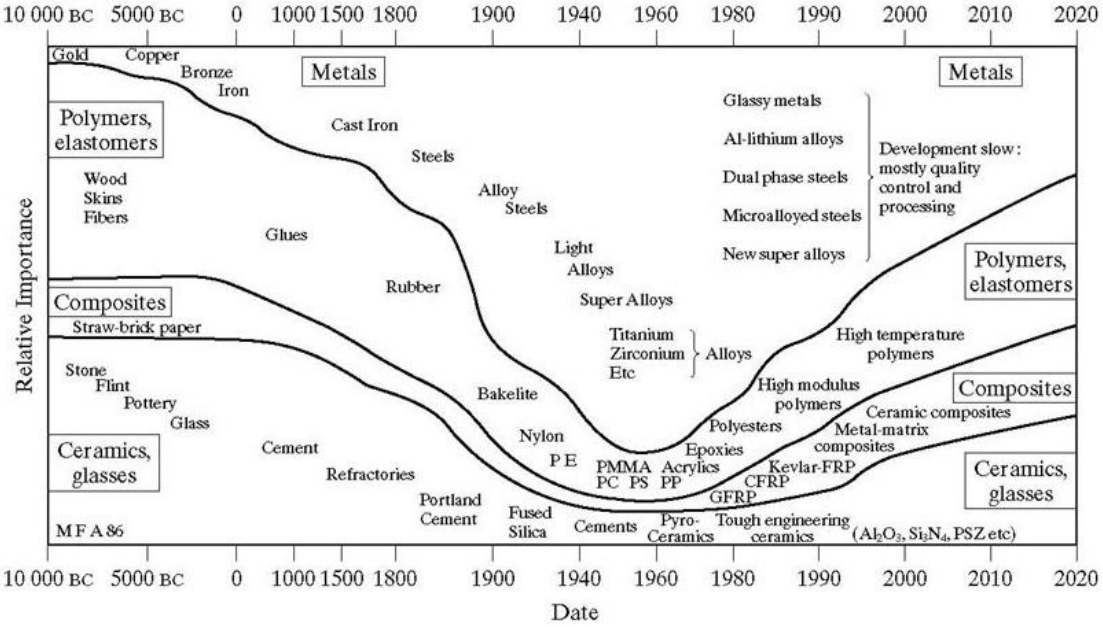

Figure 1. Evolution of engineering materials [1]

The use of polymers in sliding contacts should not neglect the triboelectric effect. An electrostatic charge can be generated on the polymer surface, resulting from friction with another material [13]. On polymers, which are good insulators, this frictional electrostatic charge accumulates during the successive cycles of rubbing until it reaches a certain saturation value and cannot be easily leaked to the ground, as in metals. Its generally non-uniform distribution depends on the nature of rubbing and may extend beyond the contact zone. This will in some degree affect the wear behavior of polymers exposed to dry friction, even if they have self-lubricating capabilities.

In this context, the aim of this thesis is to contribute to a better understanding of the tribocharging behavior of polymers in dry sliding contact, with the possibility to optimize and control the process. The study was conducted in three phases: (1) development of experimental devices for the generation of electrostatic charge on the surface of polymers and measurements of the electrical potential and the charge of the specimens; (2) characterization

of the state of charge and its influence on the dry friction between polymers; (3) optimization of the tribocharging process and validation of statistical tools for its control.

The dissertation is organized in four chapters. The first one is a study of the state of the art, to have a clear view of the current state of research in the field of triboelectricity. A review is made of the main studies related to tribological properties of polymer-on-polymer sliding friction by considering the effect of normal force, sliding velocity, surface roughness, temperature, and humidity. A special attention is given to the researches aimed at showing how the electrostatic charge generated by triboelectric effect alters the tribology of the dry contact between polymers. Furthermore, several studies related to the comparison of the charge evolution and the potential decay between tribocharging and corona discharge mechanism are also discussed in this chapter, to point out that both wear and triboelectric charge can be a hazard to the industry. However, by optimizing and control the tribocharging process, this electrostatic charge can be either prevented, when representing a hazard, or used in energy harvesting devices.

The second chapter provides essential information on the laboratory bench that was designed to investigate the tribocharging behavior of polymers on back-and-forth sliding contact. It presents the characteristics of the specimen and the supporting instruments. The procedures employed for carrying out the experiments and perform the statistical control of the tribocharging process are also thoroughly described.

The third chapter presents the experiments carried out for evaluating the effects of several factors that affect the tribocharging process, such as Young's modulus and micro-hardness value, surface temperature, surface geometry and texture direction during friction. The study also compares in terms of surface distribution and time decay the charge generated by triboelectric effect with the charge deposited by corona discharge.

The fourth chapter is devoted to studying the multivariate optimization model of tribocharging in function of the normal force applied, the number of cycles' and sliding speed. Furthermore, a selected optimal combination of the factors has been employed to set up a control chart for the statistical monitoring of the tribocharging process.

The general conclusion, which closes the dissertation, is accompanied by a synthesis of the main contributions that the thesis makes in the field studied, as well as the statement of the promising perspectives opened by this work.

CHAPTER I
STATE OF THE ART

A basic application of frictional energy was used by palaeolithic civilization to produce fire due to temperature increase in sliding contact. Friction converts useful kinetic into thermal energy or heat. Thus, our ancestors realized that rubbing some sticks against each other produces the energy needed to start the fire, which in turn gave them to heat, light and kept them safe from wild animals. They also realized the importance of sliding speed for increasing the heat generated and accelerate the process. When using a string and bow to handle the stick with one hand while the other gave a normal load to it, ignition of fire become easier with increasing the rotating speed of the stick and the pressure between the bodies in contact.

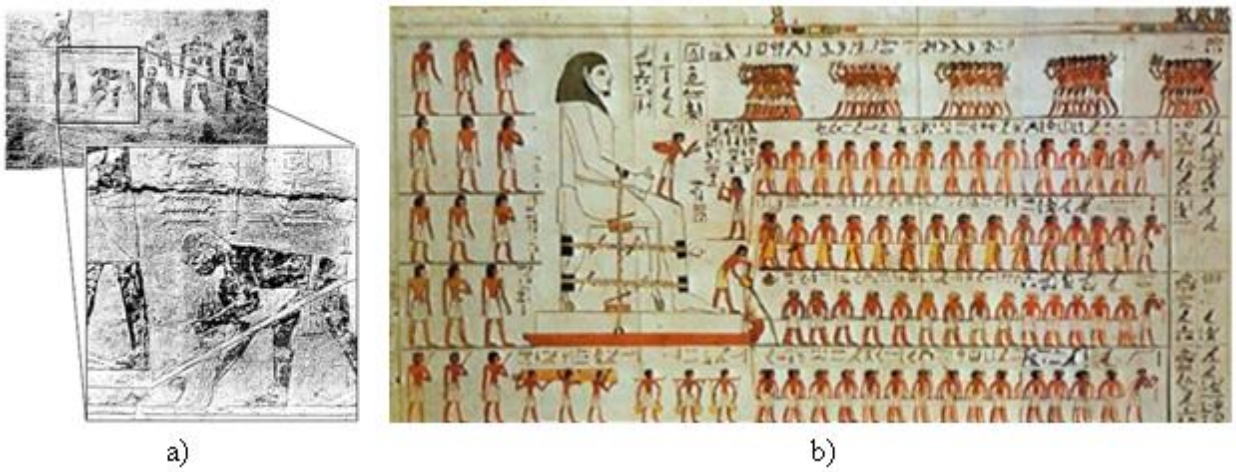

Figure I.1. a) First recorded "tribologist" pouring a lubricant in front of the sledge transporting the statue of Ti from a tomb in Saqqara, Egypt, at about 2400 B.C. [14] and b) use of lubricant on conveying the Colossus statue [15].

However, most of the effects of friction are unwanted. More than 5 000 years ago, humans started to use wheels to reduce friction in translational motion. At about 2500 B.C. Assyrian people used stone socket for the lower pivot of the door on the restoration of a temple by Gudea, Prince of Lagosh, Sumer. Depicted in **Figure I-1.a** is the first recorded "tribologist" using a lubricant (which is believed to be water, mud and olive oil) into the path of a wooden when transporting the statue of Ti, the overseer of the pyramids in Niuserre, in Egypt (2400 B.C.).

Another bas-relief, dated 1880 B.C. and coming from the tomb of Tchuti Hetep at El Berrheh , shows the same system of transport (**Figure I-1.b**), but the man pouring the lubricant is now on the pedestal of the statue and no longer in front of it. A crypt in Egypt that was dated more than one thousand years B.C. provided the confirmation of use of lubricants. A chariot in this tomb still contained some of the unique animal-fat lubricant in its wheel bearings. In China, the famous "south pointing chariot", a two-wheeled vehicle dated 255 B.C., made use of wooden differential gears, as well as of iron rings to reduce wear between moving parts. Military engineers of the Roman Empire discovered some 2000 years ago that with certain pairs of materials friction and wear may be decreased. They also realized that the application of oil films reduce friction [7,16].

About 1500, Leonardo da Vinci a designer, astronomer, philosopher, visionary engineer and artist, deduced the rules of the sliding motion of a rectangular box over a flat surface (**Figure I-2**) and introduced the concept of the coefficient of friction as the ratio of the friction force to normal load.

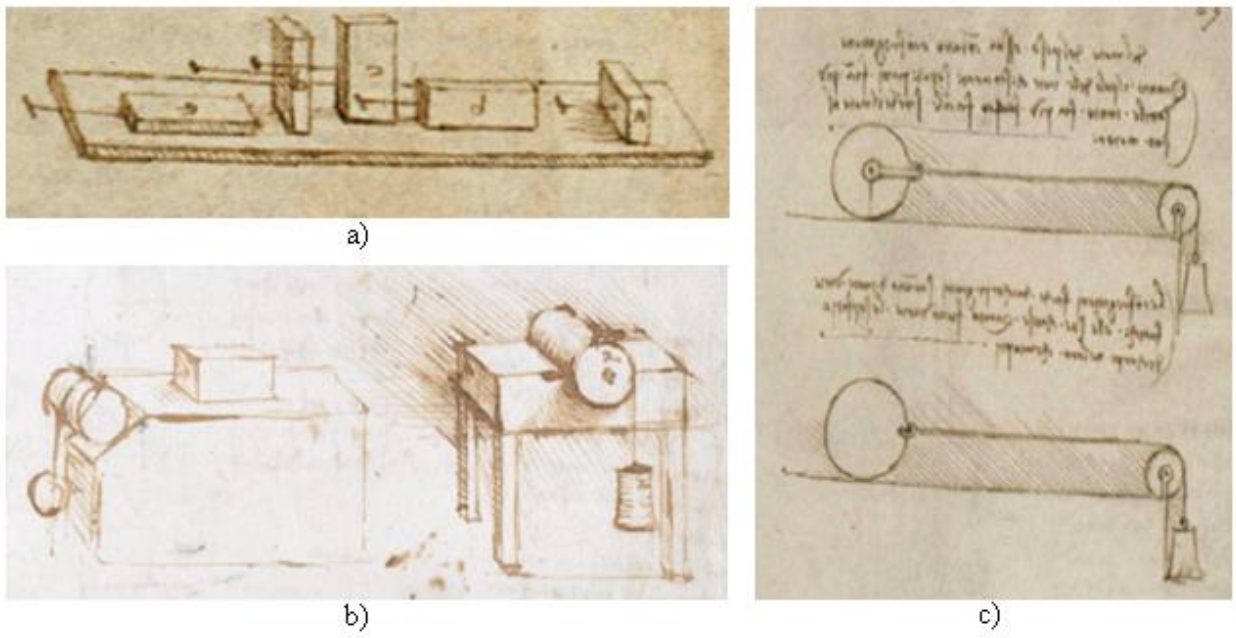

Figure I-2. a). A set of slabs in dissimilar orientations on a plane. b) a block on a horizontal surface connected by a string which passes over a cylinder to a hanging weight, and a horizontal cylinder placed in a hemi-cylindrical cavity with a string supporting to a hanging weight c) Bodies rolling and sliding on horizontal planes [17,18].

In France, in 1699, Guillaume Amontons formulated the rules of friction after investigating dry sliding between two flat surfaces. These observations were verified by Charles-Augustin Coulomb, who formulated what is known as the three laws of friction: (1) the friction force that resists sliding at an interface is directly proportional to the normal load; (2) the amount of friction force does not depend on the apparent area of contact; (3) the friction force is independent of velocity once motion starts. He additionally made a clear distinction between static friction and kinetic friction [14,19].

Coulomb observed that the static frictional force increases with time, this time dependence is varied depending on material. For example, the real contact area will rise for the micro-contacts on metallic material due to the creep processes with a faster pace at high temperature but slower when the contact area is high. The viscoelasticity of elastomer is involved in this effect since it increases with the contact area [19,20]. The non-dependency of the coefficient of friction on the normal force was confirmed for steel in contact with electro-polished aluminum, for an applied normal force ranging from 10 mg to 10 kg. This means that for a soft metallic material, the coefficient of friction remained effectively constant although the load was varied by a factor of nearly 10^6. In the case of polymers and elastomers, the range of load values for which the coefficient of friction is constant is even larger. Therefore, the behavior of these materials notably deviate from Amontons' law [21].

There are different opinions regarding the dependency of the coefficient of friction on the sliding speed. This dependency is critical in lots of applications. Thus, the decrease of the frictional force with the velocity often results in frictional instabilities [20].

Commonly, friction is related to the roughness of the surfaces. In a large domain, the frictional force is independent or only very slightly dependent on the roughness. Contrary to the expectations, the coefficient of friction for particularly soft metallic materials surfaces may be even larger than for hard surfaces. In spite of the complex dependency between friction and roughness, even very detailed contemporary investigations continue to lead to the simplest view that was already mentioned by Coulomb [20].

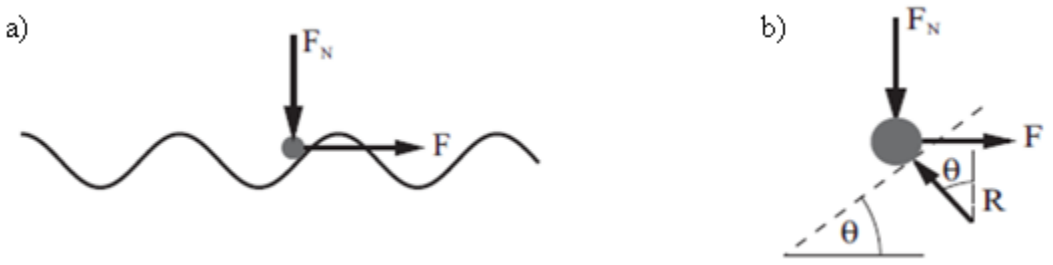

Figure I-3. Dry friction simplified model by Coulomb illustrated : a) mass point on the corrugated surface and b) detail view of this phenomenon [20].

Between the corrugated surface and the point mass, there should no longer be static friction originating even from smaller scale, the equilibrium situations are determined:

$$R\cos\theta = F_N, R\sin\theta = F \tag{I-1}$$

It follows that

$$F = F_N \tan\theta. \tag{I-2}$$

The force of static friction F_s is, by definition, identical to the maximum force F, at which equilibrium is still possible:

$$F_s = F_{max} = F_N \tan\theta_{max} \tag{I-3}$$

The coefficient of static friction is, therefore, equal to the maximum slope of the surface:

$$\mu_s = \tan\theta_{max} \tag{I-4}$$

This model provides, in a simple way, one of the most important properties of dry friction – its proportionality to normal force – and gives a simple geometric explanation for the coefficient of friction. If this is applied to sufficiently large bodies with multiple periodic "corrugations," as in the sketch from Coulomb, then the model also explains the independence of the coefficient of friction from the contact area. It does not explain, however, the observable independence (or relatively weak dependence) of the frictional force on the surface roughness.

F. P. Bowden and K. Riedler in 1935 investigate the temperature distribution in frictional contact. The thermal effects in contacts can be studied at three scale-levels: (1) the tribological system as a whole, (2) the macroscopic contact area, and (3) the micro-contacts between the rough surfaces.

While the temperature of the entire system changes slowly during the process, the temperature in a sliding contact (e.g. between two gears) can change very quickly and reach high values [20].

In 1949 F. P. Bowden and D. Tabor gave a physical clarification for the laws of friction. They stated that the true area of contact is a small percentage of the apparent contact area because of the surface roughness. The true contact area is formed by the asperities. Because the normal force rises, more asperities come into contact and the average vicinity of each asperity contact expands. The frictional force was shown to be depending on the true contact area—a considerable more intuitively satisfying argument than what the Amontons-Coulomb law allows. Bowden and Tabor argued that within these asperities all of the dynamics of friction come about. The friction hypothesis from transporting one surface up the roughness of the other surface is rejected. Adhesion was up till now disregarded, since for it true friction would have to be relative to the cross-sectional area. Real contact area for soft material like rubber will be larger than that for hard materials such as steel [5,22–24]. Regardless of finishing process is applied, all surfaces contain asperity peaks and valleys that make them rough on a micro- or nano-scale [25].

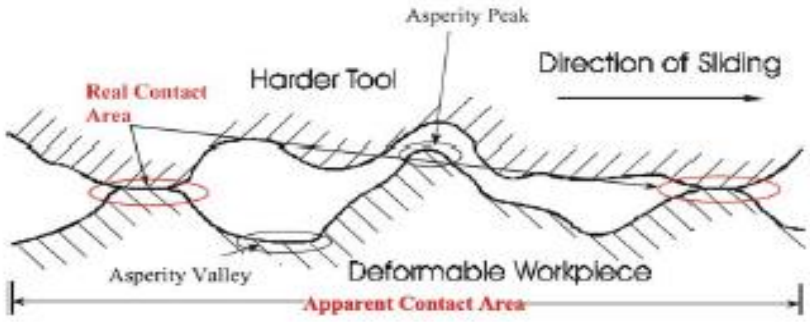

Figure I-4. Real contact area on the apparent contact area [25]

The present massive developments in mechanical design and materials technology are related to new challenges such as miniaturization, portability and functionality, which paved the way to wider application of "green" tribology. Sustainable, biodegradable, renewable energy sources and bio-mimetic are the key concepts the "green" paradigm, which can be specifically expressed in relation with tribology, thus, as most of energy dissipation by friction is transformed into heat which leads to global warming, friction minimization is one of the major objectives of "green tribology". Reducing of wear is another such objective, as it affects the lifetime of components

and generates recycling problems, in addition to debris that contaminate the environment. Both problem of friction and wear can be solved with lubrication. However lubrication can also lead to environmental damage. Thereby biodegradable lubrication or self –lubricated materials can be a solution. Surface texturing also provides a way to control friction and wear in order to obtain ecologically friendly tribo-systems. Finally a real-time condition monitoring, investigation and control of tribological systems should be applied to avoid the formation of dangerous particulates or gases [16].

In the present work the relationship between surface electrostatic charge and the coefficient of friction will be reviewed. The frictional force is defined as the force (F_T) required initiating and maintaining relative motion of two bodies under a normal load (F_N). This results in the following definition for coefficient of friction:

$$\mu = F_T / F_N \tag{I-5}$$

where μ = coefficient of friction, F_T = tangential force (N), and F_N = normal load or force (N). A coefficient of friction can only exist between two materials. The coefficient of friction is influenced by many parameters of the surfaces in contact, such as geometry, roughness, material properties, etc. The friction force, and thus the coefficient of friction, has many functional dependencies as shown below:

$$\mu = \mu(F_N, T, V, RH, R, L) \tag{I-6}$$

where *T*: temperature, *V*: velocity, *RH*: relative humidity, *R*: roughness of both surfaces, and *L*: existence of lubricants [26].

The study of the state of the art for the present work will focus on investigation of the relationship between tribological and electrostatic phenomena in polymers which are generally used as either machine elements or in energy harvesting applications. In accordance to that, firstly we will discuss the characteristics of the polymers used in this study, considering that surface condition and material properties influence the friction and wear as well as its electrostatic charge. Secondly, we will analyze the possibility of using statistical process control of the tribocharging process as part of condition monitoring which includes surfaces thermal analysis and its correlation to electrostatic charge patterns and coefficient of friction behavior.

I.1. Tribology and electrification

I.1.1. Tribology of polymers

The tribology of polymers is an extremely complex process, which has been extensively studied since the mid-20th century to the present day. Popularity of polymers is due to their structural features, unique mechanical behavior (elasticity, accommodation to shock loading, low friction and high wear resistance), and possibility to modify their properties. External liquid lubricants, which work well for other classes of materials, are easily absorbed by polymers [68]. The polymers absorption can be easily influenced by either the operating condition or environment, therefore conventional experimental methods established formerly for metals, may not be appropriate for polymers [27,28].

Wear of polymers can be classified as shown in **Figure I-5**. Each wear mechanism is governed by its own law. It is difficult to distinguish between the various types of wear, since they are inter-related and barely occur separately. Wear depends on some of the properties of the materials, such as elastic modulus, tensile strength and percentage elongation at failure (toughness), which vary notably from one type of polymer to another. Typically, high tensile strength related with a high elongation at failure promotes wear resistance in a polymer. Consequently, given all other factors remain constant, some of the linear thermoplastic polymers with semi-crystalline microstructure perform much better in wear resistance than thermosets or amorphous thermoplastics.

Usually, high tensile strength coupled with high elongation at failure promotes wear resistance in a polymer. Therefore, given all other factors remain constant, some of the linear thermoplastic polymers with semi-crystalline microstructure perform far better in wear resistance than thermosets or amorphous thermoplastics. These observations are in line with the idea that for polymers, surface hardness is not a controlling factor for wear resistance [10,28].

As a general rule, the abrasive, adhesive and fatigue wear are the most representative of the frictional behavior of polymers **Figure I-6**. Abrasive wear is initiated by hard asperities on the surface in contact, which dig into the frictional surface of the polymer and eliminate material, leading to micro- machining, tearing, ploughing, scratching and surface cracking.

The wear debris generated commonly take the shape of fine chips or flakes, identical to those produced through machining process. The abrasive wear is dependent on the shape and apex angle of the abrasive points moving along the counter-face [28].

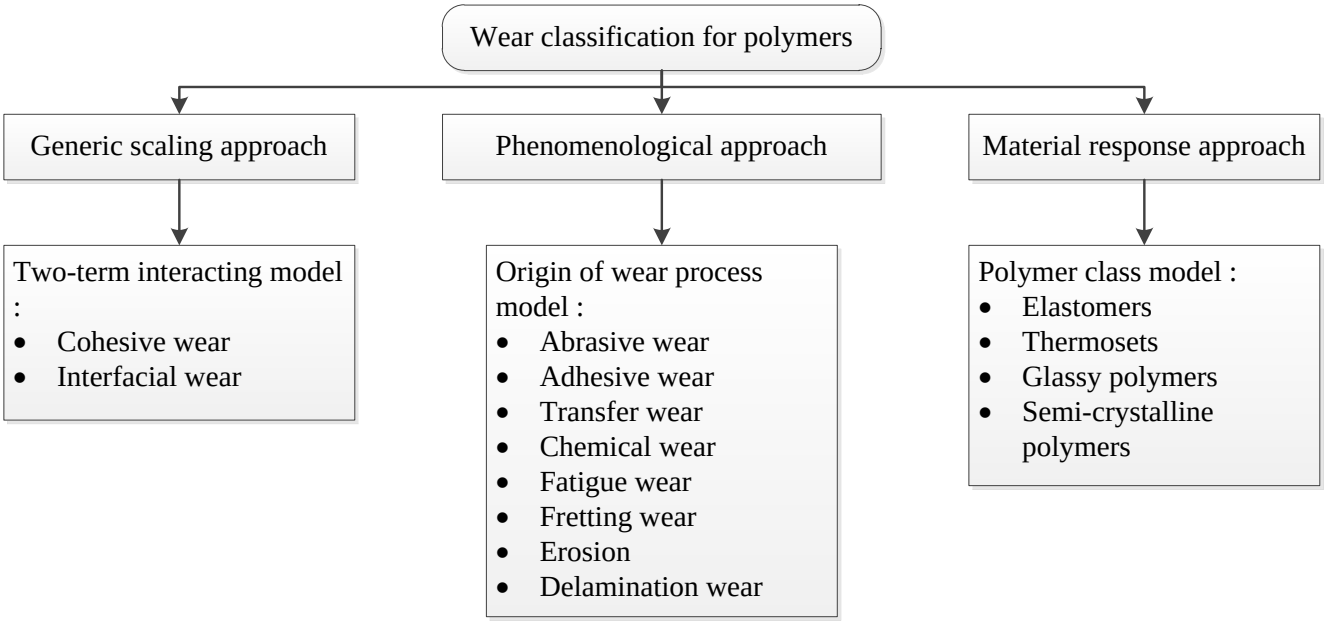

Figure I-5. Simplified approach to classification of the wear of polymers [10].

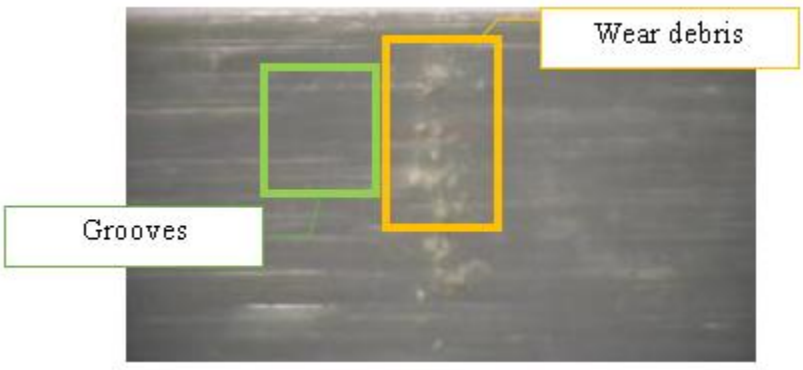

Figure I-6. Grooves across the surface of a PVC slab and wear debris of ABS after flat-on-flat rubbing (photo taken by the author, using digital microscope Makrolite II at IUT Angoulême, Université de Poitiers)

Adhesive wear occurs when two comparable hardness of flat solid bodies are in sliding contact, whether lubricated or not. Adhesion (or bonding) arises at the asperity contacts at the interface, and these contacts are sheared by sliding, which may result in the detachment of a fraction from one surface and attachment to the opposite surface. In the continuous sliding, this is possible the transferred fragment returning to the original surface. Some are ruptured by a fatigue process during repeated loading and unloading action causing formation of loose particles.

Based on experimental records of numerous unlubricated material pairs, the amount of wear is typically proportional to the applied load F_N and sliding distance x and inversely proportional to the hardness H of the surface being eroded [16,20]. Generally adhesive wear is independent of surface roughness, frequently appearing on very smooth surfaces as well as on rougher ones. Conversely, adhesive wear may change the roughness of both surfaces in contact [28].

Surface fatigue is initiated by cyclic or reciprocal stress of the surface by rolling or sliding respectively. In this type of wear, there is no observable surface modification after only one cycle. The mechanism of this fatigue wear in polymers is related to crack propagation during friction and repetitive deformation of the material. Fatigue outcomes in delamination, pitting, and crack generation. As a result of propagation and intersection of minor surface cracks that are oriented perpendicularly to the sliding direction, wear debris are formed [6,20].

Myshkin [27] has summarized articles related to tribology of polymers, including the relationship of normal force applied , sliding velocity, and the effect of temperature on friction coefficient, as shown in tables I.1. to I.3. Although most metals and many other materials obey the first law well, polymers often do not. However the third law defines the independency of the coefficient of dynamic friction (μ_d) with the effect of sliding velocity which is typically true over quite a wide range of velocity, although at high sliding speeds (tens to hundreds meters per second for metals) the coefficient of dynamic friction falls with increasing velocity [27,29–31].

Effect of temperature on frictional contact of polymeric material will be discussed as well in this present work, with reference also to the generation of electric charge. Temperature increase during sliding or rolling contact will affect the friction and wear behavior of materials, as well as the static electric charge generated on the surface.

Table I-1 : The effect of load on friction coefficient [27,30,32–35]

Author (s)	Materials and load applied	Graphical representation
Bowers, Clinton, and Zisman (1953)	2-15 N, steel-polymer (PTFE, PFCE, PVC, PVDC, PE)	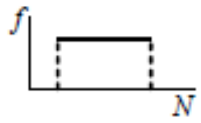
Shooter and Thomas (1952)	10-40 N, steel-polymer (PTFE, PE, PMMA, PC)	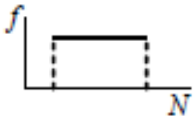
Shooter and Tabor (1952)	10-100 N, steel-polymer (PTFE, PE, PMMA, PVC, nylon)	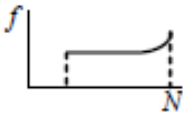
Rees (1957)	Steel-polymer (PTFE, PE, nylon)	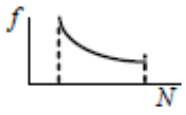
Bartenev (1981), Schallamach (1952)	Steel-rubber	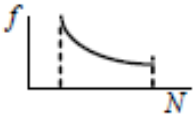
Kragelskii (1982)	Steel-rubber	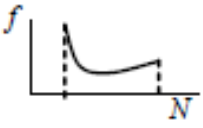
Cho (2016)	0.05 – 5 N, polymer-polymer (BOPP, HDPE, PE, PTFE, HDPE, PU)	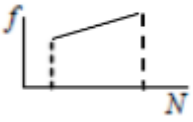
Looijmans (2018)	0.2 – 0.5 N, diamond-polymer Isotactic polypropylene	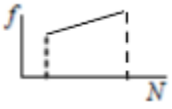
Wang (2018)	10 – 60 mN, steel- mineral and polymer 1-SiO_2, 2-PTFE, R11 acrylic formulation	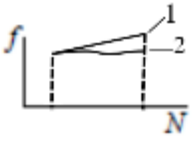

Table I-2 : The effect of sliding speed on friction coefficient [27,30,32–35]

Author (s)	Materials and sliding speed	Graphical representation
Shooter and Thomas (1952)	0.01–1.0 cm/s, steel–polymer (PTFE, PE, PMMA, PC)	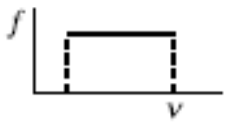
Milz and Sargent (1955)	4–183 cm/s, polymer–polymer, 1—nylon, 2—PC	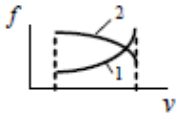
Fort (1962)	10^{-5}–10 cm/s, steel–polymer (PETF)	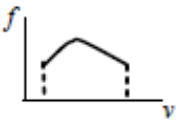
White (1956)	0.1–10 cm/s, steel–polymer (1—PTFE, 2—nylon)	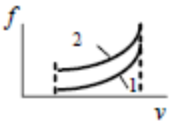
Flom and Porile (1955)	1.1–180 cm/s, steel–polymer (PTFE)	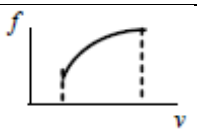
Oloffson and Grablen (1947)	1.5 cm/s, polymer–polymer (fibers)	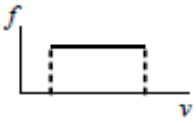
Bartenev and Lavrentev (1981), Challamach (1955)	Steel–rubber	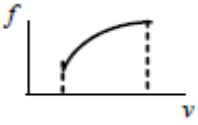
Cho (2016)	0.1 – 1 m/s, polymer-polymer (BOPP, HDPE, PE, PTFE, HDPE, PU)	
Looijmans (2018)	10^{-1} – 10^{2} µm/s, diamond-polymer Isotactic polypropylene	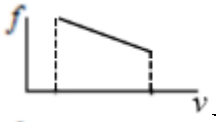
Wang (2018)	0.5 – 2.5 mm/s, steel-polymer R11 acrylic formulation	

Table I-3 : The effect of specimens temperature on friction coefficient [27,32,36]

Author (s)	Materials and temperature	Graphical representation
Shooter and Thomas (1952)	20–80 °C, steel–polymer (1—PS, 2—PTFE)	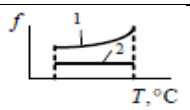
Ludema and Tabor (1966)	-50 to +150 °C, steel–polymer (1, 2-PCTFE, 3-PP) 1-v=3.5x10^{-5} cm/s, 2, 3-v=3.5x10^{-2} cm/s	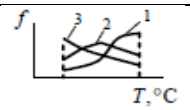
King and Tabor (1953)	-40 to +20 °C, steel–polymer (1-PE, 2-PTFE)	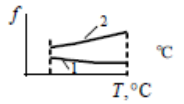
Schallamach (1952)	20–200 °C, steel–rubber	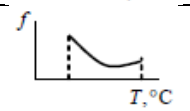
Rojsatean (2017)	23°C and 80°C, metal – polymer ABS and ABS compounds 1 – kinetic CoF and 2 – static CoF	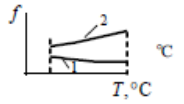

I.1.2. Physical mechanism of triboelectrification

The first scientific reference to the triboelectrification phenomenon is due to Thales of Miletus (640-546 B.C.), who rubbed amber with several materials such as silk cloth, cat's fur or wool, then used the electrostatically charged amber to attract another materials identified as light threads, straw, hay, dried leaves, feathers, and lint [37–39]. Triboelectric effect can be explained by several physical mechanisms, consisting in the transfer of: electrons, ions or material during the contact. One of the surfaces becomes negatively charged and the other becomes positively charged. The charge polarity concept was introduced by Du Fay in 1733, the terms "positive" and "negative" being actually coined by Franklin in 1740. The law of charge interaction was formulated by Coulomb in 1785. The magnitude of charge transfer usually increases with contact roughness, contact area, and contact velocity [40,41].

The triboelectric series proposed by Wilke specifies the polarity of charge acquired after contact, sliding or rolling between any two materials (table I-4) the material at the top end will lose or donate electrons to lower acceptor material on the list. The order of the materials in the series may vary, as it depends on factors such as the surface roughness, purity of the material, moisture, humidity, and the surface condition/real contact area during rubbing [41,42].

Table I-4: Various triboelectric series [40]

	Series 1	Series 2	Series 3	Series 4	Series 5	Series 6	Series 7
Donor of electrons Acquires positive charge	Human hands						
	Asbestos			Lucite 2041			
	Rabbit's Fur			Dapon			Nylon 6.6
	Acetate			Lexan 105	Plexiglass		Cellulose
	Glass			Formvar	Bakelite	Rabbit's Fur	Cellulose Acetate
	Mica			Estane	Cellulose Acetate	Lucite	Polymethyl Methacrylate
	Human hair		Polyox	DuPont 49000	Glass	Bakelite	Polyacetal
	Nylon	Wool	Polyethylene Amine	Durex	Quartz	Cellulose	Polyethylene Terephthalate
	Wool	Nylon	Gelatin	Ethocel 10	Nylon	Acetate	Polyacrylonitrile
	Fur	Viscose	Vinac	Polystyrene 8X	Wool	Glass	Polyvinyl Chloride
	Lead	Cotton	Lucite 44	Epolene C	Silk	Quartz	Polybisphenol Carbonate
	Silk	Silk	Lucite 42	Polysulphone P-3500	Cotton	Mica	Polychloroether Penton
	Aluminum	Acetate Rayon	Acryloid A101	Hypalon 30	Paper	Wool	Polyvinylidine Chloride
	Paper	Lucite, Perspex	Zelec DX	Cyclolac H-1000	Amber	Cat's Fur	Poly2.6-Dimethyl Polyphenylene Oxide
	Cotton	Polyvinyl Alcohol	Polyacrylamide	Uncoated Iron	Resins	Silk	Polystyrene
	Steel	Dacron	Cellulose Acetate/ Butyrate	Cellulose Acetate Butyrate	Metals	Cotton	Polyethylene
	Wood	Orlon	Acysol	Epon 828/V125	Rubber	Wood	Polypropylene
	Amber	PVC	Carbopol	Polysulphone P-1700	Acetate Rayon	Amber	Polytetrafluoroethylene
	Hard rubber	Dynel	Polyethylene terephthalate	Cellulose Nitrate	Dacron	Resins	
	Mylar	Velon	Polyvinyl Butyral	Kynar	Orlon	Metals	
	Nickel, Copper	Polyethylene	Polyethylene		Polystyrene	Polystyrene	
	Silver	Teflon			Teflon	Polyethylene	
	UV Resist				Cellulose Nitrate	Teflon	
	Brass, Stainless Steel				PVC	Cellulose Nitrate	
Acceptor of electrons Acquires negative charge	Gold						
	Polyester						
	Celluloid						
	Styrene						
	Acrylic						

I.1.3. Triboelectric charge of material polymers

Aforementioned contact charging may be due to the transfer of either electrons or ions (positive or negative) from one surface to another, as well as to the displacement of material which is already electrically charged as graphically represented on **Figure I-7**. The explanation of the triboelectric phenomena becomes complicated when one of the materials is an insulator, because of the lack of knowledge regarding the charge carriers that can be transferred between surfaces. Unlike with conductive metals, electrons in the insulator do not have a single energy level. "The energy of an electron in an insulator is a function of its surface impurities, and the materials' chemical and atomic structure" [43] . Negative electrical charges are carried by electrons which are subatomic particles and in metal conductors electric currents involve their movement. Nevertheless either a negative or a positive charge can be transported by an ion, known as anions and cations respectively.

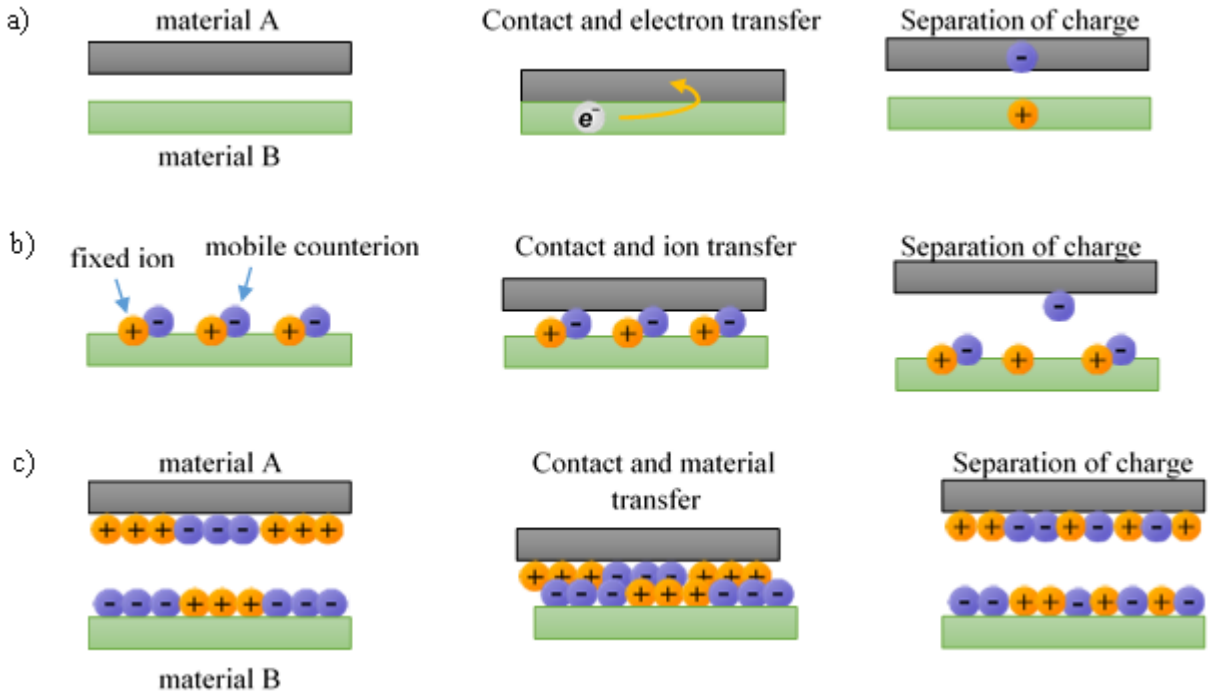

Figure I-7. Contact charging mechanism; a) electron transfer; b) ion transfer; c) material transfer [44,45]

An anion has a net negative charge because the number of electrons exceeds that of the protons. Conversely, a cation has fewer electrons than protons, consequently granting it a positive charge. Cations and anions can be polymer fragments, molecules or even atoms. Beside two previous mechanisms, material transfer during contact is also possible and results in charge exchange. In polymers this phenomenon is related to wear mechanism [13,43,45,46].

Tribocharging between insulators is more difficult to understand as compared to metal-metal or metal-insulator contact charging. Hogue et al. (2007) verified that insulators do not have free or nearly free exchangeable electrons on physical contact, thereby charged material or ions transfer during tribocharging process may play a more important role [47].

Coulomb's law expresses the force acting between two point electric charges q_1 and q_2, separated by a distance r_{12} when the charges have similar polarity, they will repel each other, otherwise they reciprocally attract, as represented in the **Figure I-8**. The magnitude of the force between the particles is:

$$F_{12} = F_{21} = \frac{k|q_1||q_2|}{r_{12}^2} \tag{I-7}$$

the proportionality constant *k* being $9 \times 10^9 N.{}^{m^2}/_{C^2}$, and the vector expression:

$$\overrightarrow{F_{21}} = \frac{kq_1q_2}{r_{12}^2} \cdot \frac{\overrightarrow{r_{12}}}{|\overrightarrow{r_{12}}|} = -\overrightarrow{F_{12}} \tag{I-8}$$

Figure I-8. The force between charges [48]

The approach of the present study aimed at relating tribological and electrical charging effects in polymers is somewhat similar to the one of Descartes et al [49], who correlated the mechanical and electrical behaviors of the wheel-rail contact.

I.1.4. Corona charge of materials polymers

Corona discharge is broadly used in many industrial applications including water treatment, surface treatment, dust removal, electrostatic precipitators, photocopiers, printers and electrostatic separation. Comparing to tribocharging process, corona offers a quite controllable, uniform, predictable charge, can be used on a wide range of material and may repeated without significantly changing the surface roughness. Corona discharges have been extensively studied in relation with energy losses on transmission line, disturbance of radio signals, insulation faults, etc [45,50–53]. F.W. Peek (1915) described the critical visual corona point as a soft violet light in the dark space, at the tip of a metal rod, when energized at a voltage beyond a certain threshold. The visual effect is accompanied by a hissing noise as the electric potential gradually increases between the smooth conductors of a transmission line or between concentric cylinders of electrostatic precipitators [54].

By definition, corona discharge is a gas discharge where the geometry limits the gas ionizing processes to high-field ionization region(s) around the active electrode(s). According to the polarity of the active electrode(s), the discharge's named positive, negative, or bipolar [55]. The common setup for corona discharge involves a sharp metal point or a thin conductive wire, connected to a high-voltage supply.

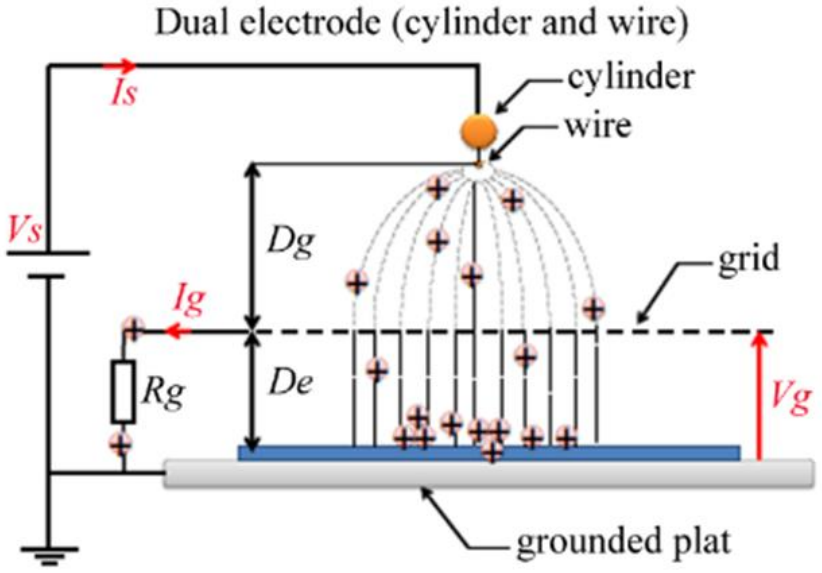

Figure I-9. Triode configuration corona system (dual wire-type corona electrode, grid and grounded plate) [56]

By increasing the amplitude of the voltage applied, the electric field strength might exceed the breakdown threshold in a volume of a few cubic millimeters in the proximity of this electrode. Equal numbers of positive and negative ions are produced in this region, with the negative ions attracted to the positive electrode and neutralized, and the positive ions repelled from the electrode thus moving away towards the nearest grounded region [57].

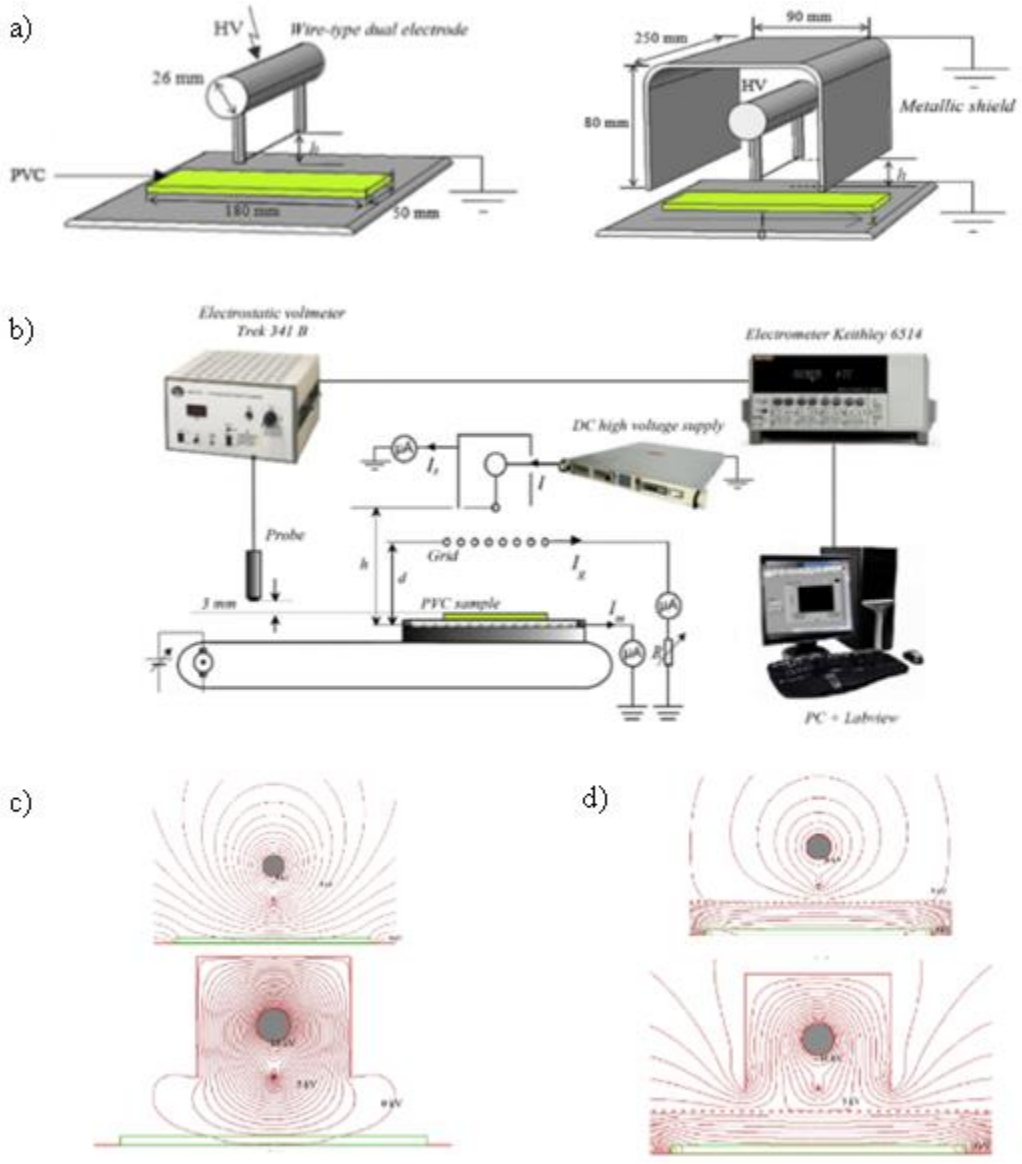

Figure I-10. Grounded shield model by Reguig in a) wire-type dual electrode, and b) triode system, then c) and d) respectively the numerical charge analysis with a "superficial charge simulation program" [58]

Corona discharge using the triode configuration is illustrated in **Figure I-9**. The ions produced by the electrode during the discharge are driven through a grid electrode towards the grounded plate. However, most of the ions are collected by the grid electrode and flow to the ground through a resistor (*Rg*). The current *Ig* through this resistor imposes the grid potential $Vg = Rg \times Ig$ The intensity of the electric field between the grid and the grounded plat is controlled by the potential *Vg*. From the moment the discharge is initiated, the potential of the sample surface placed on the ground plane progressively increases until reaching the potential of the grid [56]. Reguig et al. [58] used grounded shield to optimize the corona discharge as shown in the **Figure I-10a**. The discharge zone is larger, while the current generated is higher.

Positive and negative corona discharges respectively generate different types of ions $CO^+, C^+, C_2O^+, C_3O_2^+, CO_2^+, H_3O^+, CHO^+, CHO_2^+$ and $O^-, O_2^-, O_3^-, CO_3^-, CO_4^-, H^-, OH^-$ [59]. A comparison between of the two types of corona discharge[60] is given in the table I-5. Their visual aspect, which was previously investigated by Peek (1915) [54], can be examined in **Figure I-11**.

Table I-5. Comparison between the discharge in positive polarity and negative polarity.

Positive polarity	Negative polarity
Silent Discharge	Noisy Discharge
Less ozone production	High ozone production
Lower discharge current	Higher discharge current
Strong ionic wind	Weak ionic wind
Steady state current	Less stable current (Trichel pulses)
Light up (continuous glow) along the wire	Dots light along the wire
Lower corona losses	Higher corona losses

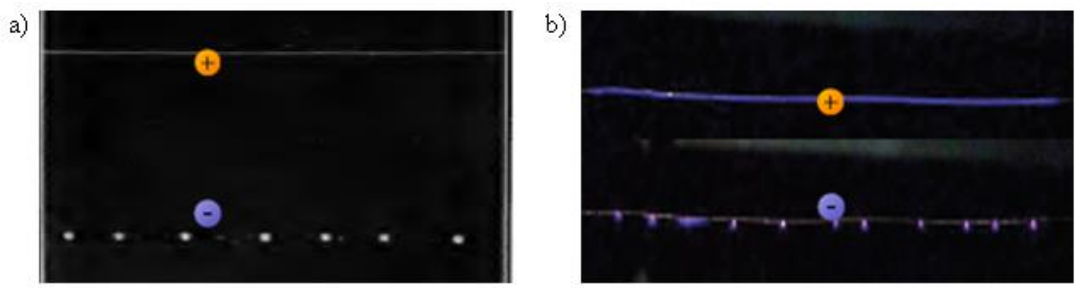

Figure I-11. Photographs of the light appearance in different polarity of corona discharge by a) PEEK [54] and b) Reguig [60].

I.1.5. Tribology effect and electrostatic phenomena

I.1.5.1. Role of friction and wear

Energy lost due to friction and wear is a concern in many industrial sectors. According to Chattopadhyay [3] in Germany the economic loss due to friction and wear ranges between 5% and 8%, The energy efficiency can be improved by reduction of tribology losses in major sectors such as power generation or transportation. In industrial machine tools, the wear processes of the interacting surfaces reduce their lifetime, as shown in the **Figure I-12**.[61,62].

Recent study by Holmberg [63,64] who investigated the global consumption due to friction on several processes found in heavy duty vehicles, friction in the engine consume 33% of the fuel energy. Thus, 180.000 million liters of fuel were wasted worldwide in 2012 for this reason. With reduction of friction, the annual benefit would be 280.000 million euro, fuel efficiency would improve by 200.000 million liters, and CO_2 emission would reduce by 530 million.

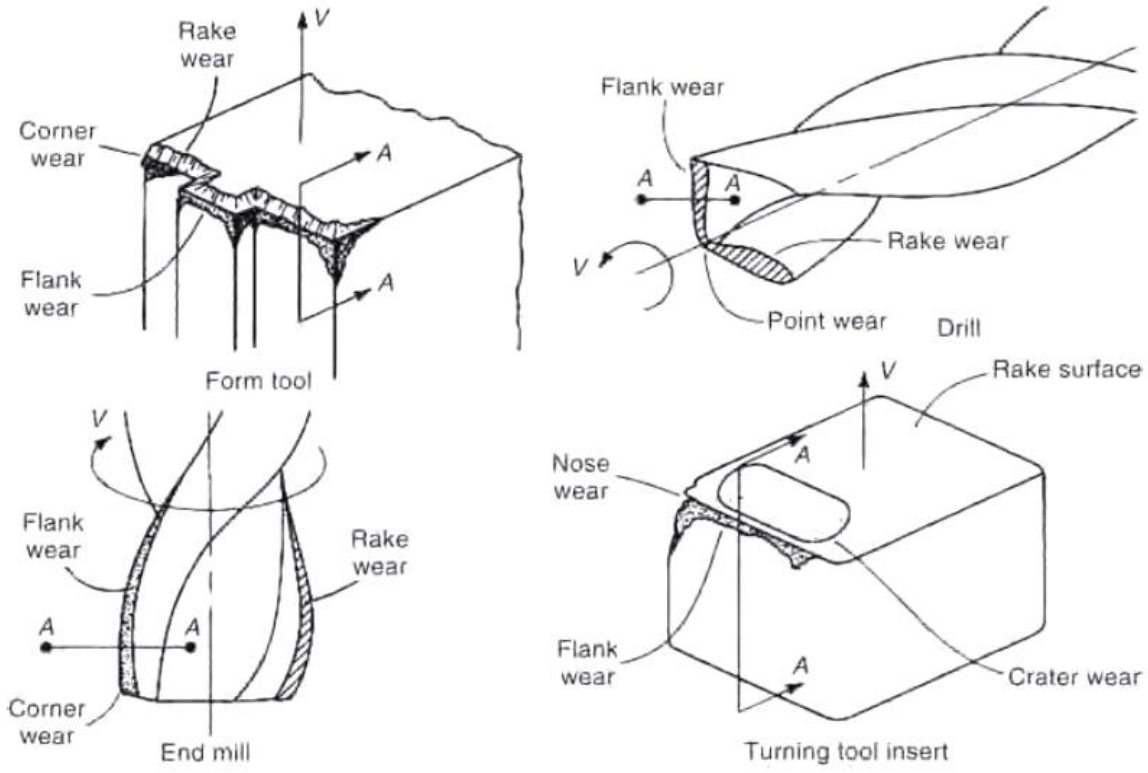

Figure I-12. Typical surfaces wear of common tools due to friction [3].

In the mining industry, where Indonesia is ranked 7th in the world [65], friction and wear loss of mechanical assemblies reached 40% of total energy used. Friction reduction could save of 31.100 million euros, 280 TWh of energy, and 145 million tons of CO_2 emission (table I-6). Remarkable technologies as potential solutions are: wear reduction in critical parts (rock crushing or rock drilling), surface treatment and microstructural material design, thin surface coatings, surface texturing, thick composite coating, optimizing the crusher and grinding mill design [66].

Table I-6. Potential of energy, cost, and emission saving by new tribological technology on short term (10 years) and by nation expected based on their participation of the international mineral raw material production [65].

Production of mineral raw materials (Excluding petrol and gas)	Energy savings (TJ/a)	Cost savings (million euro/a)	CO_2 emission reduction (million tons/a)
World (100%)	995.000	31.100	145
China (33%)	335.000	10.400	48,6
USA (12%)	120.000	3.730	17,4
Australia (7,9%)	78.600	2.420	11,5
Russia (7,1%)	70.600	2.210	10,3
India (6,4%)	63.700	1.990	9,3
South Africa (4,7%)	46.800	1.240	6,8
Indonesia (4%)	40.000	1.300	5,8
Brazil (2,1%)	20.900	650	3,0
Canada (2%)	20.000	620	2,9
Finland (0,02%)	200	6.2	0,03

Prospective mechanisms to decrease friction in paper machines include the application of low-friction and highly durable coatings, surface engineering as well as texturing, low-viscosity and low-shear lubricants and fluids, innovative additives, new materials in seals [67]. As results in the short term (approx. 10 years) of annual worldwide economic saving could attain 2.000 million euros, energy consumption would reduce by 36.000 GWh, and CO_2 emission will diminish by 10.6 million tons.

These statistical data confirm that friction and wear incur losses in several industrial sectors. The losses could be reduced through optimum equipment design and statistical process control.

I.1.5.2. Electrostatic applications and hazards in industry

Static electricity in industrial process is sometimes an advantage and other times a disaster. In fact the benefit of electrostatic phenomena is common and widespread, as for instance in ink jet printers and electrophotography for charging the ink drop or the toner. Applications of the electrostatic separation technique provides benefits in various industrial field such as mining, coal, food, and waste processing. Electrostatic atomization and spraying are also widely used in painting or agricultural devices, with the purpose of droplet transfer efficiency. Related to pollutions from either a solid (dust or smokes) or a liquid (mist) there are electrostatic precipitators which are commonly used in living environments and work places for air cleaning purpose.

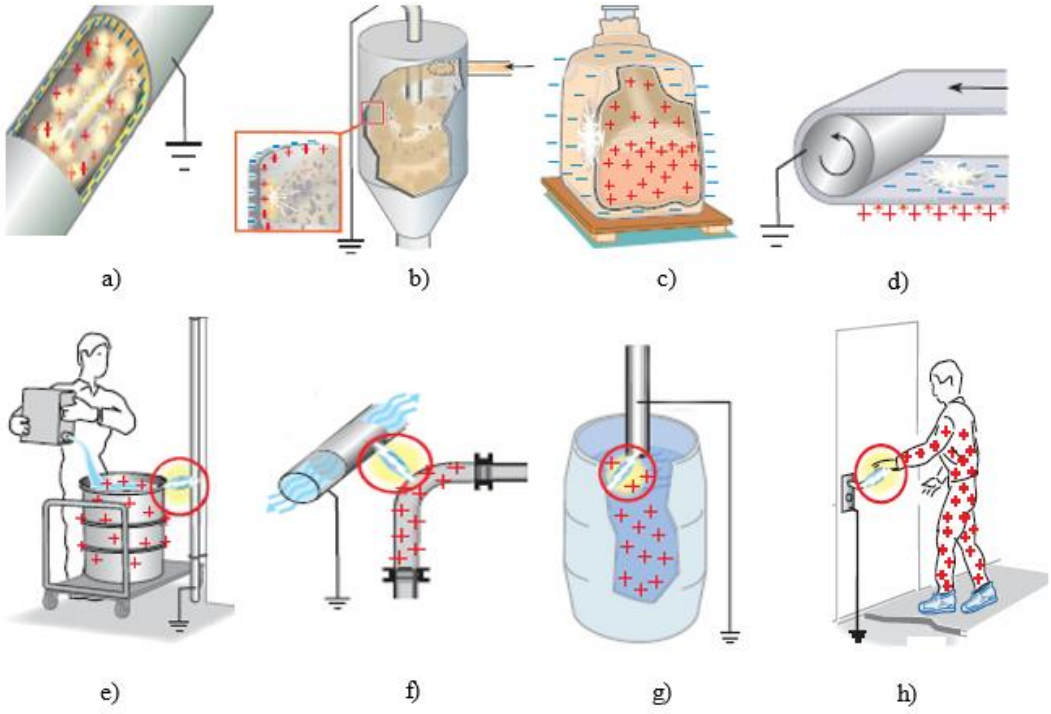

Firgure I-13. Frictional electrification in a) pipe, b) dust separator, c) container for bulk products, d) rotating belt/conveyor, e) metal drum, f) metal elbow, g) plastic container, and h) person [68].

Besides those already mentioned situations, static electricity can also be profitable in such applications as electrostatic coalescence, electro-rheology, flat panel displays, ozone generation, surface treatment, and enhanced mass transfer operations and chemical reactions [57,69,70].

Electrostatic ignition hazards represent a major issue in many industries. Electrostatic spark discharges can be at the origin of explosion, fire or both as shown in the table. Generally, industrial materials can be electrostatically charged in the production or handling processes due to friction as illustrated in **Figure I-13**. Frictional electrification appears in the industrial processing involving : (1) insulating materials/tools or coated with insulators (**Figure I-13a** to **I-13d**); (2) ungrounded conductors (**Figure I-13e** to **I-13g**); (3) operators wearing insulating clothes or shoes (**Figure I-13h**) [68,71–73]. In the present study this phenomenon of charge generated in insulating materials due the friction has been investigated in laboratory scale experiments, since the connectivity to the ground or selection of insulating materials as machine parts in industry are important issues in industry.

I.1.6. Triboelectric energy harvesting

Von Guericke developed the first rotating static electricity generator using a sulfur sphere, which was described in his manuscript *Experimenta Nova Magdeburgica*, published in Amsterdam in 1672 [38]. Nowadays nanoscale triboelectric energy harvesting is a hot topic. Indeed, on one hand triboelectrification is an effect that frequently occurs in human daily life, and on the other hand energy problems have drawn global attention as well as green resources consideration.

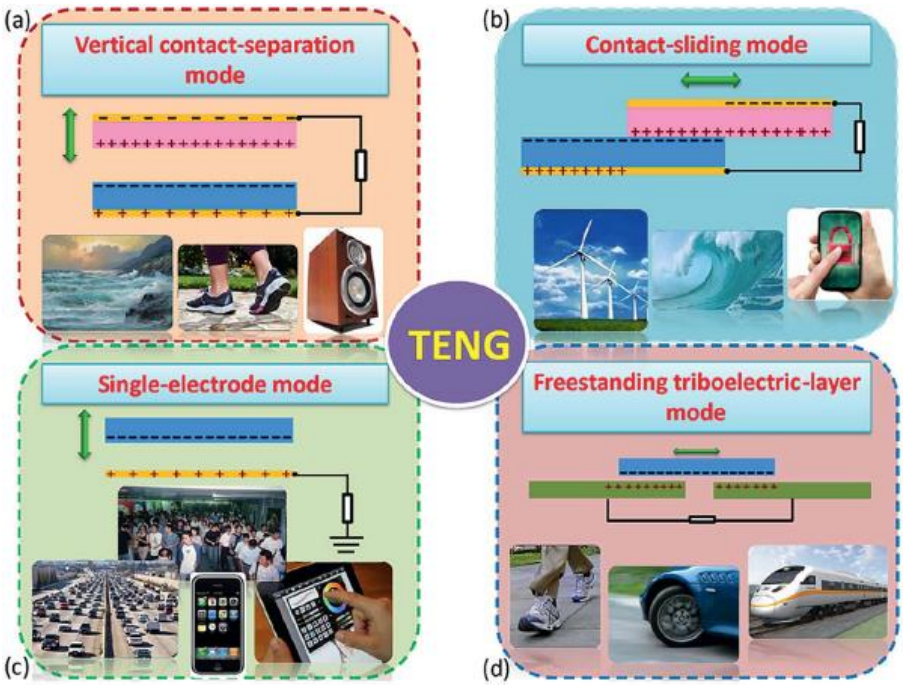

Figure I-14. The four fundamental design of TENG [74]

Zhong Lin Wang demonstrated the potential of using organic materials like paper and polymers to convert mechanical energy into electricity. Depending on the pattern of its source movement, there are four fundamental design of triboelectric nanogenerator namely: vertical contact-separation, contact sliding, single-electrode mode, and freestanding triboelectric-layer as shown in **Figure I-12** [74].

Massive development of triboelectric nanogenerators embrace several sectors including wearable devices which harvest energy from human movements [75–83], wind energy harvester [84–87], wave energy harvester [88,89], machine element harvester which gather wasted friction energy from a machine [90] and self-powered devices or sensors [91–95]. Present study will address two problems related to the triboelectric nanogenerators, more specifically the measurement of the electrostatic charge at the surface of polymers as well as the influence of the environmental conditions [96,97].

I.1.7. Tribology and electrification properties

The number of tribology applications using polymers is rapidly increasing and concern bearings, gears, shafts, pumps, conveyer chains, seals, fluid meters, belts, tires and wheels. The problem is that the study of polymer-on-metal or polymer-on-polymer sliding contacts (and especially the associated triboelectric effect) is not as advanced as that of metal-on-metal sliding, [26].

Tribocharging is mostly apparent in insulators, while in conductors, the charge can rapidly dissipate when in contact with other conductive objects [40]. Since electrostatic charge on the surface of either insulators or non-grounded conductors dissipates slower than that of a conductor connected to the ground, friction behavior will depend on the electric charge on the surfaces in contact. Alahmadi [98] performed experiments to observe the friction coefficient between PMMA sphere on the PTFE and steel surface on isolated and grounded condition. The samples showed relatively have lower friction coefficient on isolated than grounded arrangement. Alahmadi stated that electrostatic charge accumulated on the surface as the attractive force which leads to increase in friction coefficient. This was more significant for lower values of the normal load. Alahmadi mentioned that electrification on the isolated test specimen is lower than another one which connected to the ground. This is interesting point to discuss since PMMA and PTFE are non-conductive polymers.

Galembeck and Burgo [99,100] conducted several experiments related to surface charge and friction coefficient, CoRR measurements adopted the ASTM standard (G194-08). PTFE plane was used as a runway of a glass bead (P_1) after being pre-charged by rubbing against felt with adjusted pressure as shown in **Figure I-15**. The glass bead sample was placed on the chosen high of an aluminum smooth slope with 10° of inclination, then coefficient of rolling resistance calculated with simple formulation:

$$CoRR = h/d \tag{I-9}$$

where, h is the chosen high of glass bead starting point and d is the distance traveled along the PTFE plane. The potential decay of PTFE is slow, therefore enough time to mapping the surface potential and glass bead samples can be prepared with confidence. The result indicates that rolling friction of glass balls increases with the level of charge at the surface of the PTFE plane.

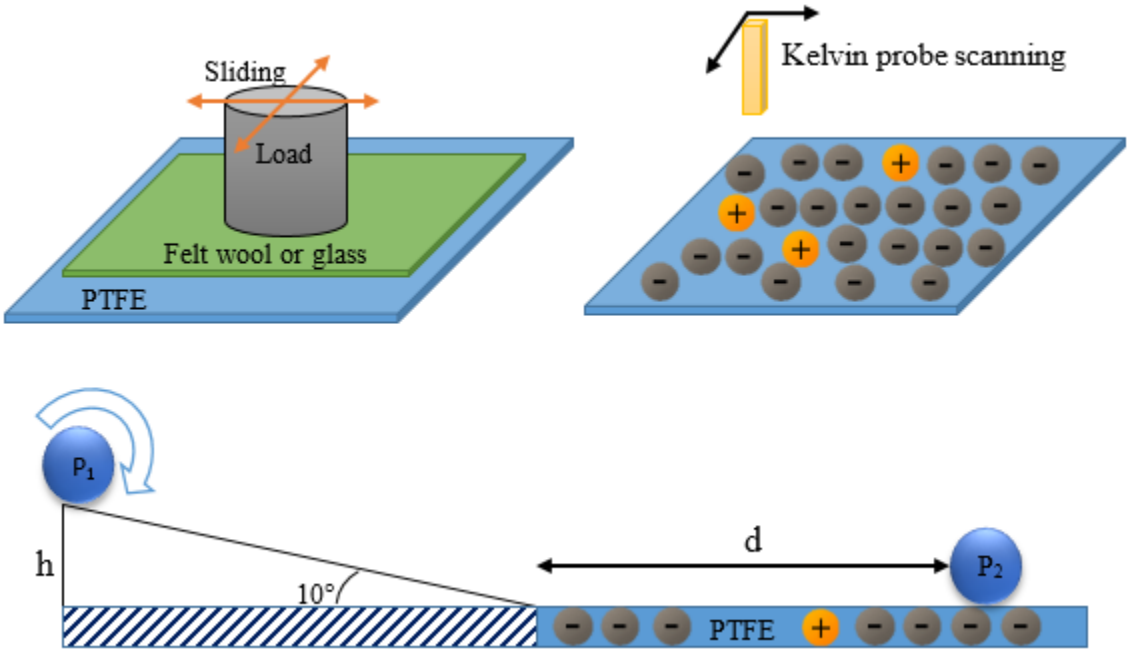

Figure I-15. CoRR measurement adopted ASTM G194-08 [100]

This result of Galembeck were in agreement with the experiments of Ishida in Japan [98] related to wheel-rail interface. The friction coefficient of the wheel was slightly larger on the electrified rail than on the non-electrified one (**Figure I-16**) [101].

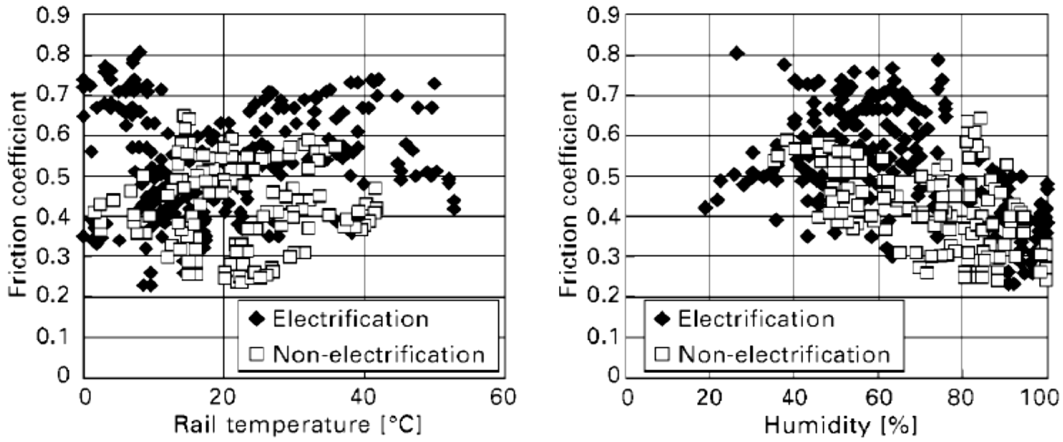

Figure I-16. Relation between friction coefficient and electrification of wheel-rail contact [101].

I.2. Modeling, Optimization and Control of Tribo-electrostatic Processes

Tribology and electrostatics are complex sciences, hence the diversity on their mutual interactions is not surprising. Maintain under control the tribo-electrostatic processes is a crucial aspect in many industries. Electrostatic discharges due to the accumulation of triboelectric charge on insulating bodies is a major source of hazards in chemical, pharmaceutical and electronic industry. In other cases, such as the electrostatic separation of granular plastic mixtures, the triboelectric effect is beneficial and should be enhanced. However the triboelectric effects can be eliminate or prevent either by apply antistatic agents or optimize the process of frictional charging. [61,102].

I.2.1. Condition monitoring

"To make the best choice between extended total life and less investment in replacement parts by proactive maintenance or, alternatively, reduced maintenance, preferably only when indicated by condition monitoring, is a typical task for life cycle engineering. However, facts and data are needed based on comparable experience and reliable predictive tools, when such decisions are to be taken in the conceptual stage, there are similar tradeoffs between initial investment, performance, maintenance costs and possible degree of recycling" [103].

The present study will simultaneously monitor friction, wear and triboelectric charge generation of polymers in sliding contact.

1.2.1.1. Laboratory sliding tribometer

The Hertzian theory relates to non-adhesive contact between two spheres or a sphere with a plane, taking into account the elastic deformation properties of the materials. Theoretically, such a contact appears as a point for two spheres or a line for cylinders in parallel contact. The JKR (Johnson, Kendall, Roberts) theory is an improvement over the Hertzian model, as it includes the adhesion phenomena **Figure I-17**. Hertz theory is illustrated in **Figure I-18a** for the contact between two spheres and in **Figure I-18b** for the contact between two cylinders [29,104,105].

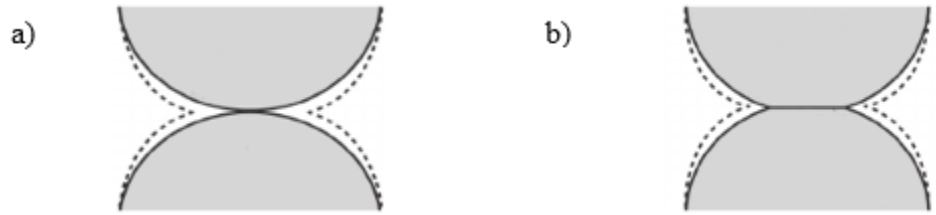

Figure I-17. Models of mechanical contact by a) Hertz fully elastic model and b) JKR fully elastic with adhesion in the contact area.

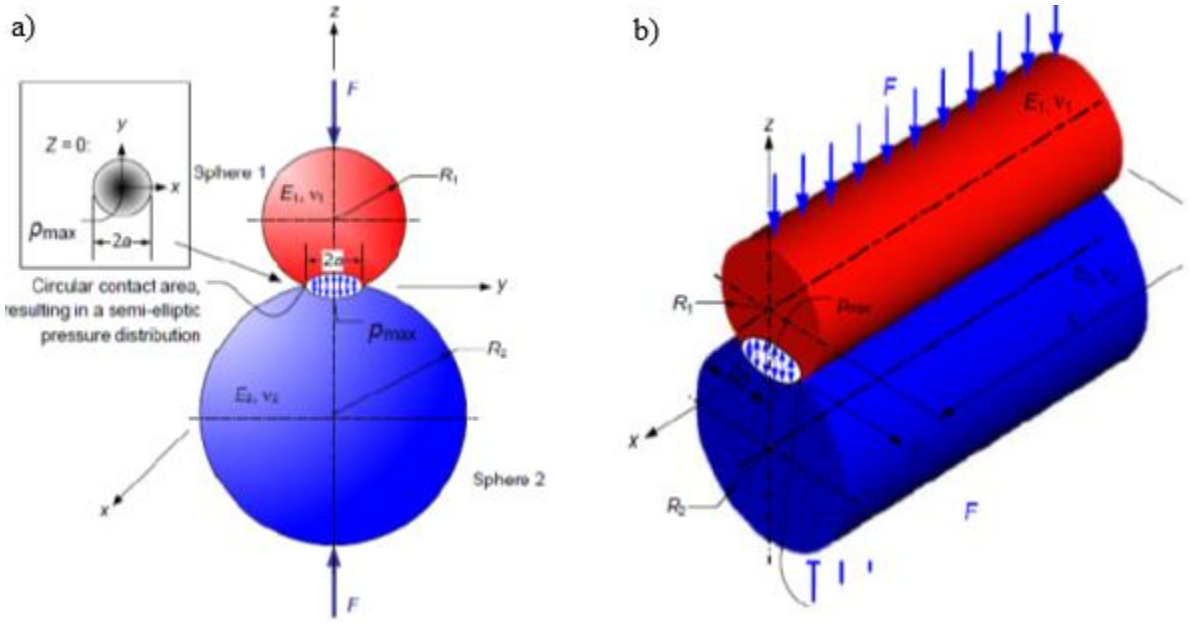

Figure I-18. Models of Hertzian contact a) between two spheres and b) between two cylinders with parallel axes [104].

In accordance with Hertz contact model (**Figure I-18a**) between two spheres of radii R_1 and R_2, the radius of contact area a is given by:

$$a = \sqrt[3]{\frac{3F\left[\frac{1-v_1^2}{E_1}+\frac{1-v_2^2}{E_2}\right]}{4\left(\frac{1}{R_1}+\frac{1}{R_2}\right)}} \quad \text{(I-10)}$$

where E_1 and E_2 are the elastic moduli, v_1 and v_2 are the Poisson's ratios of spheres 1 and 2 respectively. The maximum contact pressure at the center of the circular contact area is:

$$P_{max} = \frac{3F}{2\pi a^2} \quad \text{(I-11)}$$

the depth of indentation "*d*" is related to the maximum contact pressure by:

$$d = \frac{a^2}{R} = \sqrt[3]{\frac{9F^2}{16RE^{*2}}} \quad \text{(I-12)}$$

where R is the effective radius defined as $\frac{1}{R} = \frac{1}{R_1} + \frac{1}{R_2}$, for v = 0.33. The maximum shear stress occurs in the interior at z ≈ 0.49a.

In the case of the contact between two parallel cylinders of radii R_1 and R_2 (**Figure I-18b)**, the force is linearly proportional to the indentation depth, so that the half-width *b* of the rectangular contact area can be expressed as:

$$b = \sqrt{\frac{4F\left[\frac{1-v_1^2}{E_1}+\frac{1-v_2^2}{E_2}\right]}{\pi L\left(\frac{1}{R_1}+\frac{1}{R_2}\right)}} \quad \text{(I-13)}$$

where L is the length of contact, E_1 and E_2 are the elastic moduli, and v_1 and v_2 are the Poisson's ratios, for cylinders 1 and 2, respectively. The maximum contact pressure along the center line of the rectangular contact area is:

$$P_{max} = \frac{2F}{\pi bL} \quad \text{(I-14)}$$

The term "tribometre" was invented by Goldsmith in 1700 to designate a device meant to measure friction. At present, the meaning of the term tribometer has been expanded to an instrument used to measure friction, wear, or both. A laboratory bench simulating the load, the speed and the lubrication conditions of industrial machinery facilitate the study of wear-related phenomena. A microscope can be used to evaluate the surface condition, and accurately predict the lifetime of the components [106,107]. Basic principle of this tribometer can be illustrated by

Leonardo da Vinci's static friction test using inclined plane (**Figure I-15**). Present-day tribometers mimic reciprocating machine elements such as piston and slider-crank mechanism shown in the **Figure I-19a**. Other configurations, such as those illustrated in **Figure I-19b** to **I-19d**, are commonly used to estimate the nominal contact pressure and contact area, using Hertz formula. Symmetrical arrangements such as face-to-face and ring-on-ring device which are respectively shown in **Figure I-19e** and **I-19f** are sometimes used to study wear [106,107].

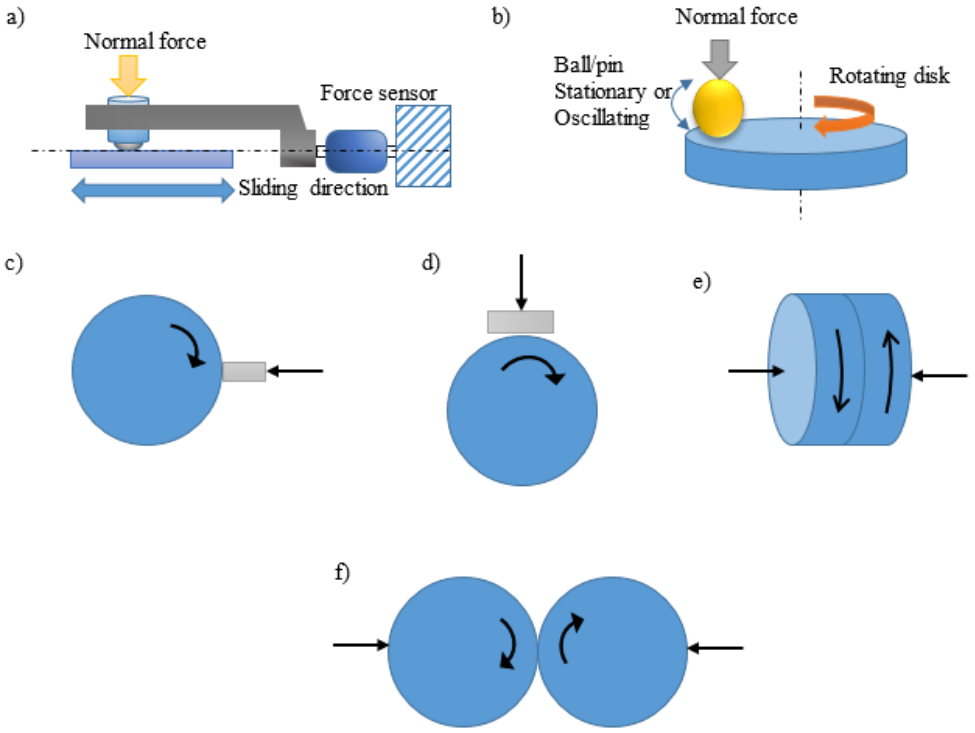

Figure I-19. Basic principal of wear test a) reciprocating test, b) Ball/pin-on-disk, c) a pin-on-a rim, d) a block loaded against a ring, e) face-to-face, and f) ring-on-ring [30,31,106].

Selection of a tribometer is a delicate issue, as the instrument should simulate the industrial process and facilitate the study of wear or friction behavior of given machinery. Typical wear studies and appropriate tribometer categories are summarized in Table I-7 [7]. In the present study, the wear mechanism is similar to the situation of "dry sliding wear under non-ambient conditions". To meet this requirement, a special room with controllable temperature and humidity has been built, considering that these ambient conditions have also a strong impact on electrification [108,109].

Table I-7. Prevailing wear conditions and type of tribometer [7].

Mechanism	Tribometer
Abrasive	Apparatus involving abrasive paper or bed of sand
Cavitational wear	Specimens mounted in stream of air or liquid jet mixed with abrasive particles
Dry or lubricated sliding wear under ambient conditions	Specimens slid against a moving counter-face (which may also be a specimen) either by rotation or reciprocating movement. Lubricant supply system fitted for lubricated tests
Dry or lubricated sliding wear in non-ambient conditions	Specimens and moving counter-face enclosed in chamber fitted with heating, refrigeration and/or vacuum pumping system to maintain a specialized environment
Fretting/fretting fatigue	Specimens slid against the counter-face at very small amplitude. Apparatus can be fitted with chamber for specialized environments
Wear in pure rolling or combined with sliding	Specimens in form of rollers and spheres and constrained to move at specified speeds. Apparatus can be fitted with chamber for specialized environments
Impact wear	Apparatus containing hammer to impact wearing specimen. Can be fitted with enclosing chamber for non-ambient tests
Diffusion or solubilization wear	Cutting tool as specimen. Cutting performed at high surface speed Specimens immersed in molten test material and rotated to accelerate wear
Hydrodynamic and elastohydrodynamic lubrication	Idealized conformal and non-conformal contacts devised with purpose of displaying mechanism involved in the formation of lubricating films
Boundary and solid lubrication	Apparatus involving sliding wear at low velocities allowing the monitoring of the friction coefficient

I.2.1.1. Surface electric potential cartography

Baytekin et al. [110] observed the surface charge in tribocharging experiments over various type of materials i.e. silicon, aluminum, polytetrafluoroethylene (PTFE), polycarbonate (PC) and polydimethylsiloxane (PDMS). They concluded that mosaic charging is a common feature of triboelectrification. Moreover, this mosaic reflects the imperfection of contact during frictional charge. **Figure I-20** illustrated the possible scenarios of mosaic charging and the result of Kelvin Force Microscopy (KFM) scanning.

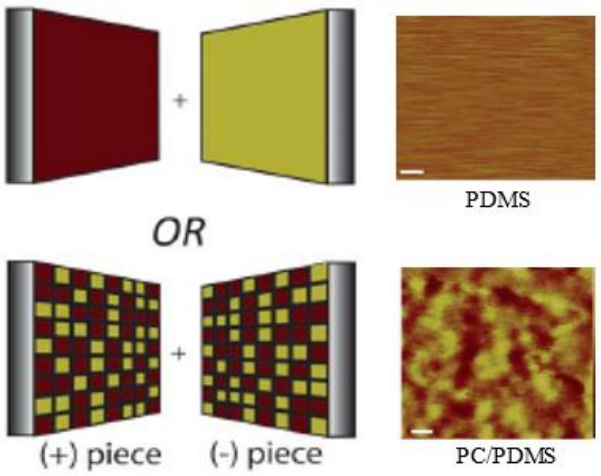

Figure I-20. Surface charge mosaic the scenario and results PC against PDMS [110].

A thorough study of static charge patterns of tribocharged Polytetrafluoroethylene (PTFE), poly (methyl methacrylate (PMMA) and polyethylene (PE) was conducted by Burgo et al.[111]. They eliminated the residual charge by soaking the polymer samples in ethanol for 2 hours prior to experiments of tribocharging. In a first set of experiments, square sheets of 400 mm^2 or 3600 mm^2 were rubbed with a disk of polymer (Ø = 10 mm or 25 mm) at 5.000 rpm for 3 s. In a second sets of experiment, a 3600 mm^2 square sample was placed on a planetary shaker to accommodate glass spheres (Ø = 1 mm) or PTFE pellets (5 × 5 × 1 mm^3) at 5 Hz of reciprocating frequency and 10 mm of amplitude for 60 minutes. The surface potential measurement ranged within ±3300 V at 25 mm^2 of dimensional resolution, as the results shown in the **Figure I-21**.

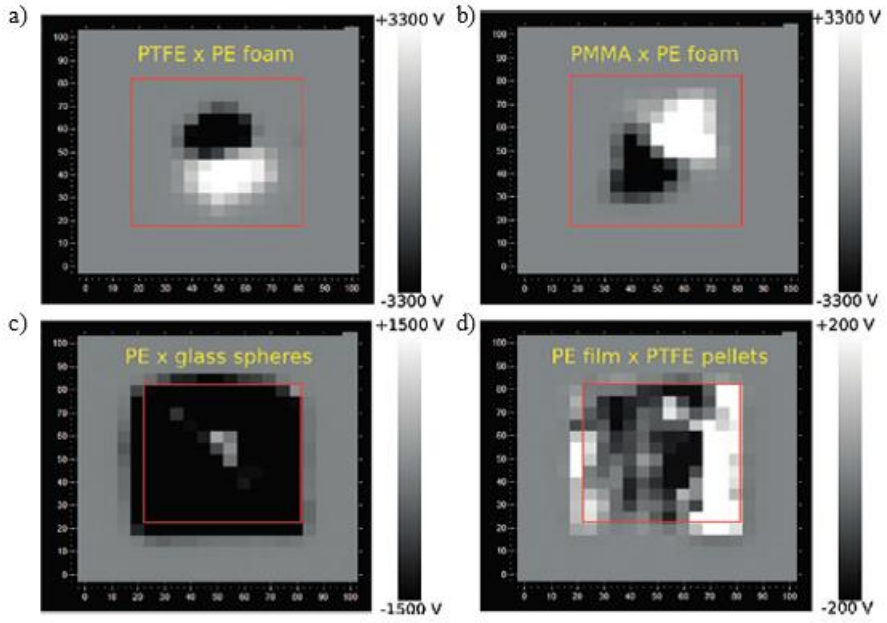

Figure I-21. Macroscopic potential patterns obtained from a) PTFE, b) PMMA which rubbed with PE and PE surface after rubbed with c) glass spheres, d) PTFE [111].

Tribometer instrumentation in these circumstances was employed as tribocharging device not only to simplify the characterization of wear and friction phenomena but also to facilitate the study of the tribocharging effects. Sensors have an important role in monitoring the triboelectrification process and need to be placed as schematically shown in the **Figure I-22a** [112,113], which displays the design of tribometer integrated with an LVDT (linear-variable-differential-transformer) to inspect the perpendicular displacement of the pin against the disk, an infrared thermometer to observe the temperature of the disk, and a laser probe to supervise the wear profile and depth.

Hiratsuka et al. [108] designed a tribocharging device (**Figure I-22b**) to make easier the switching of the rotational direction, the control of the slip ratio, the charge monitoring, and the simultaneous measurements of triboluminescence and tribocharging. A special tribocharging device equipped with a stepper motor was used by Liu et al. [114], as illustrated in the **Figure I-22c**, to generate charge, on the surface of nylon, PP, and PTFE samples rubbed against stainless steel, analyze its decay, and establish a triboelectric series.

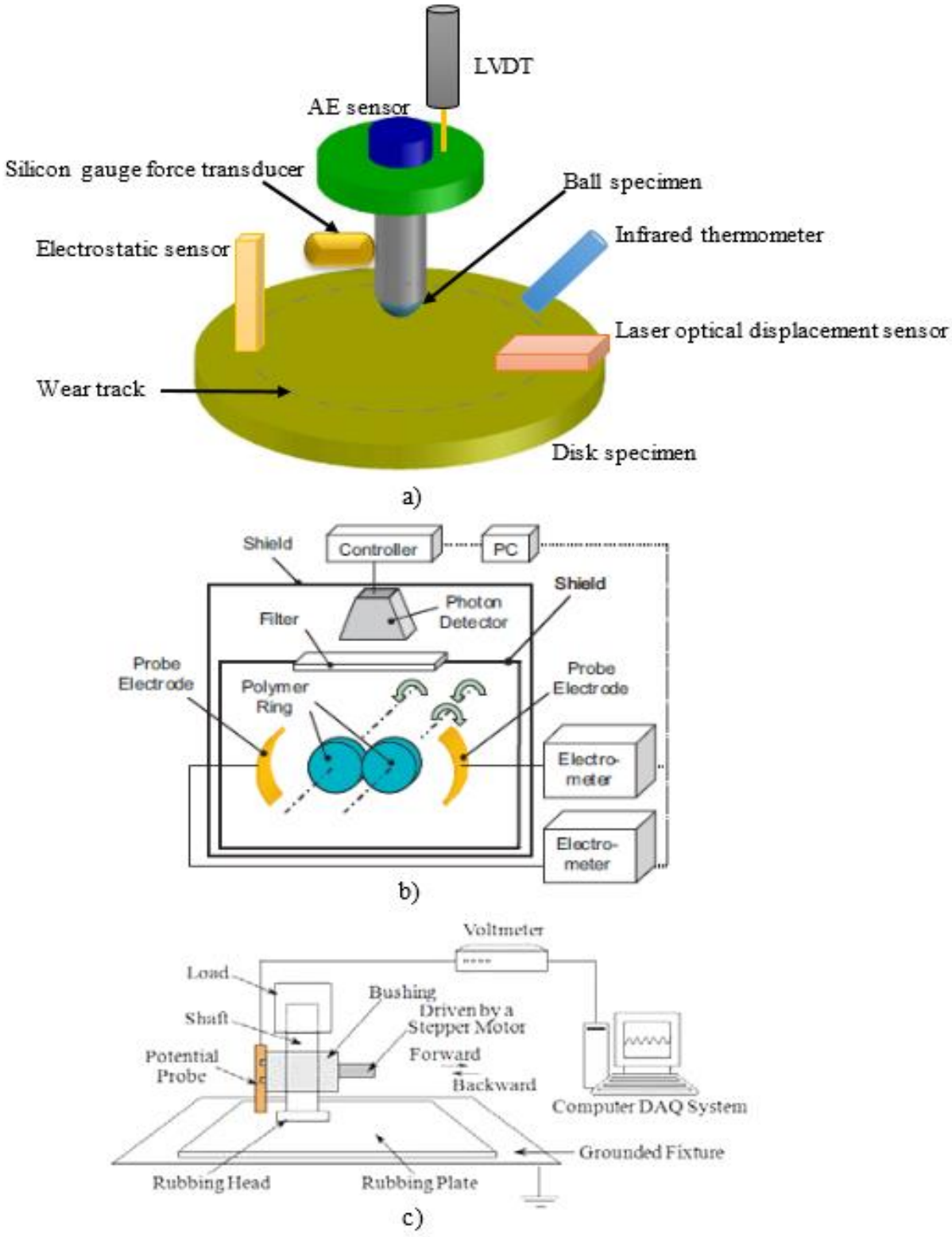

Figure I-22. Types of tribometers with integrated sensors: a) pin-on-disk [112,113], b) ring-on-ring [108] and c) reciprocating pin-on-plat [114].

I.2.1.2. Surface potential decay

Surface charge decay measurement may in some situations be used to evaluate the resistivity of a material [115,116]. In industrial applications, understanding the surface charge decay is fundamental to materials selection, considering the risks related to the accumulation of charge [52,71]. Several studies demonstrate that the moisture adsorption induced the increasing of material conductivity [117,118] either on hydrophobic or hydrophilic polymers [77].

Figure I-23 describes the surface charge decay phenomenon which can be explained by several factors such as charge injection, internal conduction, polarization, charge decay into air or gas, surface conductivity, and piezoelectric phenomena [114,119,120].

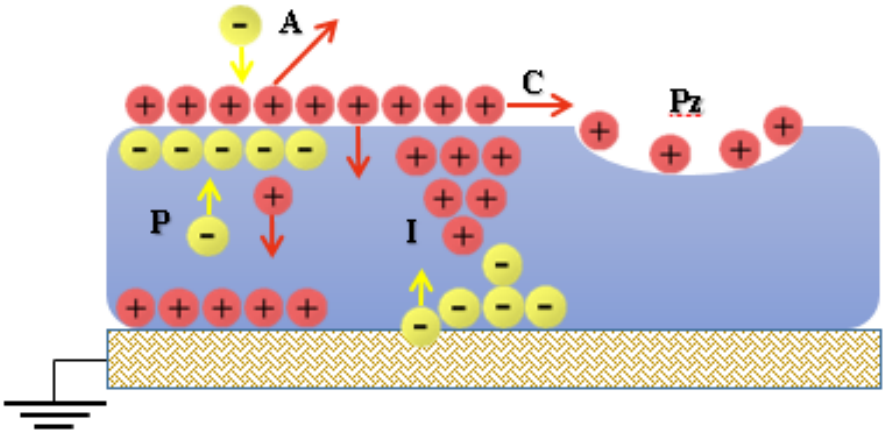

Figure I-23. Different possible mechanisms to explain the decay of the electric potential at the surface of an insulating slab: internal polarization (P), decay through the polymer bulk / charge injection (I), decay through the air or gas (A), surface conduction (C), and piezoelectric phenomena (Pz) [114,119,120].

I.2.2. Design of experiments and statistical process control

Response surface methodology or RSM is part of Design of experiment (DOE), for analysis and modeling of problems which contain response of interest using a compilation of mathematical and statistical procedures to optimize the response with engaging of several variables and the objective. For example, an engineer may wish to find the levels of force (x_1) and cycle (x_2) of a process that maximize the electrostatic charge generated on the surface (y). According to this method the tribocharge is a function of the levels of force and cycle [121–124].

Quality improvement in industry may require the application of RSM. For instance, Xiao et al. [125] applied it in a friction materials development research. He found five ingredients that were statistically significant and deserve to be studied further. In the study of tribological performance of dry sliding, Peng Chang et al. 2015 [126] have used RSM method to show the connection between control factors i.e. talc filler, loads (10, 20, and 30 N) and sliding speeds (0.2094, 0.4188, and 0.6282 m/s), and the responses: the average coefficient of friction (CoF) and the wear rate. The results successfully shown that all three factors have significant effects on both responses, and the predicted optimized sliding conditions were confirmed by experiments. A recent study conducted by Rashid et al. [127] applied factorial experimental design technique to find the optimum combination of applied normal force (30, 50, and 70 N), and sliding speed (2.6, 3.9, and 5.2 m/s) at a constant sliding distance of 5000 m under dry sliding condition. Rashid revealed that volume loss and coefficient of friction decrease for treated material. Moreover, normal force has the most significant effect on the wear, while sliding speed has no significant contribution to the volume loss.

Dascalescu et al. [128] successfully applied factorial DoE to the study of triboelectric charging of mm-size polyamide particles in the polypropylene box of a vibratory feeder. The solutions to improve the electric charging are pre-conditioning of material surface and increasing the number of collisions between particles and the walls of the tribocharging devices. He also used DoE to evaluate the tribocharging of powdery material in compressed-air devices [129]. The response function was the charge/mass ratio of the material collected in a modified Faraday cage and the factors under his investigation were the injection-, dilution- and vortex- air pressure. The latter was found to be the most important factor. Furthermore, DoE method also satisfactorily applied to the study of corona discharge [130], a charging mechanisms that will also be employed in the present thesis.

Statistical process control (SPC) has been successfully applied in the field of electrostatic processes. Medles et al. [131] demonstrated that the application of SPC could reduce the variability which affects the output of the process (**Figure I-24**) and enhance the ability to detect the out-of-control situations. According to Senouci et al [132,133] control charts are powerful tools to monitor the evolution of an industrial process. The researches proved the effectiveness of multivariable control charts to detect any out-of-control situations.

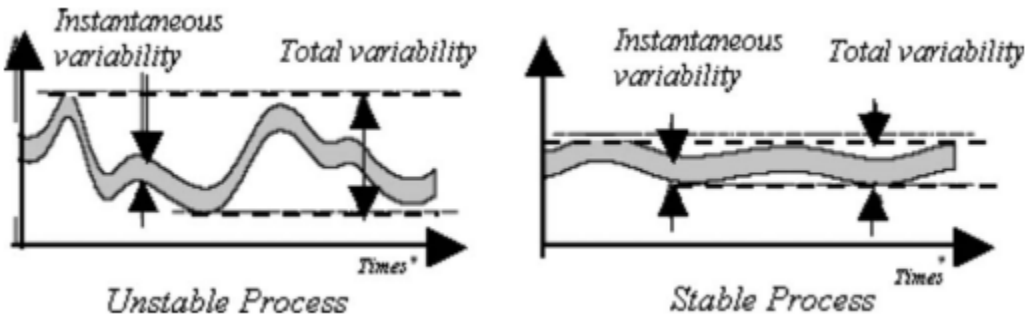

Figure I-24. Unstable and stable processes.

Buda et al [134] applied statistical process control on the tribocharging process of granular materials. *X*-bar and *R* control charts were employed to monitor the process and detect the occurrence of two disturbances, i.e. the variation of granule size and the slow-down of the feed rate. The conclusions regarding the effect of particle size was then employed by Zeghloul et al [135] in developing a tribo-aero-electrostatic process of plastic separation.

I.3. Conclusions

The application of polymer as industrial light-duty components is increasing. This justifies the increasing research efforts related to the study of frictional electrification of polymers. In many cases, the objective is to prevent static charge build up on the surface, and the use of anti-static agents can be the solution. However, the anti-static agent may not resist as the wear appears and surface eroded. In other cases, the aim is to harvest the charge generated by triboelectric effect. This implies the development of technical solutions to enhance this effect and generate more energy. Hence this study was focused on the tribocharging behavior of polymers and the optimization of the frictional charging process.

Tribocharging is a phenomenon influenced by several relatively easy-to-control factors: the contact force, the speed of friction, the number of frictional cycles, the surface temperature, the moisture as well as the ambient humidity and temperature. The nature of the materials in contact may affect the charge polarity and the friction behavior.

The tribology of polymeric materials is well consolidated field of research. However, the electrification during frictional contact has been the object of only a limited number of studies. One of the major difficulties of these studies is that the measurements of tribology phenomena such as the correlation between the friction coefficient and the surface static charge are affected by the fact that some of surface characteristics change during friction. The experimental benches to the development of which the author contributed are expected to facilitate the study of the trboelectric effects.

Design of experiments (DoE) methodology enables the modeling and optimization of complex physical processes. Therefore, it will be used to achieve the optimum design of tribocharging processes that make the object of this thesis. Furthermore, employing the technique of statistical processes control should pave the way to industrial applications of polymer tribocharging.

CHAPTER II
MATERIALS AND METHODS

Material selection is an important stage in industrial design. This is specifically true in the application of polymers, which are presently more and more broadly used, because of their advantageous functional, aesthetical and sustainability features. However the choice of polymers for the design of mechanical parts should take into account the phenomena of friction, wear and electrostatic charge with which they are associated, and which can be either useful or hazardous, depending on the field of application. The present study of the tribocharging properties of polymers has been carried out on slabs of Polyvinyl Chloride (PVC), Acrylonitrile Butadiene Styrene (ABS), Polyethylene (PE), Polypropylene (PP), and Polystyrene (PS). According to the available statistical data [136], the European industry demand by polymer type in the period during 2013 to 2015 was the highest for Polyethylene (29%), followed by Polypropylene (19%), Polyvinyl Chloride (10%), Polystyrene (7%) and Acrylonitrile Butadiene Styrene (less than 5%). The characteristics of the polymer materials that were the subject of the study are presented in sub-chapter II-1.

In order to demonstrate the feasibility of tribocharging and compare it with corona charging, two experimental benches were designed. These installations are described in sub-chapter II-2.

The various measurement techniques used to compare tribo- and corona-charging, as well as to evaluate the surface charge decay are described in sub-chapter II-3, together with the design of experiments method that enabled the modeling of physical processes.

II.1. Material characterization and sample preparation

Generally, the polymers are divided into two different classes based on their behavior in the presence of heat. The first class is thermoplastics, which can be heated and reformed frequently. The present study is focused on the tribocharging of these polymers. The other type of polymers are thermosets, which cannot be re-molded after the hardening process.

Thermoplastic materials demand in agriculture, in industry (electrical, electronic, automotive, etc.), in building and construction, in packaging, and in household goods manufacturing is mainly related with their specific properties: high resistance to impact, low thermal as well as electrical conductivity, good recyclability, and reforming capabilities, high chemical resistance, low weight, high strength, good aesthetical value, with hard crystalline or rubbery surface finish. Their sensibility to sunlight or fire exposures can be controlled by adding UV filters or flame retardants.

II.1.1. Thermoplastic materials

The present work focused on the tribological and electrostatic behavior of particularly thermoplastic materials [1]**.** The challenge was to advance the knowledge of the mechanisms involved in the generation of electrostatic charges in dry frictional contacts.

Polyethylene (PE) before-mentioned as the most widely-used thermoplastic material, can be found in food or oil containers, cable insulation, artificial joints and toys, not only because it is cheap, inert and easy to mold, but also because of its high resistance to most water-based solutions, including salt water, because of its good electrical insulating characteristics and because of its low dielectric losses. Moreover, PE is non-toxic so that can be implanted in the human body (artificial artery, heart valves, and hip-joint cups). Generally, there are two types of polyethylene on the market, high-density polyethylene (HDPE), having the recycling code “2”, a stiffer and stronger type used for pipes and containers, and low-density polyethylene (LDPE), which is less dense than water and has the recycling code “4”. Other types of polyethylene are linear low-density polyethylene (LLDPE), very low-density polyethylene (VLDPE), and “Super PE”, which is resistant to petrol, corrosive substances and cosmetics.

Polypropylene (PP), almost similar to PE in production quantity and form, is stable for most aqueous solutions including salt water, but without fire retardants and stabilizers it is flammable and degrades in sunlight. This polymer is low-cost, ductile and light but has low mechanical strength. It is more rigid than PE, can be used in higher temperature than HDPE, having a melting point about 165-170°C, and it is remarkable for its stiffness, transparency, and range of acceptable colors. PP with recycle mark code "5" is particularly inert, easy to recycle ; it can be incinerated to recover energy.

Polyvinyl Chloride (PVC) is one of the cheapest and most versatile polymers, tic in regular operating condition. In its genuine form, PVC is brittle, rigid, and heavy, but after applying plasticizers it becomes elastic and soft as rubber. In contrast, by reinforcement using glass fibers, this material becomes strong, stiff and tough so that can be used for flooring, roofs, and building panels. PVC has excellent resistance to acids or bases as well as good barrier properties to atmospheric gases, in spite of its poor resistance to some solvents. Special high-temperature incineration is required for safe recycling of this material (recycling code "3") since thermal degradation releases HCl, chlorine, and another toxic compounds.

Polystyrene (PS), having the recycling code "6" is brittle and cracks easily but is optically clear, easily-molded and the cheapest of all polymer foams. Polybutadiene was used to enhance its mechanical properties, with the consequent loss of optical transparency. PS is suitable for use as food containers or packaging each time when optical attractiveness is important as well as the low-cost. Furthermore, its strength at low temperature makes it suitable to use in interiors of freezers and refrigerators.

Acrylonitrile-butadiene-styrene (ABS) is resilient, tough, easily molded, and typically opaque. Therefore, it is used for the casing of computers, telephones, automotive parts, medical instruments, toys, and several household electronic appliances since it has in-self-extinguishing features. ABS is hygroscopic and does not resist to petroleum, but is easily recyclable (code "7" classified as "other polymers").

II.1.2. Characterization method

Electrical resistivity influences the decay of electric charges while thermal conductivity influences the state of heating and the evolution of the thermal field generated by dry friction and

this could lead the variation of surface moisture. According to Cartwright et al. [137] and Mukherjee et al. [138] the magnitude of the charge generated through friction is strongly related to the surface moisture and the relative humidity of the ambient air. This phenomena was recently studied by Biegaj et al. [139] who show that the surface chemistry and humidity not only affect the charge but also the surface potential decay ; high humidity facilitates faster charge decay.

Chemical investigation was made with a Fourier Transform Infrared (FTIR) (**Figure II-1**) spectrophotometer that uses IRAffinity-1 optical system. It relies on a Michelson interferometer to analyze the origin state and possible changes in the polymer composition due to friction or electrification. The infrared spectra of the polymers under study are given in **Figure II-2**.

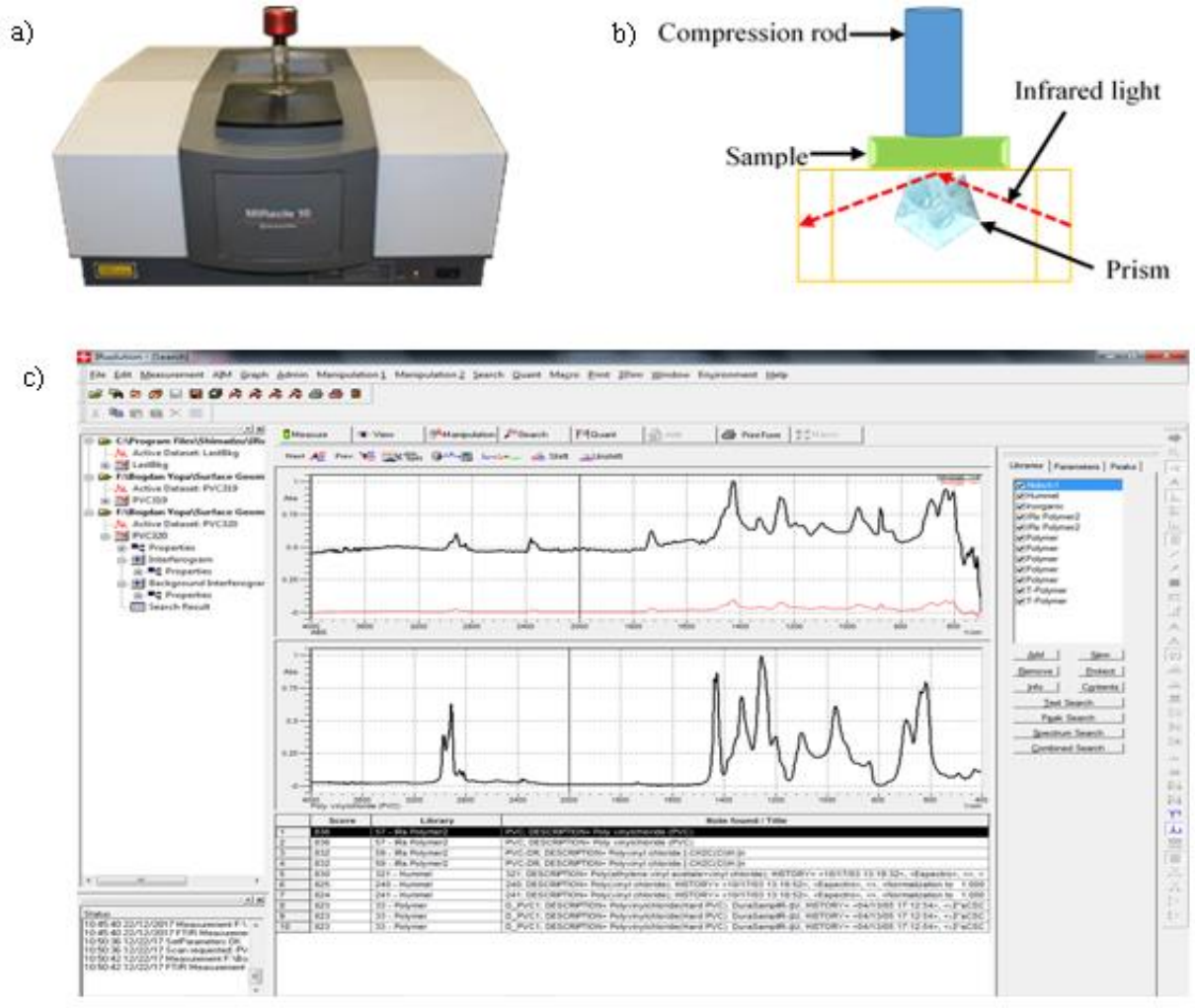

Figure II-1. a) FTIR spectrophotometer MIRacle 10 single reflection ATR and b) schematic diagram of the optical system, and c) analysis of contaminant by combining with the spectrum library of substances

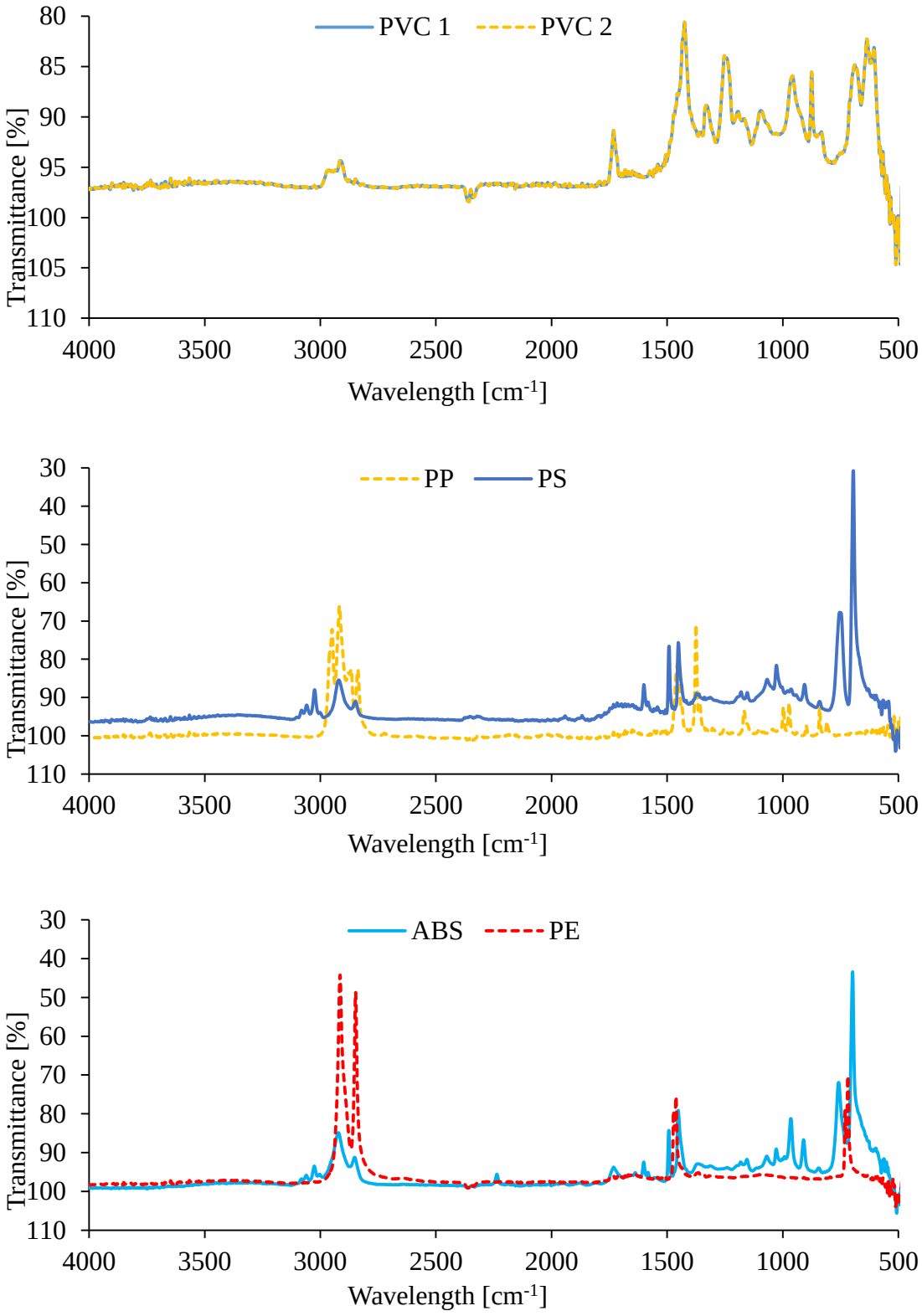

Figure II-2. Spectrometric result of materials used in present study

Failure in machine components originate from fracture or excessive deformation, hence material in this study should be tested to determine the acceptable "stress" (i.e., load per unit area). A basic mechanical test has been done using tensile testing machine Zwick/Roell Z010 (**Figure II-3**) to find out modulus of elasticity, yield strength, ultimate tensile strength, and strain (the ratio of the change in length).

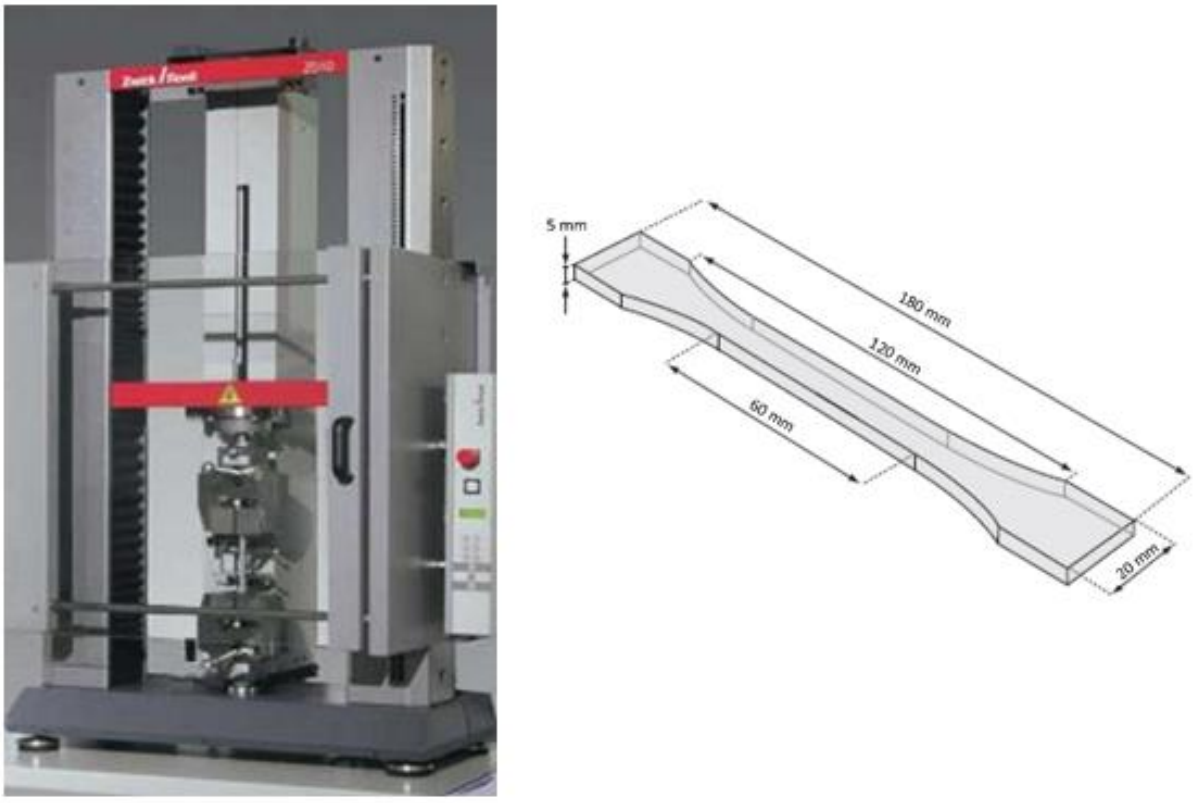

Figure II-3. A universal testing machine for tensile test and the specimen model

Micro-hardness test was conducted using Shimadzu HMV-G21 (**Figure II-4**) with Vickers indenter so that can lead to determine the resistance of scratching, abrasion, bending or cutting of the materials. In the present study the goal of this test is to evaluate a variety of polymers specimen ranging in quality from soft to hard. This compact design of Micro Vickers hardness tester has built-in CCD camera (1), USB to PC communication port (2), automatic high speed reading (3), facility to read scratched surface (4), a stable frame that is devoid of angles (5), test condition assist function (6), multi turret (7), ultra long life illumination (8), low test force ability (9), electromagnetic test control (10), fracture toughness measurement (11), measurement mode settings (12), routine inspection graphs (13), and automatic lens switching (14).

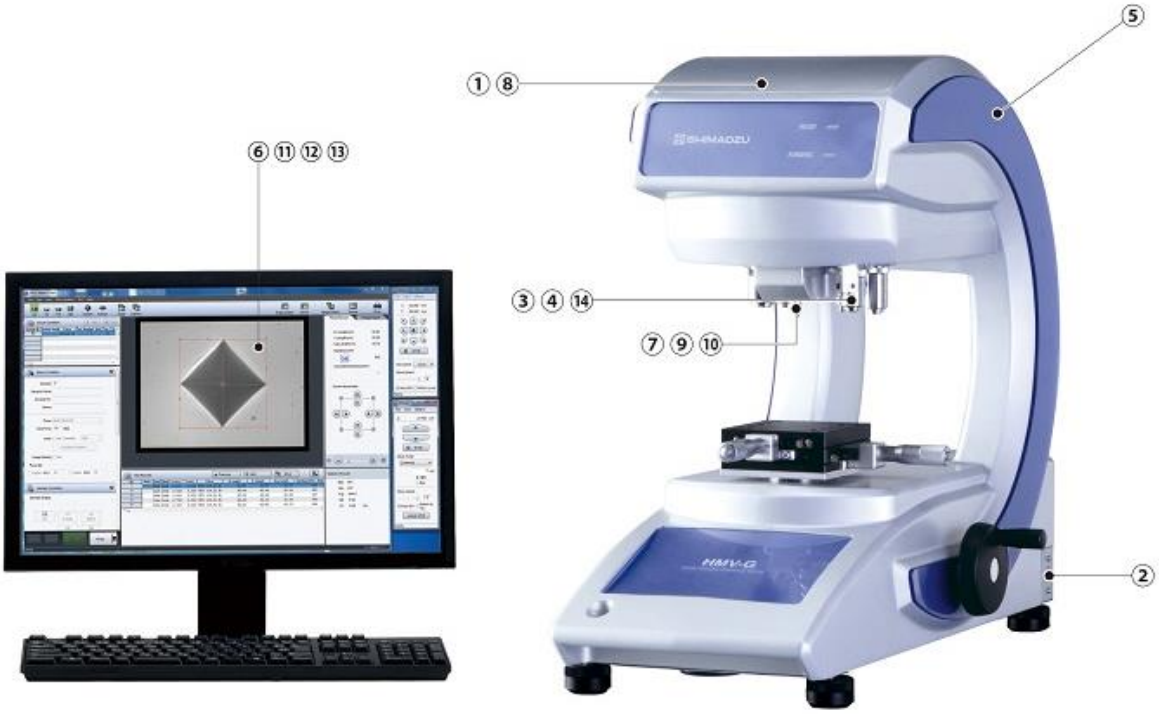

Figure II-4. Micro-hardness testing machine and the associated software.

High-quality digital imaging of sample surface depends on the accuracy of microscope optical performance. Therefore full high-definition microscope Makrolite II was employed to investigate sample surface condition. Microscopic analysis is an appropriate preliminary stage before roughness testing, since anisotropy of polymer surface may affect friction behavior as well as the generation of electrostatic charge. Correlation between surface condition (roughness and texture) on friction behavior has been studied by several researchers[140–144]. **Figures II-5b** and **II-5c** show the texture due to manufacturing on the surface of hard PVC and ABS respectively, while the other materials have smooth and shiny surface or no texture. The different alignment of surface texture used when rubbing the pair of two slabs of polymer are illustrated in **Figures II-5d** to **II-5f**. Sample A is stationary with a fixed position while sample B slides along the surface of sample A with a back and forth movement. The orientation of the texture lines are referenced to the sliding direction where the texture lines are either parallel with or perpendicular on the sliding direction. The three possible combination are shown in **Figures II-5d** to **II-5f**.

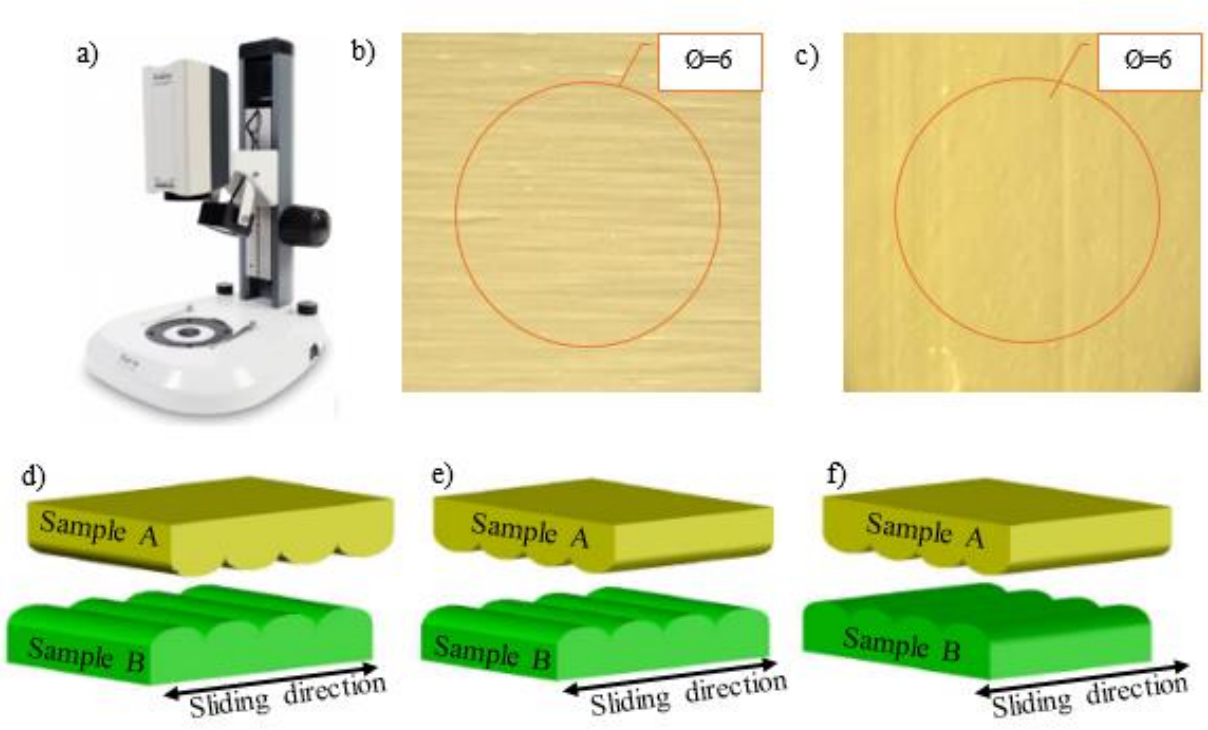

Figure II-5. Surface texture investigation using a) Makrolite II microscope on b) PVC sample and c) ABS sample. Surface texture position in sliding contact of d) both orthogonal, e) orthogonal-parallel and f) both parallel, refers to sliding direction.

A high precision 3D profile, non-contact analysis tool Talysurf CCI 6000 and a portable contact roughness meter Mitutoyo, model SJ-210 (**Figure II-6**), were operated to determine the metrology of the specimens. As mentioned before, specifically for PVC and ABS, the roughness test should be conducted in two directions, taking into account the textures due to manufacturing. Interestingly, this origin texture is appropriate to use as a variable in the comparative study of different roughness. Indeed, since there is no treatment needed to modify the roughness, the surface physicochemical characteristics remain unchanged. The standard used for the measurement of roughness was ISO 1997. The evaluation conditions were made for a profile of type R, with Gaussian filtering type. The number of samples was N = 5, the low-pass filter had a wavelength Ls = 2.5 μm, and the high-pass filter had a length Lc = 0.8 mm.

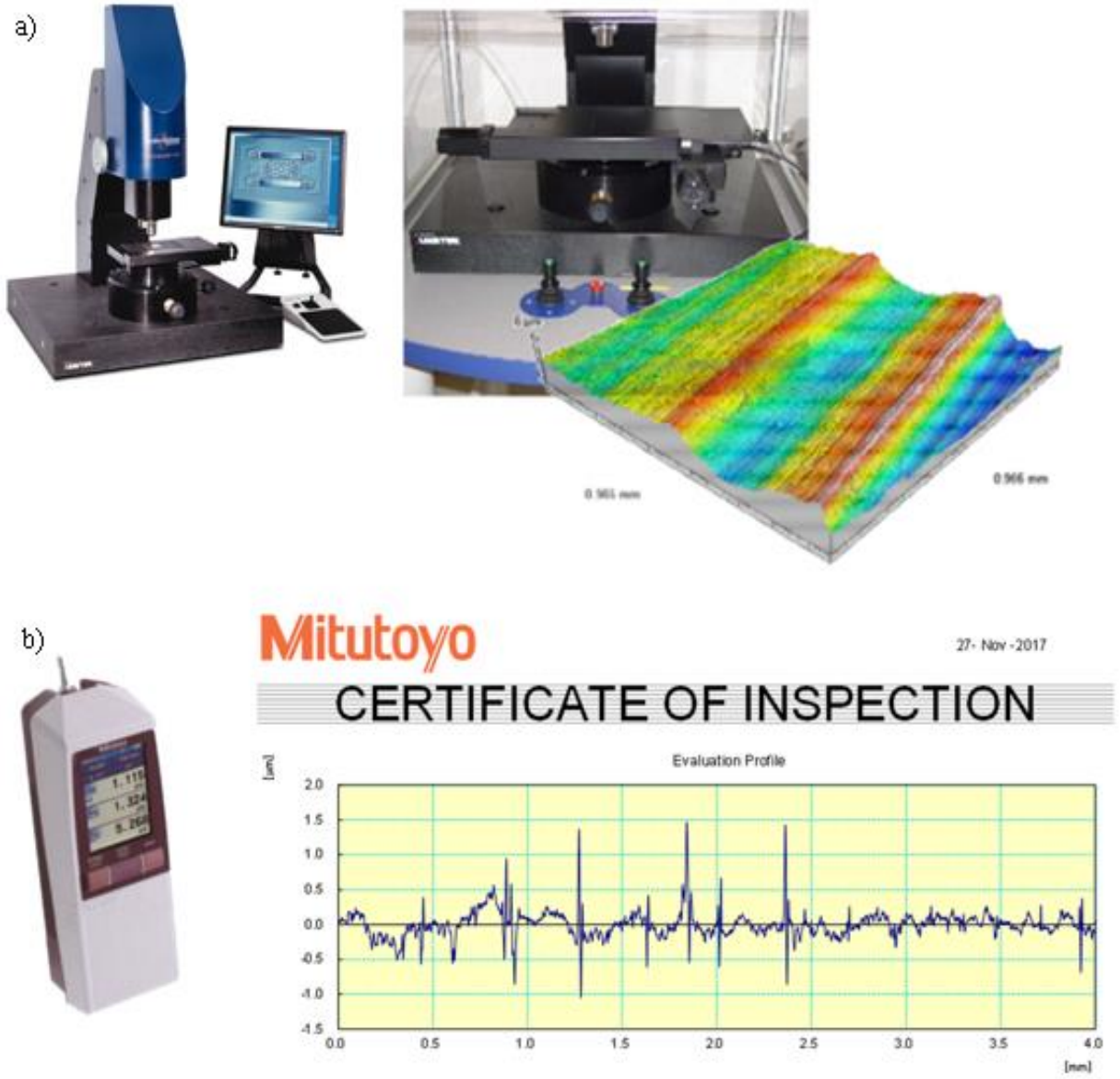

Figure II-6. Surface metrology instruments: a) interferometer Talysurf CCI 6000; b) surface roughness tester SJ-210

Based on the series of material tests described above and the literature review [1,145], **Table II-1** summarizes the main mechanical, electrical, and thermal properties of material under this study. Thus, the interpretation of the experiments of tribocharging should take into consideration these data.

Table II-1. Properties of materials used in this study

Materials	PVC	PS	PE	PP	ABS
Young's Modulus (GPa)	2.14 – 4.14	1.2 – 2.6	0.62 – 0.86	0.9 – 1.55	1.1 – 2.9
Yield strength (MPa)	35.4 – 52.1	28.7 – 56.2	18 – 29	21 – 37	18.5 – 51
Tensile strength (MPa)	40.7 – 65.1	35.9 – 56.5	21 – 45	28 – 41	27.6 – 55.2
Hardness-Vickers (HV)	10.6 – 15.6	8.6 – 16.9	5.4 – 8.7	6.2 – 11	5.6 – 15.3
Electrical resistivity (μohm.cm)	1×10^{20} – 1×10^{22}	1×10^{25} – 1×10^{27}	3.3×10^{22} – 3×10^{24}	3.3×10^{22} – 3×10^{23}	3.3×10^{21} – 3×10^{22}
Relative permittivity	3,1 -4,4	3,0 - 3,2	2,2 -2,4	2,1-2,3	2,8 – 3,2
Thermal conductivity (W/m.°C)	0,147-0,293	0,121-0,131	0,403- 0,435	0,113-0,167	0,188
Max. service temperature (°C)	60 – 70	77 – 103	90 – 110	100 – 115	62 – 77
Melting point (°C)	100 – 260	~240	125 – 132	130 – 171	-
Glass transition (°C)	80	95	-125	0	105
Initial Roughness (Ra) (μm)	0.13 ± 0.02 0.82 ± 0.1	0.08 ± 0.01	0.16 ± 0.03	0.02 ± 0.004	0.18 ± 0.02 0.3 ± 0.1
Arithmetic mean height (Sa) (nm)	1.79 ± 0.06 3.51 ± 0.02	0.58 ± 0.05	0.11 ± 0.02	0.79 ± 0.1	0.6 ± 0.02 1.6 ± 0.3

II.1.3. Samples preparation

The polymers used, delivered in plates of 1 m × 2 m, were cut by water jet into test pieces in 5 different forms (**Figure II-7**) which a) to c) used as top sample, while d) and e) employed as bottom sample. The thickness of each specimen is 5 mm except for the ABS which has a thickness about 6 mm. These dimensions were imposed by the aim of the study, as the frictional charge depend on surface geometry.

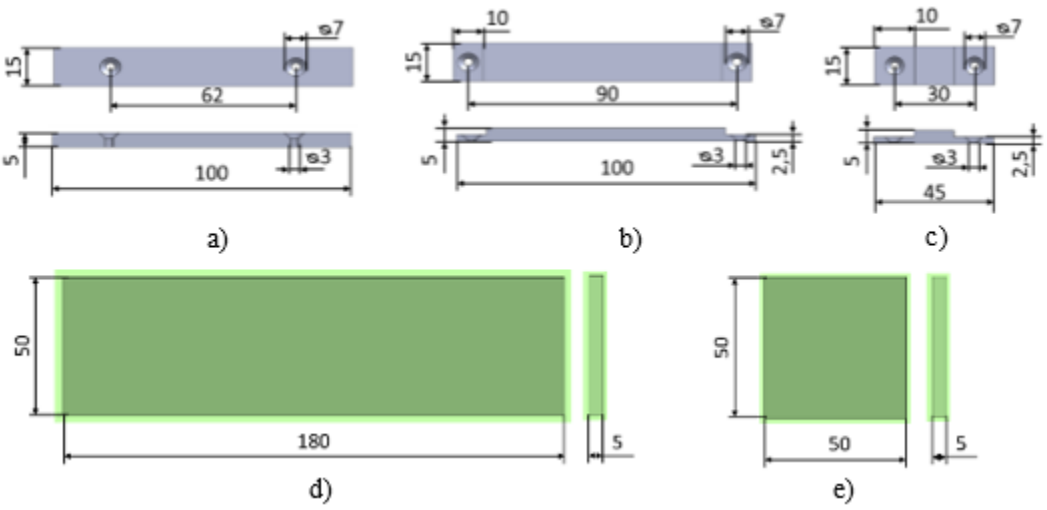

Figure II-7. Dimensions and geometries of the samples

The sample orientation due to the different geometrical configuration is important to study, since the distribution of electric charge depends on the real contact area (RCA). **Figure II-8** illustrates the friction track which can change according with the configuration. A wider contact surface b) and d) will result in a high and evenly distributed electrostatic charge, however, in order to achieve this results frictional contact between surfaces shall be uniform as well. However, using a smaller size of the top sample makes it easier to adjust the contact area. The different surface of contact geometry can vary the contact pressure and influence the electric charge generation.

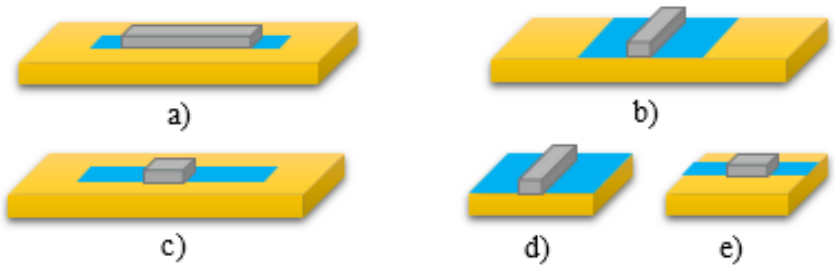

Figure II-8. Orientations of surface in contact

The residual charge at the surface of these samples is neutralized using a commercial ionizing system (electrode ECA 88 BS and high-voltage supply SC 04 B, 5 kV, 7 mA, manufacturer: ELCOWA, Mulhouse, France). Treatment were carried out before the experiments; the samples were placed at 5 cm below the neutralizing electrode and exposed for 3 seconds to the bi-polar electric charge generated by the ionizing system, as shown in **Figure II-9**. Corona ionizers generate ions by applying a high voltage to the very sharp tip of the electrodes.

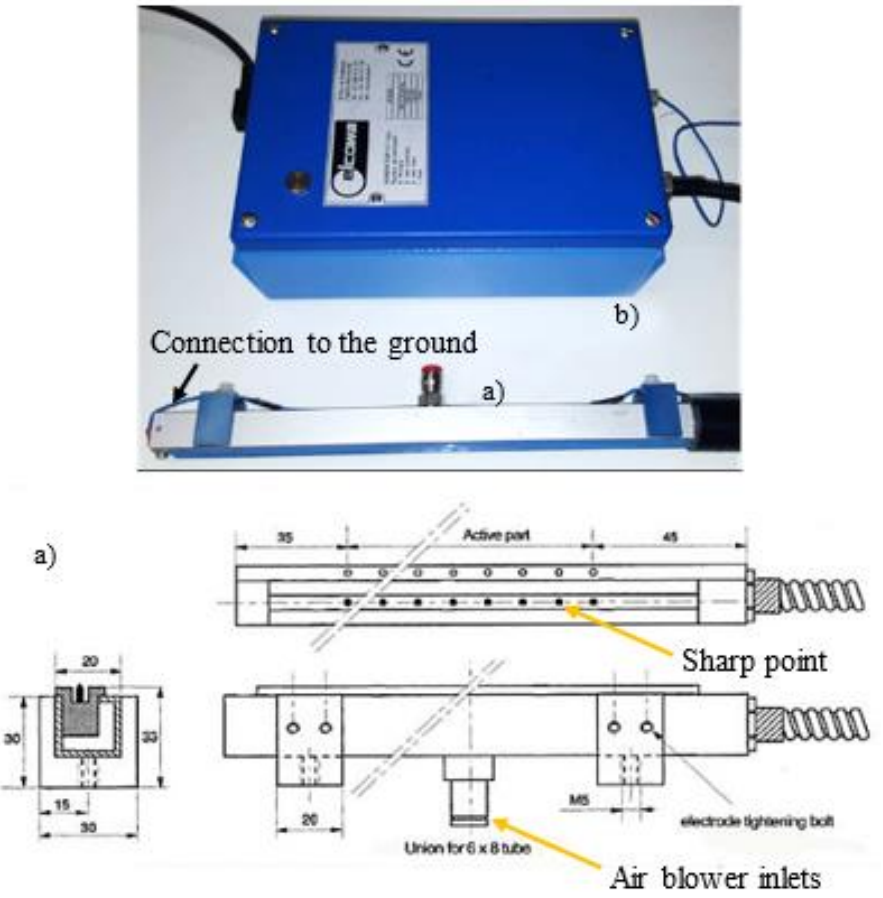

Figure II-9. Ionizer system: a) Electrode bar and b) High-voltage supply.

II.2. Tribocharging and corona discharge experimental benches

The first bench is a modified linear tribometer designed for the study of dry-sliding contacts between solids. The second is a triode-type corona electrode system, the design of which enables the comparison between two particle charging mechanisms: “ion bombardment” and “triboelectric effect”. These benches are located in a special room, to minimize the impact of the environment on the tribo- and corona-charging processes. The third bench makes possible the measuring of the distribution of the electric charge at the surface of the polymer slabs either tribocharged by dry-sliding contact with other bodies or exposed to corona discharge generated by the triode-type electrode system.

II.2.1. Tribocharging device

Tribometer are commonly used to study friction and wear processes. The purpose of this section is to describe a modified linear tribometer that enables the accurate evaluation of the tribocharging effect of sliding dry contact between polymer slabs by monitoring the rubbing conditions (normal contact force and relative displacement between samples) and the electrostatic charge generated. The study involves rectangular or square polymers slabs in flat-on-flat contact in a linear reciprocating motion (back and forth) [146].

The experimental bench was designed to meet the following features: automation of sliding motion to set the specific cycle and speed; adjustable load system; rigid sample holder to assure the stability of rubbing process; precise measuring equipment of the normal load and of the tangential force, for real time recording of the data during experiments [147,148].

The custom-designed tribocharging device is shown in the **Figure II-10**. The upper specimen (A) is fixed on a support (4) which allows, via a spherical joint, the adjustment of the flatness of the contact between the test slabs. Two perpendicular linear bearing provide vertical movement for normal contact loading. The lower support (5), which carries the specimen (B), is driven in a back-and-forth sliding motion in the horizontal direction thus ensuring the tangential loading of the contact. A lever system (7) is provided for finely adjusting the intensity of the normal contact force measured by an "S" shaped resistive gauge force sensor. The displacement of the lower support in the horizontal direction is ensured by a carriage block bearing on a rail system (6). The movement of the carriage (6) and thus of the test piece (B) is measured by a displacement sensor (9). The reciprocating motion is provided by a linear motor (1) transmitted to the rod which able to reach the speed of 150 mm/s. The amplitude of the sliding can vary by changing the position between limit switch (14). This system with linear motor was designed to replace the previous system, which consisted of a rotational motor with crankshaft system (15) with maximum speed 250 mm/s. Comparing with rotational motor system, the linear motor perform better accuracy and is easier to control. The force sensor (8) identical to the sensor (7) is inserted into the kinematic chain of tangential motion. Thus, it continuously measures the tangential force of contact between the two test pieces.

Signal conditioners (9 and 10) for the displacement and force sensor, respectively provide power to the sensors and provide the analog signals of the measurements to the acquisition card (12). The measurement is operated by a LabView software (13) in command of the acquisition and visualization of sensor measurements.

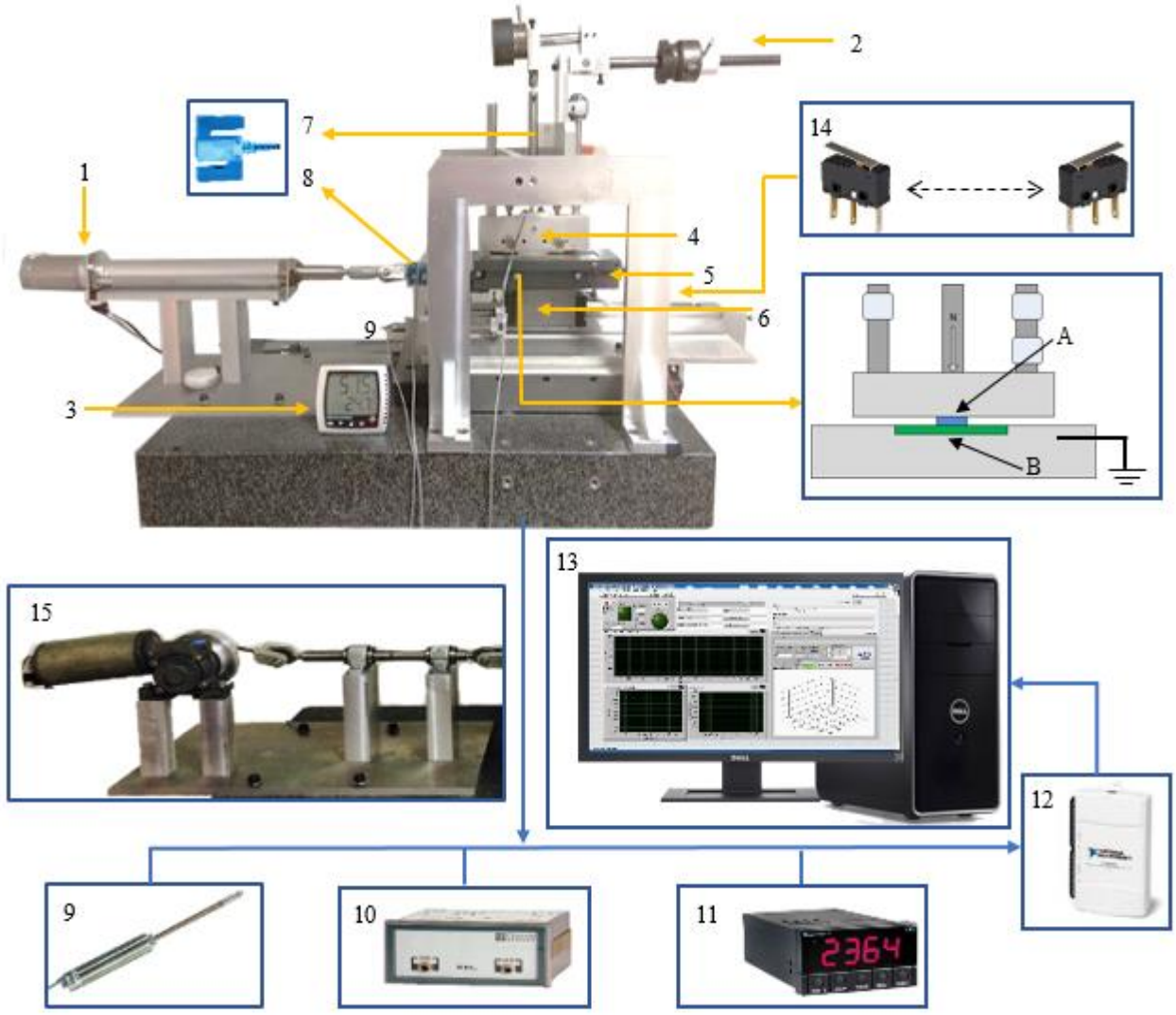

Figure II-10. Tribometer flat-on-flat experimental bench: A- Upper specimen only can move in vertical direction; B- Bottom specimen subjected to a reciprocating translation; 1- Linear motor; 2- Normal force control system; 3- Thermometer and hygrometer; 4- Upper specimen support; 5- Bottom specimen support; 6- Linear bearing supported guidance; 7- Normal force sensor; 8- Tangential force sensor; 9- Linear displacement sensor; 10- Displacement sensor conditioner; 11- Force sensor conditioner; 12- Data acquisition card; 13- Labview acquisition interface; 14- Limit switch; 15- Rotary motor

II.2.2. Real time control system and condition monitoring

A data acquisition system was designed to simplify the control of the different factors that affect the tribocharging process: sliding speed, normal force, and number of sliding cycles, as well as the monitoring of several responses: normal force variation, tangential force variation, and linear displacement. The LabView implemented integrated user interface (figure II-11) enables the operator to impose the sliding speed, the number of rubbing cycles (a) and the information about variables used in the experiment (b) namely motor speed, stroke, normal force, ambient relative humidity, air temperature and nature of sample pairs. During the tribocharging process, LabVIEW will record and graphically show the variation of tangential force (c), normal force (d), and linear displacement (e).

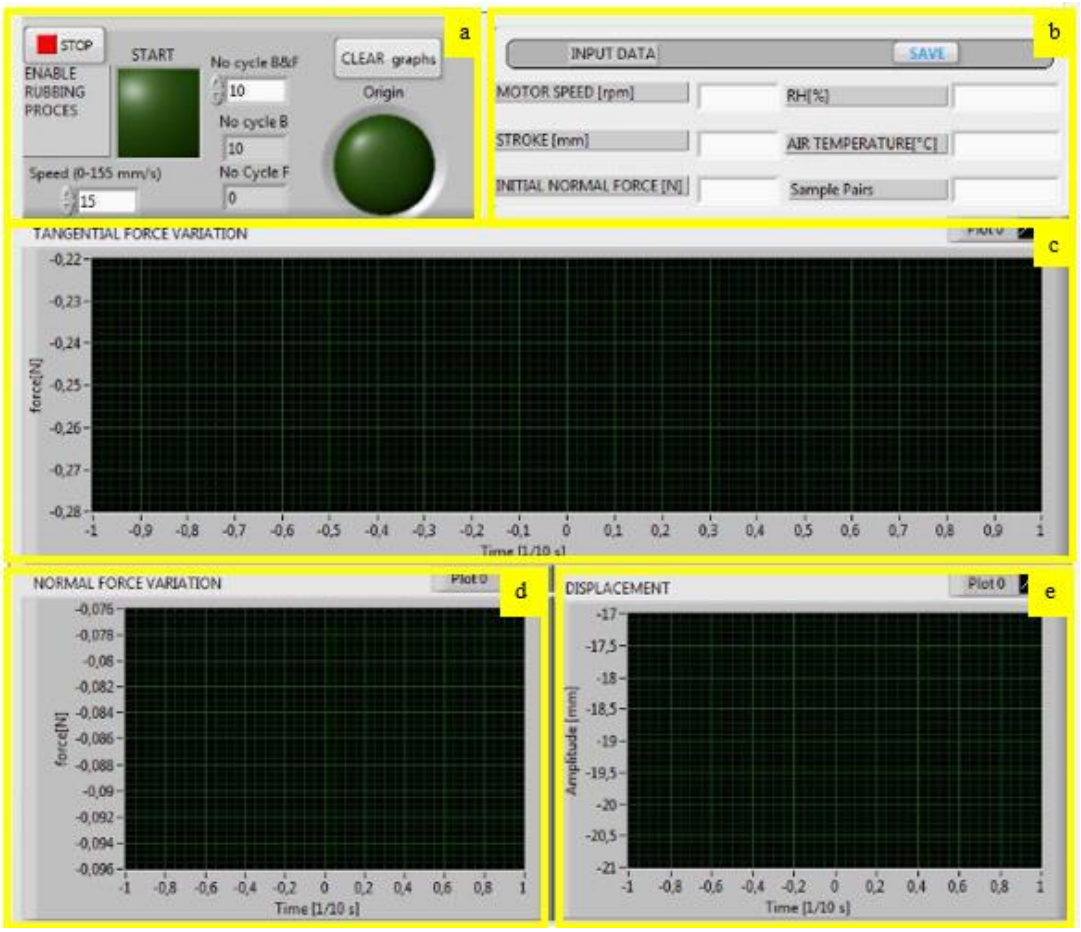

Figure II-11. Real time control system and condition monitoring: a) Speed and cycle input panel; b) Information variable in used; c) Variation of tangential force; d) Variation of normal force; and e) Linear displacement with amplitude.

Calibrating of measurement device has been done regularly to ensure the quality of results. The normal force is measured over a range of 0 N to 20 N and that of the tangential force up to ± 15 N. The force sensors operate with resistive gauges (JPRM model STC 1205) with a nominal range of ± 50 N and a resolution of 0.025 N, They are powered by the conditioner (NEWPORT model INFCS) which also converts the output signal in the range of -10 V to +10 V, to make it compatible with the NI USB 6210 acquisition board. The displacement measurement is performed with the TNC model L50R LVDT sensor (Linearly Variable Displacement Transducer). The sensor allows measurement with a resolution of 0.05 mm in a range of 56 mm. The TNC model GDL conditioner supplies and converts the displacement sensor signal. Analog signals from the sensors are connected to a NI USB-6210 multifunction data acquisition board. It has 16 analog inputs (± 10 V, 16 bits, 250 kS / s), 4 digital inputs, 4 digital outputs at 5V each and two 32-bit counters.

The control of the electric motor driving the crankshaft system or the linear motor is ensured by an H-bridge electronic circuit (LMD18200T) which supplies a voltage of 12 V to 55 V with a maximum current of 6 A. The control is performed with an Arduino UNO board and LabView.

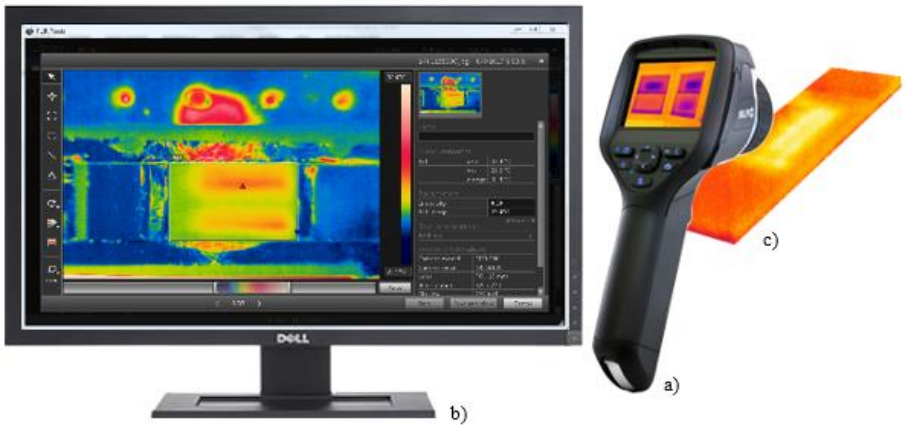

Figure II-12. Thermal imaging: a) Thermal camera Flir E60, b) User interface, and c) Sample investigated

Wear tracks or hot spot investigation was carried out using thermal imaging camera Flir E60 (**Figure II-12**, so that contact failure or suspected charged area can be detected as soon as possible using online monitoring. The temperature range is -20°C to 650°C, the thermal

sensitivity of less than 0.05 °C at 30 °C. Thermal camera calibration is done by heating the material in an oven to a certain temperature to ensure the camera reads correctly.

II.2.3. Corona discharge

The corona charging is made with a wire-type dual electrode (Tungsten wire with diameter 0.2 mm supported by a metallic cylinder diameter 26 mm) used in a triode configuration (**Figure II-13**), energized from an adjustable HV supply of negative or positive polarity (-30 kV, 0.3 mA, model T1CP 300 304 n/p, ISEG). The type B sample is placed on the grounded plate (3). The distance between tungsten wire (1) and sample is 30 mm and grid (2) placed between them. Grid voltage can be set with connection to arrangement of resistor (*Rg*) which connected to ammeter for measurement of current (*Ig*) of the grid. A grounded shield limits the zone affected by the corona discharge, so that its extension at the surface of the polymer sample to be similar to that obtained by tribocharging. The initial potential at the surface of the placed sample is equal to the potential of the grid calculated by:

$$V_g = R_g I_g \qquad \text{(II-1)}$$

In this electrode system, called "triode", the charges resulting from the ionization of the air are accelerated under the action of the electric field, pass through the grid and are deposited on the free surface of the dielectric. The surface potential of the dielectric increases to the level of the potential of the grid. From this moment, the field between the grid and the surface of the dielectric is zero. The ions do not cross the grid anymore. Thus the surface potential is limited by the potential of the grid.

The purpose of this study is to evaluate the distribution of electrical potential and its decay at the surface of polymers which were previously charged by corona or by tribocharging. Therefore it is important to charge the samples at levels comparable with those obtained by tribocharging. Thus, the results of previous tribocharging experiments were used as reference to set the parameters of the corona discharge, including the dimension of the grounded shield which is correlated to the stroke of sliding movement. In the other hand, corona charging process in a short time enables to generate high potential while surface properties of polymer remain un- changed, contrary to the tribocharging process, where the surfaces state changes as soon as the friction begins. Thus, such

phenomenon like the relationship between friction coefficient and surface potential charge will be easier to study with the initial charge obtained by corona discharge.

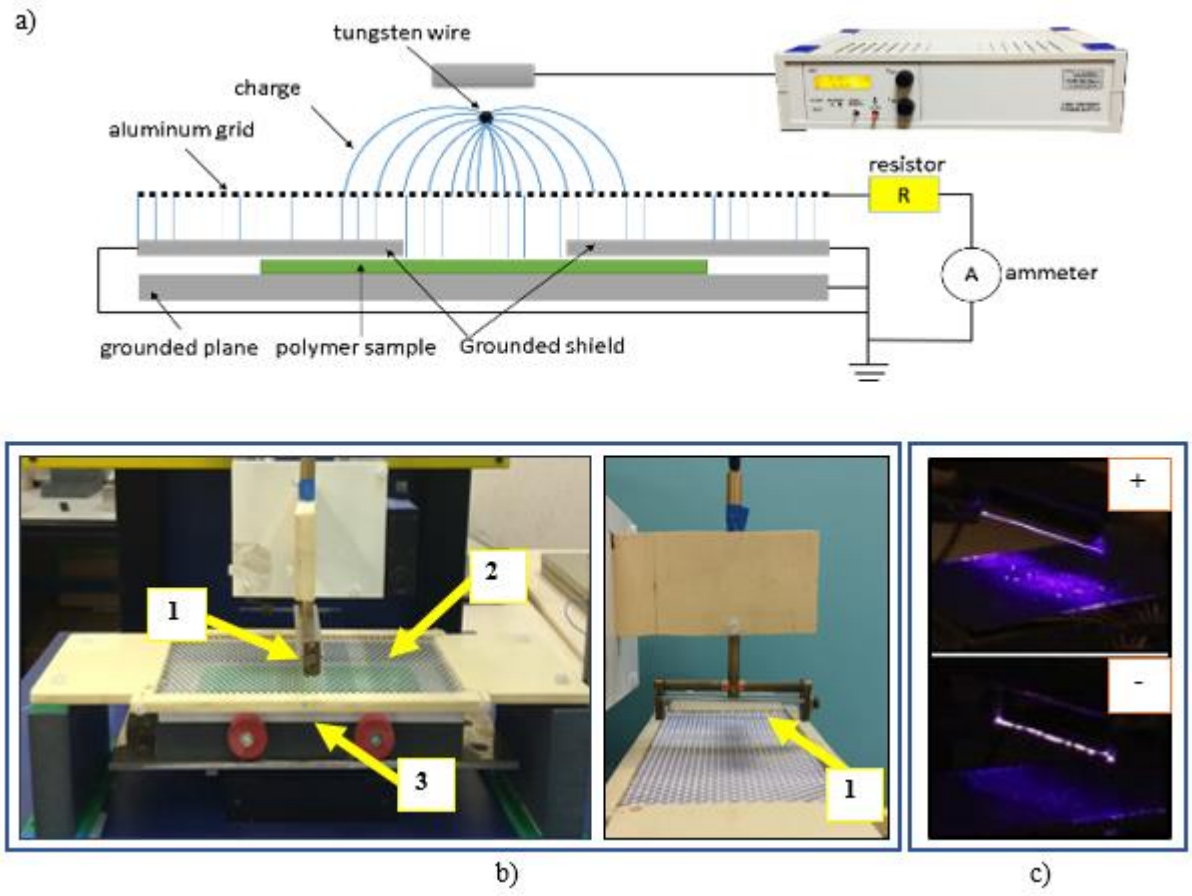

Figure II-13. Triode system of corona discharge: a) Graphical illustration, b) Photograph of the instrument, and c) aspect of corona discharge for both polarities

II.2.4. Surface charge measurement

The measurement of the electrical surface potential is a method to indirectly evaluate the distribution of the electric charge [149,150]. The experimental bench for this kind of measurement (**Figure II-14**) is composed of the lower support (1) on which the test sample (B) is placed, to be in contact with a metal plate connected to the ground and with respect to which the electric potential is measured. This support is the same as that of the linear tribometer; it is mobile and thus allows the displacement of the specimen (B) between the two installations, the one that performs the electrostatic charging by friction and another one that measures the

electrical surface potential. Having the same support gives the possibility to identify the measurement position of the electrical surface potential with respect to the contact areas. The support (1) is placed on the fixing module (2), integrated with the mobile table (3), which has a translation movement on the Y axis. The electrostatic probe (4) surrounded by an insulating support (5) is fixed on the movable arm (6), which has translational movements along the *x* and *z* axes. The movable table and the arm are part of a 3-axis positioning system controlled by the computer (7). The TREK self-compensating electrostatic induction probe, model P0865, is connected to an electrostatic voltmeter (TREK, Model 341B) that performs signal conversion. The probe - voltmeter assembly can measure a potential in the range 0 to ± 10 kV, with an accuracy greater than ± 0.1%. The response speed is faster than 0.2 ms / 1 kV. The distance between the probe and the test sample is kept at 3 mm according to the manufacturer's specifications and recommendations.

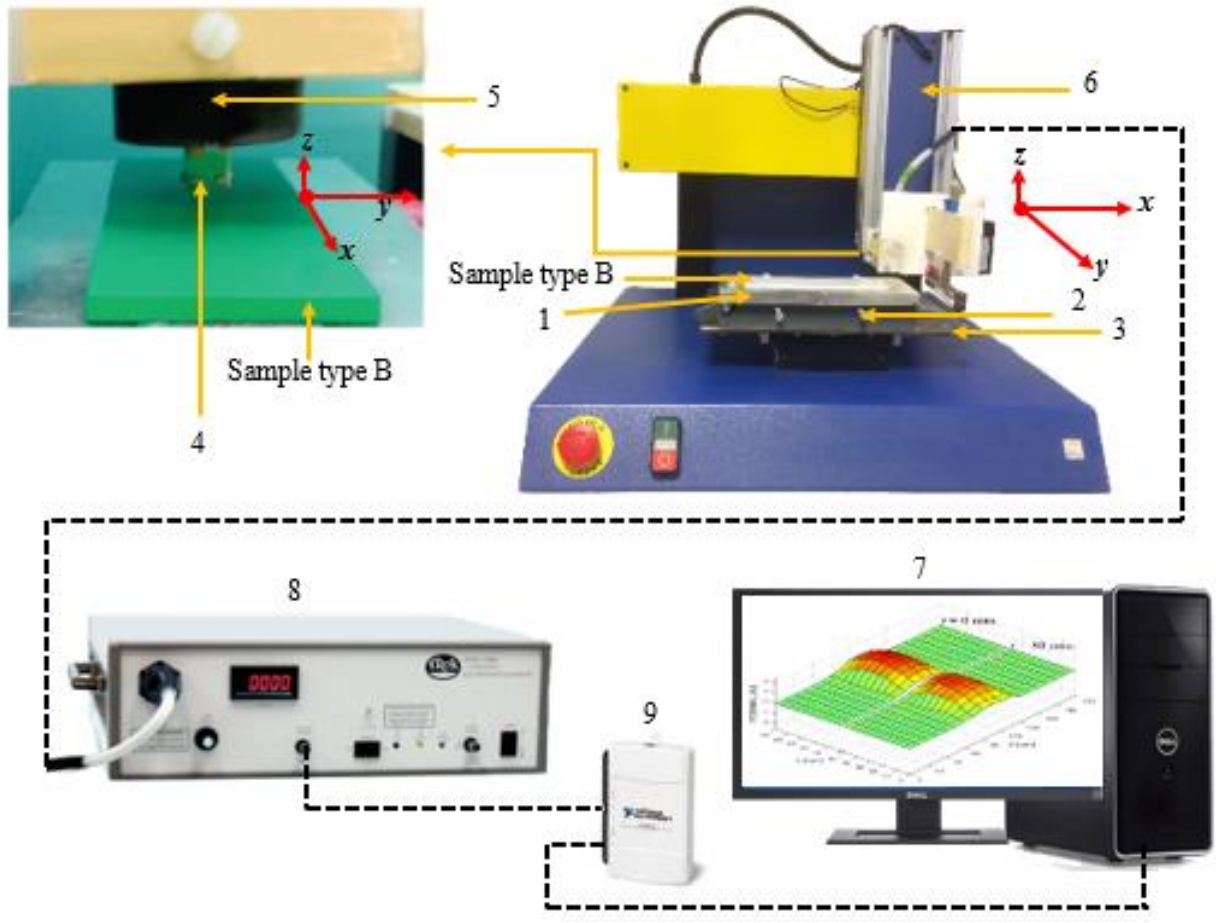

Figure II-14. Instrument for measurement of surface electric potential:

1- Bottom sample (B) support; 2- Fixing module for the bottom sample support; 3- Mobile table on *y* axis; 4- Electrostatic probe; 5- Insulating tube for probe support; 6- Arm moving on *x* and *z* axes; 7- Computer user interface; 8- Electrostatic voltmeter; 9- NI USB 6210 acquisition card.

The analog signal at the output of the electrostatic voltmeter (8) represents the electrical potential measured by the electrostatic probe, decreased 1000 times and sent to a NI USB 6210 acquisition board (9). The acquisition of data is done using a computer with a Labview software.

Mapping of the electrical potential can be done using two methods. The first is a "point by point" method: the probe is placed at a precise position and takes a measurement after 0.5 s. This time allows the probe to stabilize to achieve a precise measurement. In the second method, called "scanning", the probe takes a multitude of measurements, with a fixed sampling frequency (F_e), moving at a constant speed (v_d). The position of the measurement depends on the sampling frequency and the speed of movement. The step (p) between two measurements is:

$$p = \frac{v_d}{F_e} \qquad \text{(II-2)}$$

The area of measurement with this method is adapted to the scope of the experiment: evaluating surface charge uniformity or its decay rate. Figure II-15 describe the latter situation, where the measurement of potential decay should be fast and precise and therefore a small area of measurement has been decided (a). However in a situation where the charge is not in that area the measurement will be invalid (c), so that cartography on the whole of tribocharged area is needed before proceeding to the study of a specific region (b).

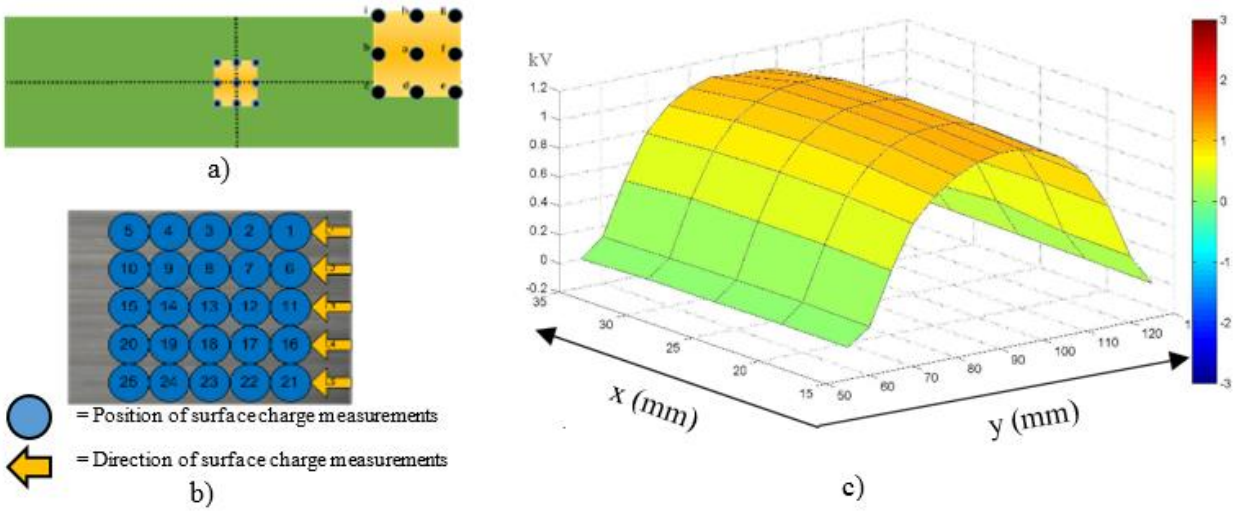

Figure II-15. Surface electric potential mapping on a) nine points and b) twenty-five points with the result c).

II.3. Design of experiments and statistical method

"Statistical process-control methods and experimental design, two very powerful tools for the improvement and optimization of processes, are closely interrelated" [121]. Design of experiment is an active method where series of tests are needed, while statistical process control is a passive method of observation of process response.

II-3.1. Design of experiments

Design of experiment is employed to obtain the maximum of information in the operation of a process with the minimum tests conducted. This method prescribes the number of experiments to be performed in order to achieve a well-defined objective and predicts the behavior of the systems in the field of use according to several factors that may vary simultaneously. Moreover, it allows to evaluate the effects of these factors and their interactions. Figure II-16 illustrate the schematic of typical process:

- Input variables u_i, with $i = 1,\ldots,m$.
- Output variables (also called responses) y_i ,with $i = 1,\ldots..,n$.

Figure II-16. General model of a system or process

In a mathematical form, a response is a function of several input variables (or factors) u_i expressed as:

$$y = c_0 + \sum c_i u_i + \sum c_{ij} u_i u_j + \sum c_{ij} u_i^2 \qquad \text{(II-3)}$$

For each factor u_i a reduced centered variable is defined as:

$$x_i = \frac{(u_i - u_{i0})}{\Delta u_i} \quad \text{(II-4)}$$

$$u_{i0} = \frac{(u_{i\,max} + u_{i\,min})}{2}\,;\, \Delta u_i = \frac{(u_{i\,max} - u_{i\,min})}{2} \quad \text{(II-5)}$$

With these notations, the response function becomes:

$$y = f(x_1) = a_0 + \sum a_{i,j} x_i x_j + \sum a_{i,j} x_i^2 \quad \text{(II-6)}$$

where x_i is -1 for the lower level of the factor ($u_{i\,min}$) and +1 for higher level ($u_{i\,max}$). The construction of centered composite design consists of adding "star points" to a complete factorial design. These points are positioned at a distance ± a from the center of the domain along the axes of the factors.

These points constitute a system in which only one factor is varied at a time. So there are *2k* star points, where *k* is the number of variables in the experiment design. Figure II-17 shows the design matrix of response surface modeling for central composite design (CCD) for which the response function of *y* can be expressed as follows:

$$y = f(x_i) = a_0 + \sum a_i x_i + \sum a_{i,j} x_i x_j + \sum a_{i,j,l} x_i x_j x_l + \cdots + a_{i,j\ldots k} x_i x_j \ldots x_k + \sum a_{i,i} x_i^2 \quad \text{(II-7)}$$

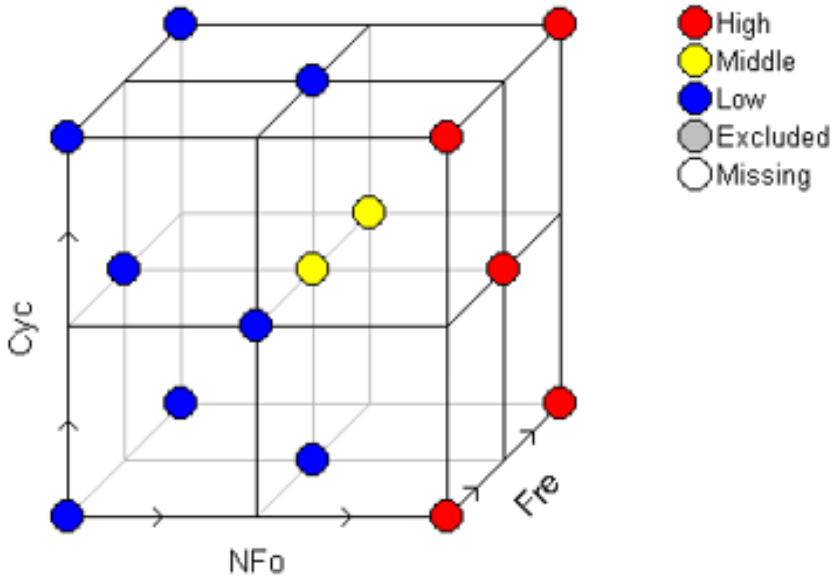

Figure II-17. Design matrix of central composite design (CCD)

II-3.2. Statistical process control

SPC techniques were used to monitor the tribocharging process. Thus, the series of experiments were performed for the optimal arrangement of control factor that had been established using the design of experiments methodology. The results of the experiments were analyzed with Grubbs' test to detect the outliers. This test involved the computation of:

$$G = \frac{\bar{X} - Xmin}{c\, S_x} \quad \text{(II-8)}$$

$$G = \frac{Xmax - \bar{X}}{c\, S_x} \quad \text{(II-9)}$$

where $\bar{X}$ is the mean value, *Xmin and Xmax* are minimum and maximum value respectively, *Sx* is the standard deviation and *c* is the coefficient of confidence of the measurement data, which refers to the Table. II-2.

Table II-2. Confidence table for *Cp*

Cp	Number Of Controlled Values										
	10	20	30	40	50	75	100	125	150	200	250
1.0	1.65	1.37	1.28	1.23	1.20	1.16	1.13	1.12	1.11	1.09	1.08
1.33	2.19	1.82	1.70	1.64	1.60	1.54	1.51	1.49	1.47	1.45	1.44
1.50	2.47	2.06	1.92	1.85	1.80	1.74	1.70	1.68	1.66	1.64	1.62
1.67	2.75	2.29	2.14	2.06	2.01	1.93	1.89	1.87	1.85	1.82	1.80
2.00	3.29	2.74	2.56	2.46	2.40	2.32	2.27	2.24	2.21	2.18	2.16

Process capability ratio (*PCR*) evaluates the ability of the process to attain the target. There are several methods to calculate the *PCR*, as follows:

$$Cp = \frac{USL - LSL}{6\, c\, S_x} \quad \text{(II-10)}$$

$$Cpk = Min\left(\frac{USL - \bar{X}}{3\, c\, S_x}, \frac{\bar{X} - LSL}{3\, c\, S_x}\right) \quad \text{(II-11)}$$

$$Cpm = \frac{USL - LSL}{6\sqrt{(c\, S_x)^2 + (\bar{X} - T)^2}} \quad \text{(II-12)}$$

where *USL*, *LSL*, and *T* are respectively the upper/lower specification limits, and the target.

Process capability *Cp* and process performance index *Cpk* are unsatisfactory if their values are below 1. The capability and the performance of a process are commonly considered as "low" if less than 1.33, "medium" when their values are in the range 1.33 to 1.66, and "high" if beyond 1.66. Taguchi index *Cpm* is the improvement of *Cp* and *Cpk*, as it directly takes into consideration the bias from the target.

The upper and lower limits of the control charts for individual values *X* and moving ranges *R* were calculated with the following formulas:

$$UCLX = T + A_4 c\,\bar{R} \quad \text{(II-13)}$$

$$LCLX = T - c\,A_4 c\bar{R} \quad \text{(II-14)}$$

$$UCLR = D_4 c\,\bar{R} \quad \text{(II-15)}$$

$$LCLR = D_3 c\,\bar{R} \quad \text{(II-16)}$$

where A_4, D_3 and D_4 have the values chosen from Table II-3, and c is a confidence coefficient depending on the number of values measured for the calculation of $\bar{R}$.

Table II-3. Coefficients for the calculation the upper and lower control limits

n	2	3	4	5
A_4	2.660	1.772	1.457	1.290
D_3	-	-	-	-
D_4	3.267	2.574	2.282	2.114

II.4. Conclusions

This chapter describes the experimental bench and the associated instrumentation employed for the study of tribocharging of polymer materials.

1. The custom-designed tribometer model that provides flat-on-flat, back-and-forth movement can be used to control and investigate the tribocharging process. Several adjustable input variables can be set such as normal force, relative sliding speed, number of rubbing cycles.
2. A special room allows repetition of experiment in relatively steady environmental condition.
3. The tribological properties of the surface and its electric potential should be analyzed, so that to understand the triboelectric effect at the surface of polymer slabs in dry sliding contact.
4. The modeling and optimization of tribocharging using the design of experiment methodology could represent a viable solution to improve the process. Statistical control can then be used to monitor the quality of the process.

CHAPTER III

TRIBOELECTRIC CHARGE PROPERTIES IN TRANSLATIONAL SLIDING CONTACT OF POLYMERS

The outcome of a triboelectrification process depends on several control variables including the normal force applied on the objects in contact, the friction speed and the number of cycles. However, the charge generated by triboelectric effect is also related to such material properties and environmental conditions as temperature, humidity, moisture, surface texture, roughness, and contact geometry. Controlling the tribocharging conditions is vital in many industrial processes, either to avoid hazards or to improve the efficiency of energy harvesting.

A preliminary tribocharging test has been done for several combinations of polymer specimens. Polyethylene (PE) typically has the lowest charge compared to the other polymers. Combination of PVC, PP, and ABS specimens can produce relatively high charge and consistent with their position in the triboelectric series. Hence, these samples have been used in the experiments described hereafter, so that to limit the dispersion of the results.

The tribocharging studies are limited by the availability of materials pairs that acquire high enough levels of charge after rubbing, in contrast with corona discharge which has similar effects on all insulating materials. Moreover, corona discharge may satisfactorily charge both rough and smooth bodies, while tribocharging is greatly affected by surface conditions. The several factors which influence the generation of electric charge are discussed in III-1.

Furthermore, the comparison between the two charging mechanisms in terms of surface charge generation and potential decay is presented in III-2. Indeed, the surface potential decay (SPD) may also be an important consideration in the selection of materials for mechanical parts of machine tools or for triboelectrostatic energy harvesters. This is why the second part of this chapter will focus on the characterization of several polymers in terms of ability to preserve a high level of charge acquired by either tribo- or corona-charging processes.

III.1. Factors affecting the tribocharging process

III.1.1. *Material properties*

The aim of the present study is to point out that the different mechanical properties of the polymers in contact may influence the outcome of the tribocharging process. The materials are characterized with a universal tensile testing machine and a hardness tester, followed by tribocharging using a laboratory bench. The distribution of charge is characterized by measuring the electric potential at the surface of the samples using the auto-compensated induction probe of an electrostatic voltmeter [151].

In order to study the effect of mechanical properties related to electrostatic charge behavior, three kinds of PVC with different hardness has been chosen. The characteristics of the three kinds of PVC can be read in **Figure III-1**. The PVC samples A, B, and C displayed different average values of Young's modulus, respectively 2.64 GPa, 2.35 GPa and 0.93 GPa, and the different average values of hardness indicated by Vickers Pyramid Number (HV) with applied test load of 245.2 mN for 5 s: 16 HV, 10 HV and 5 HV, respectively.

The electric potential was measured at the surface of the PVC after rubbed with ABS under the same experimental conditions: friction speed 20 mm/s, 6 N of normal force and 10 cycles. Surface potential cartography of the three kinds PVC samples are shown in **Figure III-2**. The surface potential cartographies suggest that a correlation exists between their mechanical properties and triboelectrification characteristics. PVC type C sample reached - 6 kV on the contact area, while the type A and B samples achieved merely -2 kV. A second series of experiments was done with a higher normal force (10 N). As a result, the surface potential of type A sample reached -5 kV in the middle area of contact. Similar maximum surface potential values were attained in the samples of type B, but the surface potential was more evenly distributed. In the case of type C samples, which are softer, the surface potential can reach about -10 kV in the middle area of contact and -5 kV around it. This result is consistent with the hypothesis of this study. The materials with higher hardness and modulus of elasticity also require higher normal force to achieve higher surface potential through triboelectrification.

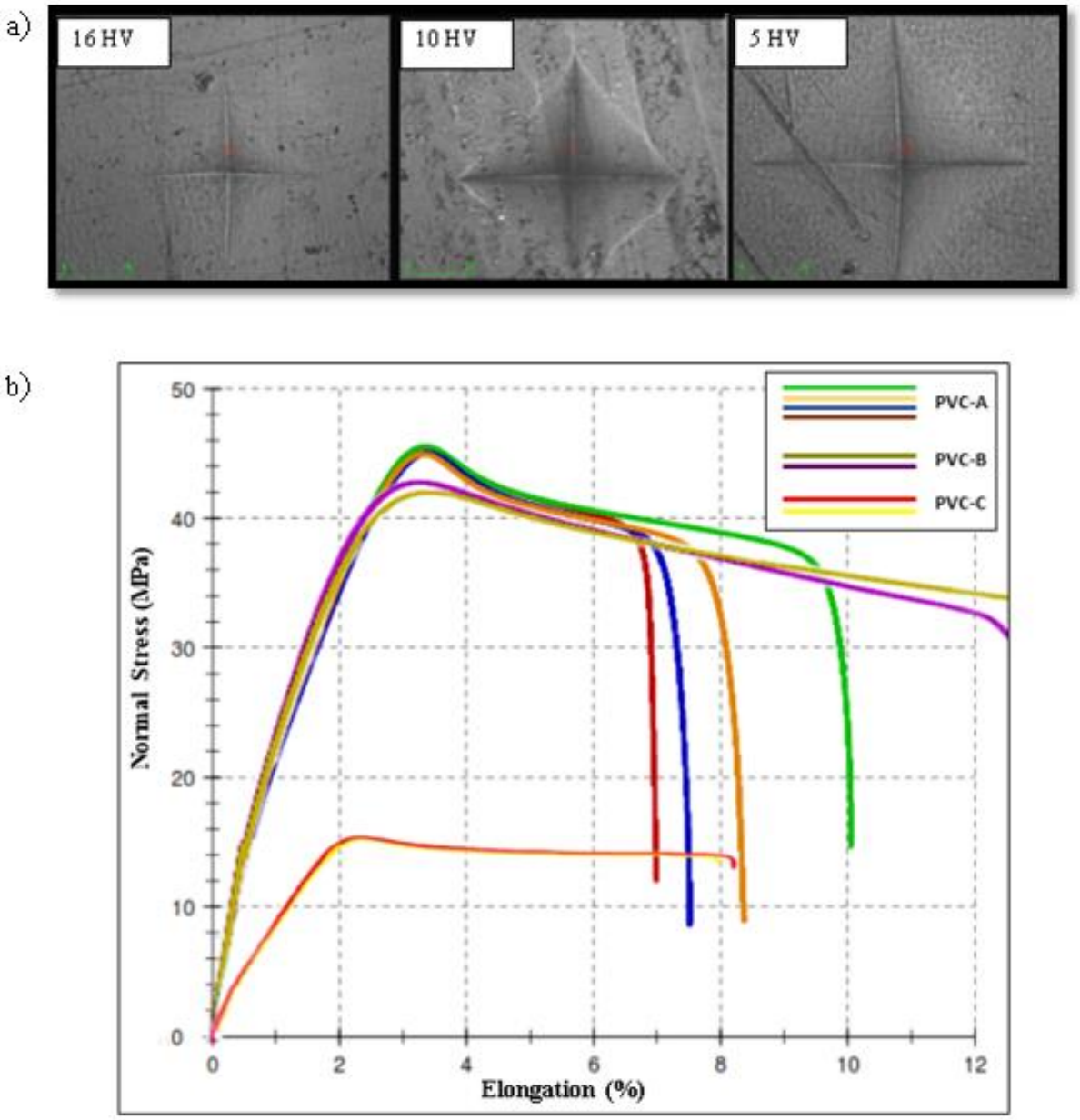

Figure III-1. Result of a) Vickers hardness test and b) tensile test, for three samples PVC – A, B and C

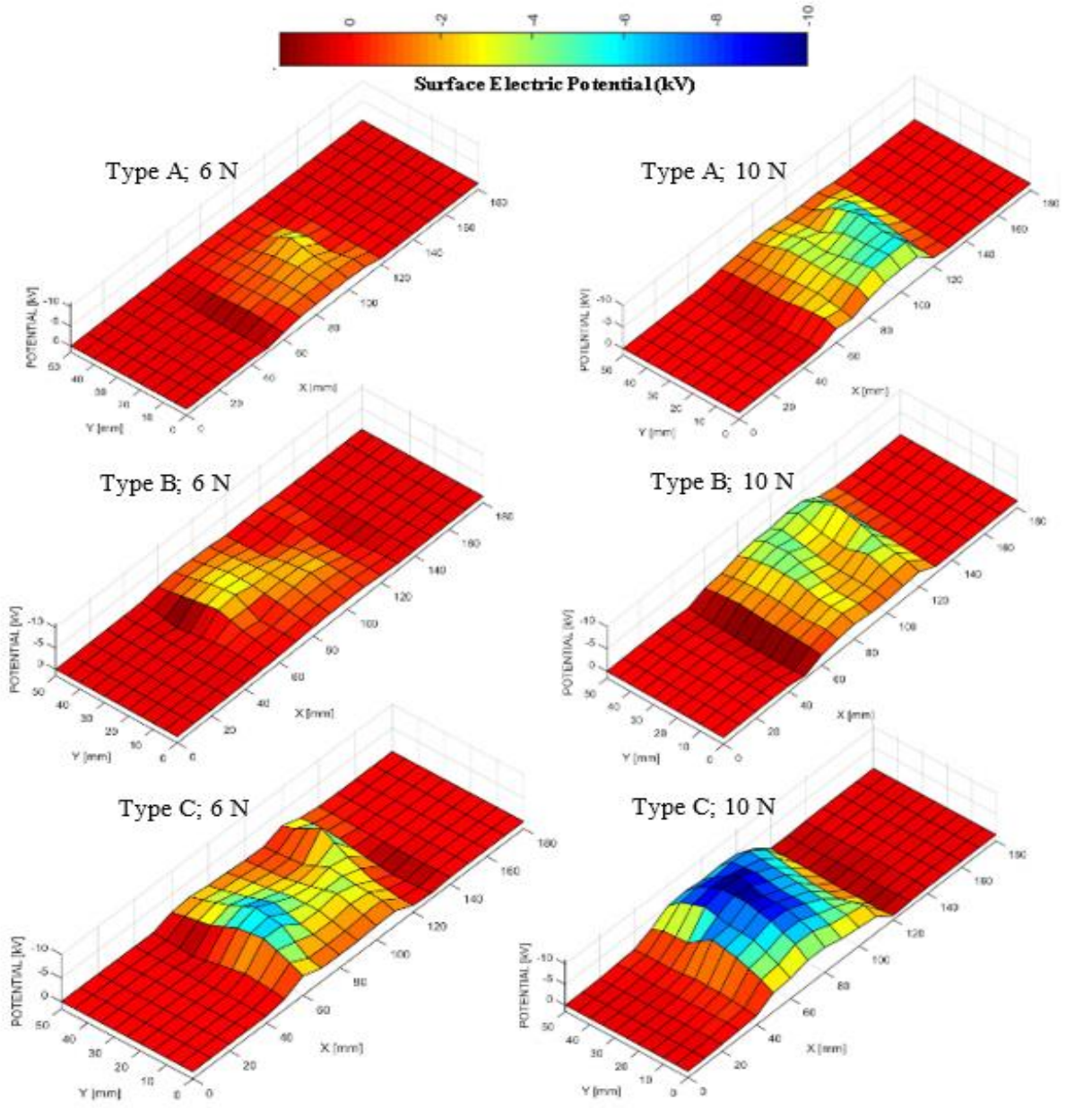

Figure III-2. Surface potential cartography of PVC samples type A, B and C

The outcome of tribocharging is difficult to predict because it does not depend only on the nature of the materials in contact, but also of several other properties: roughness, texture, hardness etc. Material with a higher hardness require higher normal force to achieve optimum surface potential; thus, a normal load of 6 N can produce the same surface potential in a softer material as a normal load of 10 N in a harder material.

III.1.2. *Surface temperature*

Temperature at the interface between two polymers may also affect friction and wear behavior [8]. The specialists call this: “thermal control regime” (Ettles, 1986). Frictional heating can cause surface temperatures to reach the melting or softening temperature of thermoplastic polymers, and this results in a drastic change in their frictional and wear behavior (Lancaster, 1971; Kennedy and Tian, 1994). In fact, Lancaster showed that the Pressure Velocity (PV) limit (a basis for setting a limit on the capability of a material pair in terms of the product of pressure and sliding speed) which is often used in the design of dry plastic bearings, is in reality a “critical surface temperature limit”; i.e., the combination of contact pressure and sliding velocity causes the surface temperature to reach the critical temperature of the material (Lancaster, 1971). Therefore this subchapter will discuss the effect of temperature on the triboelectric effect and the use of thermal field to identify the contact charging area.

III.1.2.1. Surface temperature and electrostatic charge generated

Polymeric materials are easy to mold and form when they are in high temperature condition, below their melting point. Therefore it is necessary to rigorously control the material heating, and keep it within well-specified limits. In the experiments described hereafter, a heat air blower is employed to adjust the temperature of the bodies in contact, during the process of friction. Temperature was measured with a thermal camera (camera Flir E60; thermal sensitivity <0.05°C), to verify that the material does not exceed 60° C, since material would change form or bend, which means changing the conditions of mechanical contact and hence altering the electrostatic charging. Contact model in this experiments used ABS top specimens: 5 mm x 15 mm x 100 mm and PVC bottom specimens: 5 mm x 50 mm x 180 mm.

Tribocharging setup is illustrated on **Figure III-3**. Material heating process was carried out in one of the three following modes: (1) direct heating during tribocharging (30 seconds) was pwith blowing hot air from front side; (2) same as (1) but from top side; (3) pre-heating using a spotlight. The three mechanisms of heating were verified that they did not generate electrostatic charge on the surface of sample before friction. The frictional heating in this experiment did not exceed 60° C.

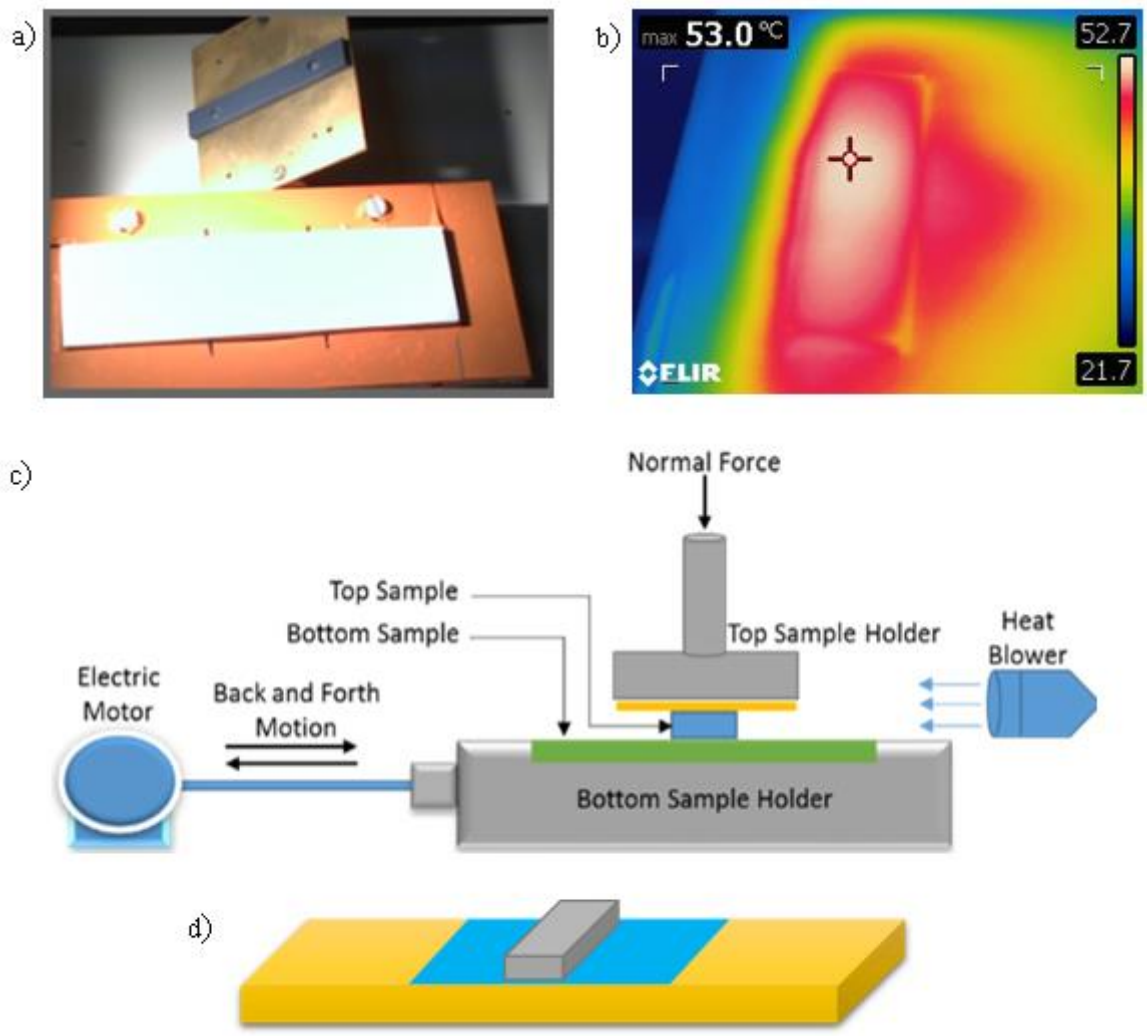

Figure III-3. Schematic representation of heating process: a) initial heating; b) heat in process; c) contact area and d) contact area.

Figure III-4 shows that heating during the rubbing process modifies the outcome of the tribocharging. Thermal treatment is more effective when hot air is blown to the material from the side rather than from the top of the sample. After 30 cycles of rubbing, the absolute value of the average surface potential was 100% higher than in the absence of heating (1100 V, as compared to 528 V). A similar effect was observed regarding the maximum potential, in absolute value, recorded in the contact area (5283 V, in the presence of heating, more than twice as high than 2416 V, without heating).

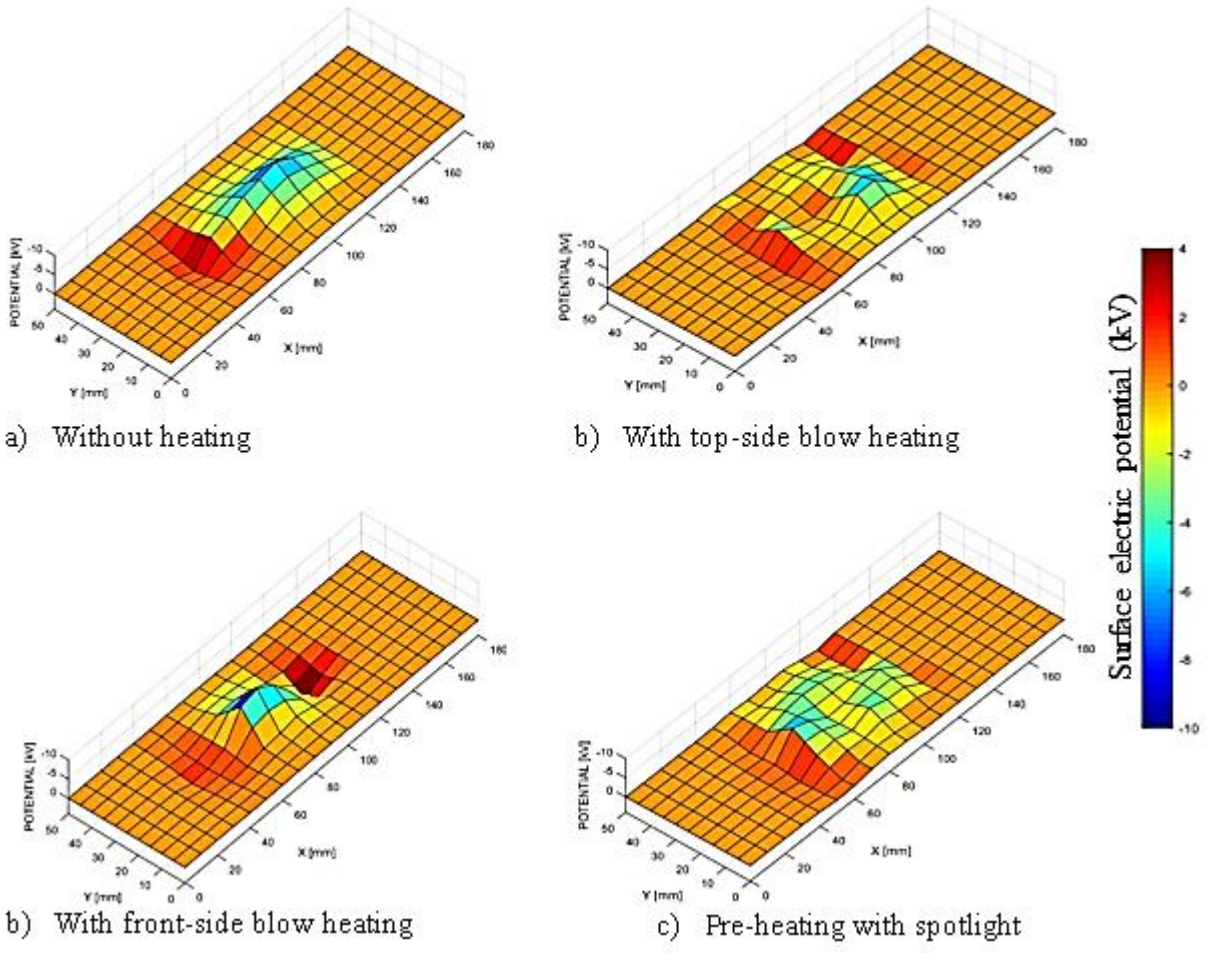

Figure III-4. Surface potential cartography after friction with and without heat treatment.

However, charged area was smaller compared to the tribocharging of sample without heat treatment (± 20 °C), this result can be justify by the fact that high temperature the increases conductivity of the surfaces in contact but enhances the interaction between them [152]. In fact surface heating with convection/radiation occurs more rapidly than with friction (**Figure III-5**), heating surface with heat blow only takes about 30 seconds to reach 60° C of surface temperature while on friction with maximum load temperature difference increased only 5° C from initial after 100 cycles or equal to 100 seconds.

Heating with convection/radiation on the surface of material in a short time and limited temperature does not have a significant impact on the surface material properties while at frictional heating rising surface temperatures also followed by wear and changes in surface conditions due to surface fatigue because of heat increasing on the surface.

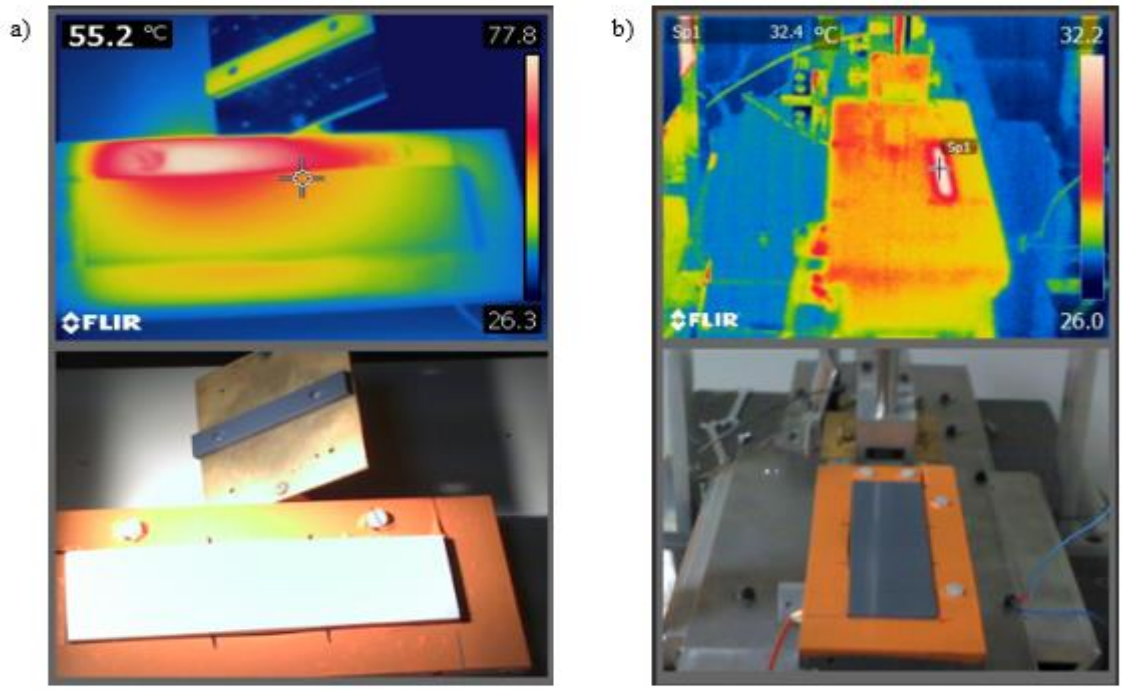

Figure III-5. Surface temperature increase due to: a) radiation heating and b) friction

Blowing hot air during the rubbing process can improve the ability of the surface to store the charge. This treatment must be administrated such as not to modify the shape of the samples and the conditions of the conformal contact between the two bodies.

III.1.2.2. Polymer surface friction trace monitoring by thermal hotspot

Monitoring of friction trace is a useful strategy to improve mechanical contact between sliding polymers. The triboelectrification process that occurs in such contacts can be used to characterize the uniformity of contact condition, so that the applied force can be adjusted accordingly. The non-uniform distribution of pressure and shear on contact will influence electrostatic charge at the surface of the sample, hence the cartography of temperature will enable the detection of excessive wear.

The frictional charge was performed used the PVC – ABS sample pairs on a triboelectric laboratory bench while the temperature was monitored by thermal camera and the charging state was evaluated by measuring the electric potential at the surface of the sample, using a non-contact electrostatic voltmeter. PVC and ABS test pieces were 5mm x 15mm x 100mm and 5mm x 50mm x 180mm respectively. The specimens were placed in a perpendicular configuration and the sliding stroke was s = 55 mm. Several parameters were set to analyze the relation of surface thermal and electrostatic potential as follows:

- F_N = 2 N, 6 N, 10 N, 14 N; Cycle = 5; v = 100 mm/s;
- F_N = 2 N; Cycle = 5, 20, 40, 80; v = 25 mm/s;
- F_N = 2 N; Cycle = 5; v = 25 mm/s, 50 mm/s, 75 mm/s, 100 mm/s;
- F_N = 14 N; v = 25 mm/s, 50 mm/s, 75 mm/s, 100 mm/s; Cycle = 5;
- F_N = 14 N; v = 25 mm/s, 50 mm/s, 75 mm/s; 100 mm/s; Cycle = 80.

Pearson's coefficient was employed to measure the strength of linear correlation between surface temperature and electric potential generated by tribocharging. The Pearson correlation coefficient (r) has values in the range from -1 to +1, while 0 indicates there is no relationship between the two variables. A value higher than 0 indicates a positive correlation (i.e. both variable increase simultaneously). Moreover, the closer is r value to 0 the larger is the variation around the line of best fit.

$$r = \frac{\sum(T-\bar{T})(V-\bar{V})}{\sqrt{\sum(T-\bar{T})^2 \sum(V-\bar{V})^2}} \qquad \text{III-1}$$

where T and V are the sample means of temperature and electric potential respectively. The significance of this correlation coefficient is interpreted in **Table III-1.**

Table III-1. Strength of Pearson's correlation coefficient

Strength of Correlation	Coefficient, r	
	Positive	Negative
Low	0.1 to 0.3	- 0.1 to - 0.3
Medium	0.3 to 0.5	- 0.3 to - 0.5
High	0.5 to 1	-0.5 to -1

Figure III-6 shows that the positive correlation coefficient between the surface temperature and the electrostatic potential ranged from 0.51 to 0.7, as function of the applied normal force, at constant number of cycles and rubbing speed. The ambient temperature and relative humidity were stable at 27° C and 50% respectively.

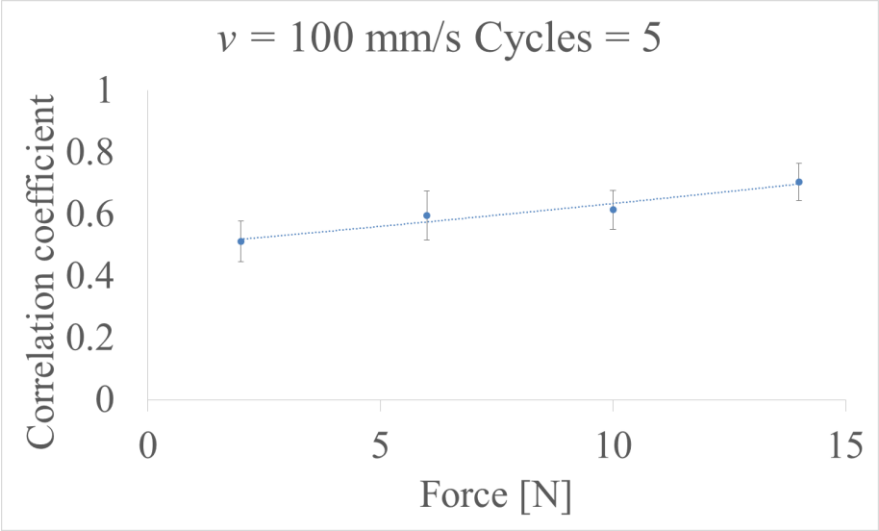

Figure III-6. Correlation coefficient between the surface temperature and the electrostatic potential, as function of applied normal force.

This correlation is illustrated by the cartographies in **Figure III-7**. The average value of the electric potential generated on the surface of rubbing area was 0.3 kV, with a maximum value of 4.5 kV for F_N = 14 N; v = 100 mm/s; Cycles = 5. In agreement with theoretical predictions, in this area of contact, the temperature and the electric potential increase with the normal force.

Figure III-8 shows the positive correlation between the surface temperature and the electric potential as function of the number of cycles' variation, at constant normal force 2 N and rubbing speed 25 mm/s which are the lowest capability of the tribocharging bench. As expected, the surface temperature as well as electric potential increase with the number of cycles. These experiments were done at room temperature 25° C and relative humidity 35%.

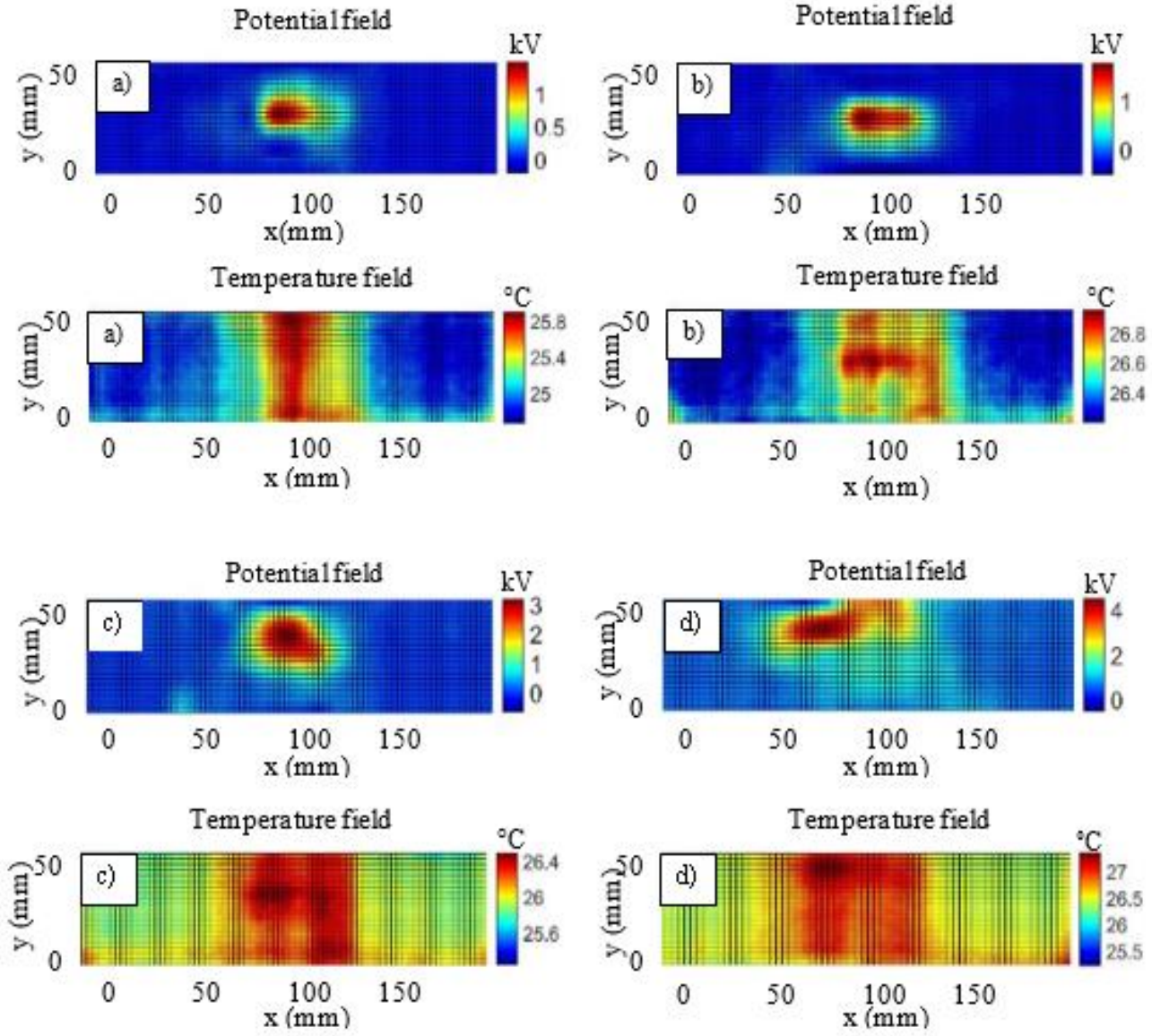

Figure III-7. Comparison between the electric potential and the temperature generated on the surface of polymer samples at v = 100 mm/s, for 5 rubbing cycles and various values of the normal force (F_N): a) 2 N, b) 6 N, c) 10 N, and d) 14 N.

The correlation coefficient for 5 and 80 cycles respectively were 0.59 and 0.82. The average surface electric potential was 0.28 kV at low number of cycles and increased to 0.44 kV at 80 cycles, while the average surface temperature rose from 26° C to 30° C.

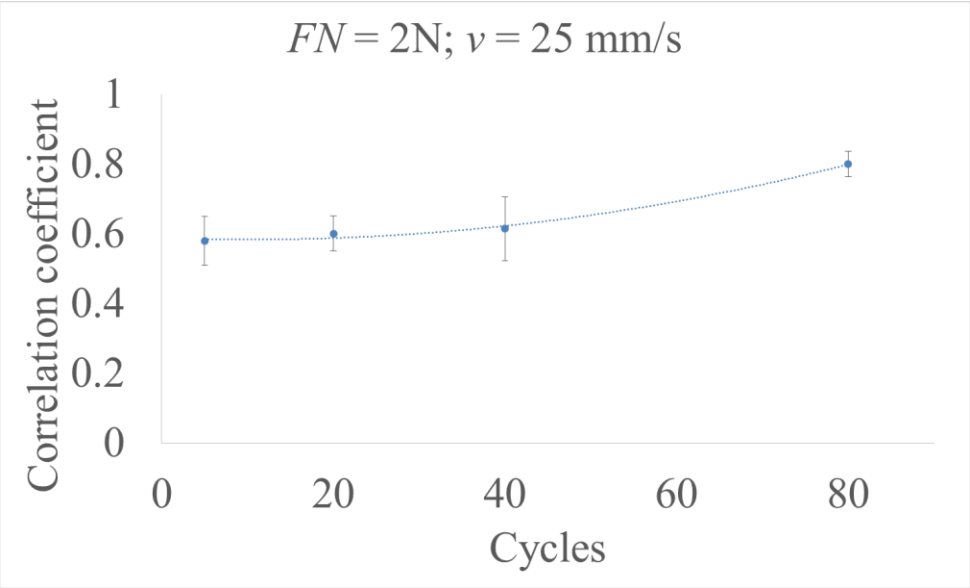

Figure III-8. Correlation coefficient between the surface temperature and the electric potential as function of the number of rubbing cycles.

The increase of the electric potential with the number of cycles is limited to a certain value, related to material characteristics and affected by the environmental conditions. After reaching this saturation potential, further rubbing will not generate significantly more charge. **Figure III-9** illustrates the correlation between the surface electrostatic potential and the temperature at various numbers of cycles.

Rubbing speed is a controllable factor but does not influence the electrostatic potential generated in the conditions of these experiments, the possible cause is stick-slip phenomenon. The occurrence of stick-slip in the system illustrated on the **Figure III-10**, was described by several researchers [152–155]. According to them, the amplitude of stick-slip in the frictional contact decreases with the increasing speed and there is a critical speed at which the stick-slip motion occurs no more. This critical speed increases with humidity and load. Furthermore, stick-slip motion is more persistent at higher load and larger size of contact spot. Plotting the tangential force against the actual displacement can be used to characterize the stick slip behavior [156].

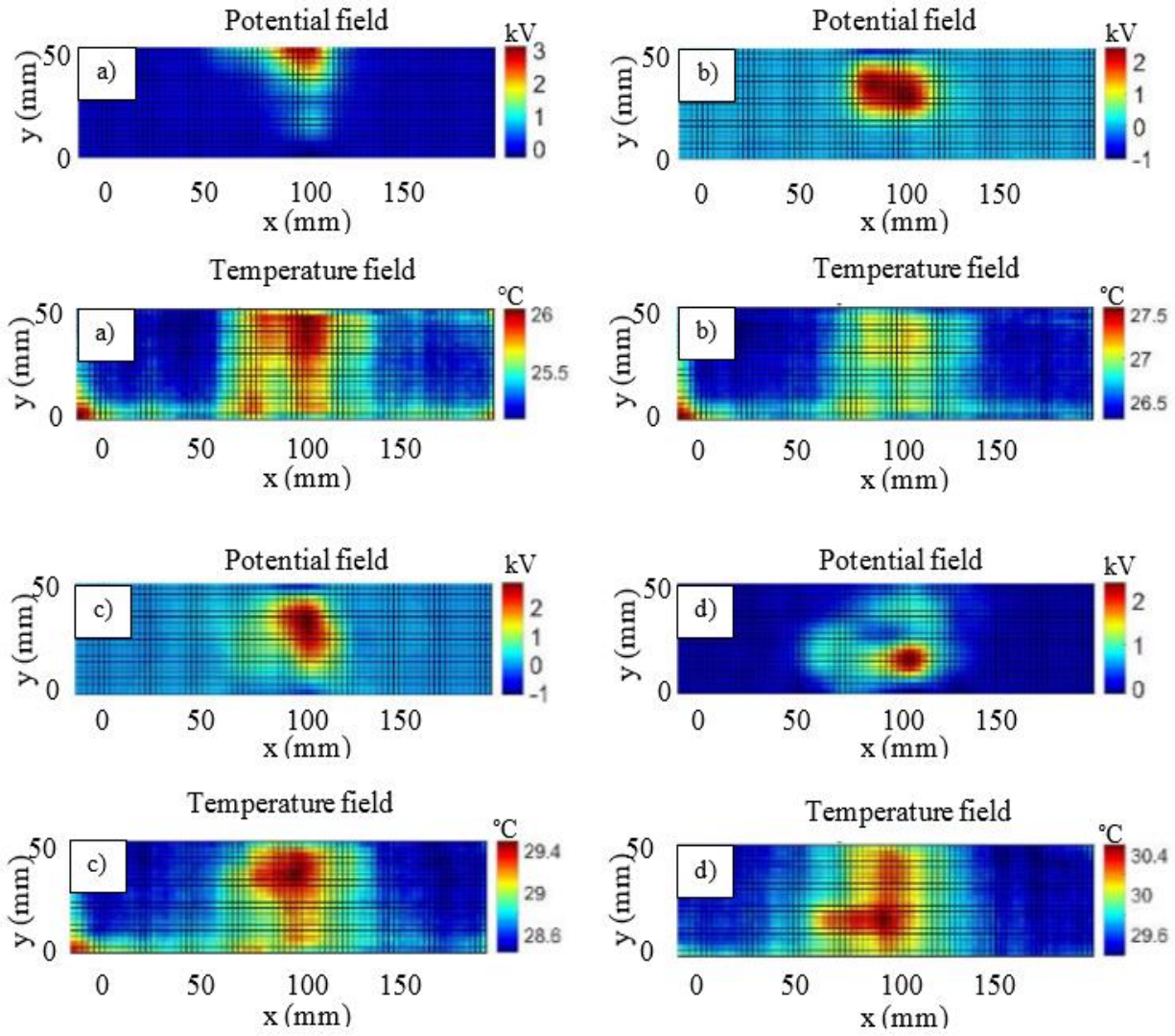

Figure III-9. Comparison between the electric potential and the temperature generated on the surface of polymer samples at applied normal force 2 N and v = 25 mm/s, for various number of cycles: a) 5, b) 20, c) 40, and d) 80.

Figure III-11 shows the positive correlation between the surface temperature and the electric potential as function of the rubbing speed in the range from 25 mm/s to 75 mm/s, while at higher speed 100 mm/s the correlation becomes positive, in agreement with predictions of previous research related to stick-slip motion phenomena. **Figure III-12** presents several electric potential and temperature cartographies that illustrate this correlation.

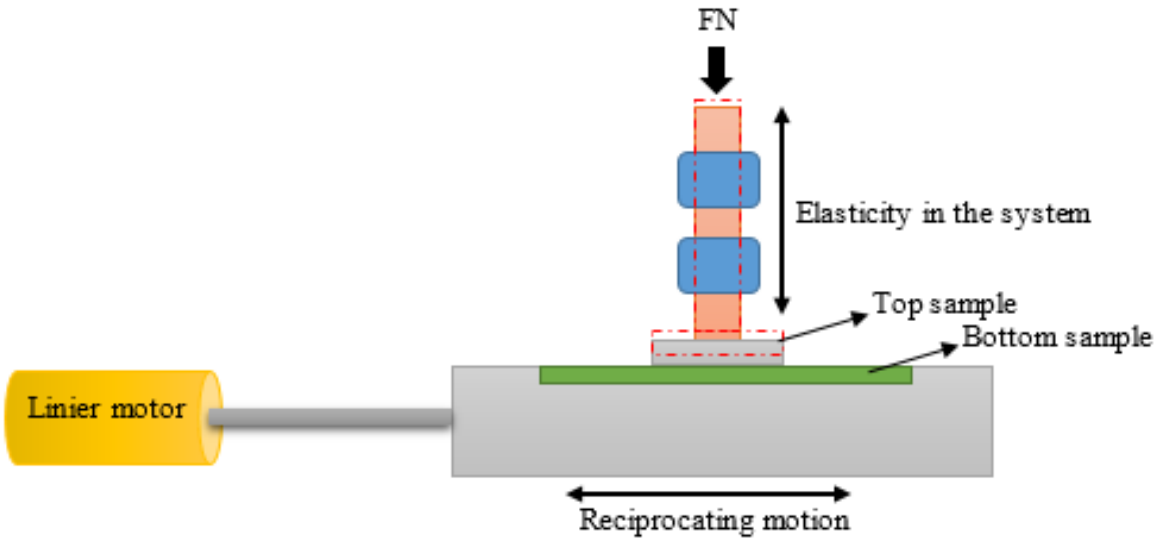

Figure III-10. Stick-slip model of the linear tribocharging system

The last two experiments were performed to verify the effect of the number of cycles on the correlation between the surface temperature and the electric potential, within the same range of speed, at a normal force of 14 N (**Figure III-13**).

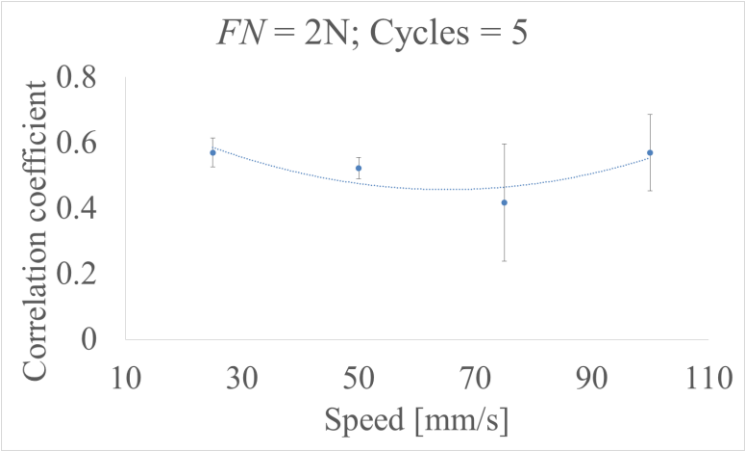

Figure III-11. Correlation coefficient between the surface temperature and the electric potential as function of the rubbing speed at 2 N of normal force and 5 cycles.

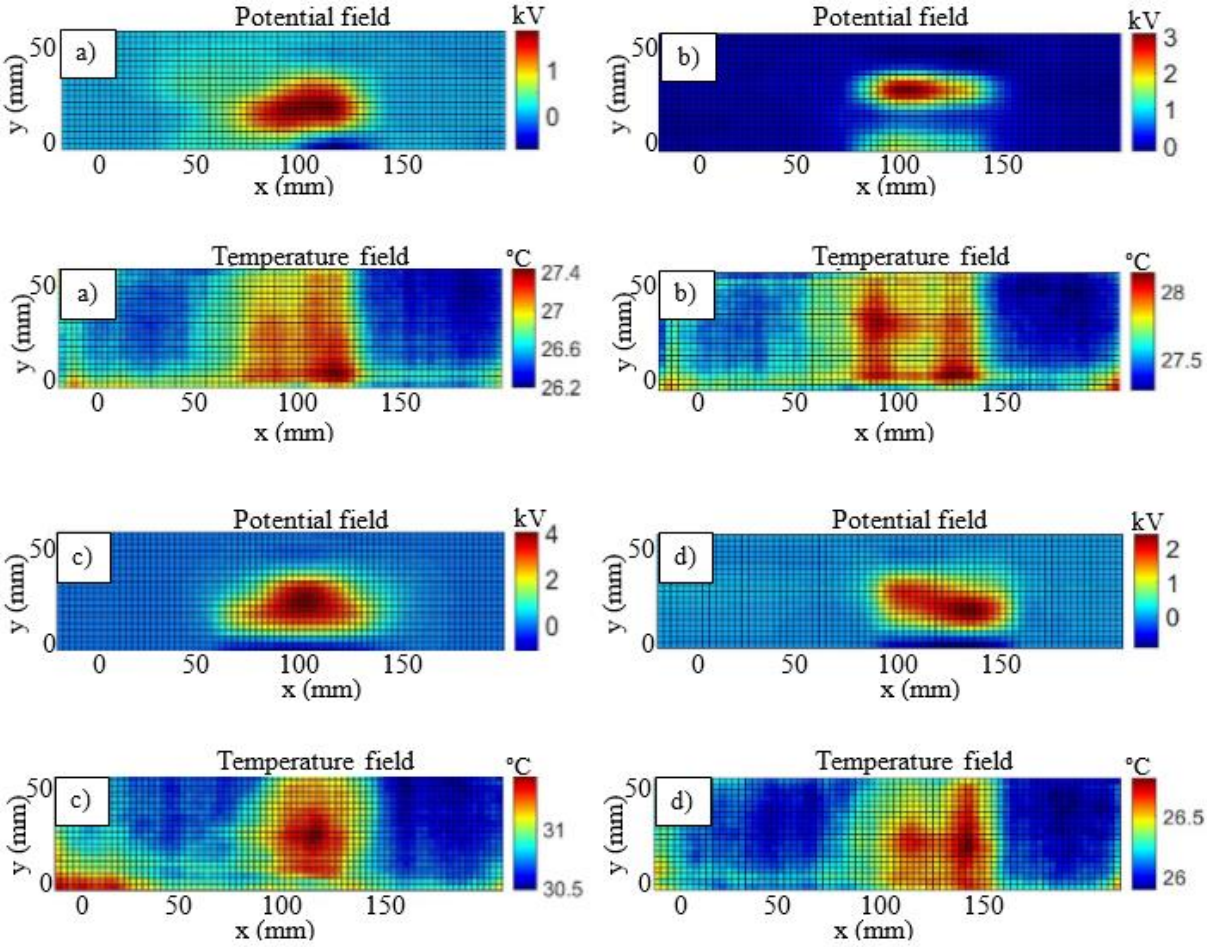

Figure III-12. Comparison between the electric potential and the temperature generated on the surface of polymer samples at applied normal force 2 N for 5 cycles, and various values of the sliding speed: a) 25 mm/s, b) 50 mm/s, c) 75 mm/s, and d) 100 mm/s.

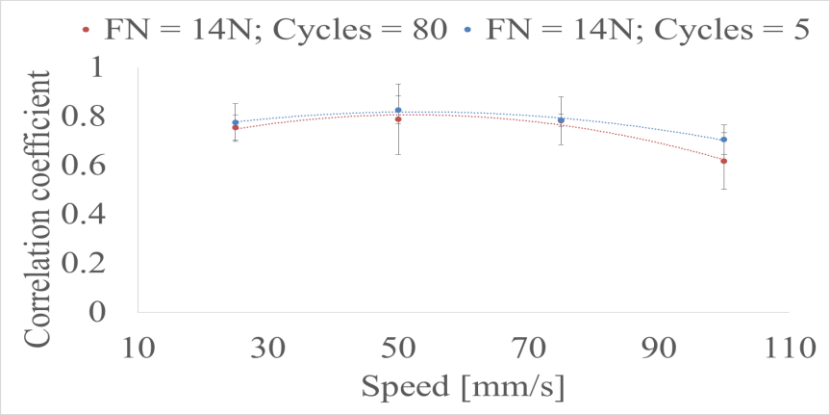

Figure III-13. Correlation coefficient between the surface temperature and the electric potential as function of the rubbing speed at 14 N of normal force, for 5 and 80 rubbing cycles.

The strength of the correlation coefficient is slightly higher at low number of rubbing cycles, because both the charge generated and the temperature increase before reaching the saturation condition. Cartographies of the surface electric potential and of the temperature are shown in **Figures III-14** and **III-15**. The speed does not influence the average value of the electric potential but may affect the contact uniformity. As a result, uneven charge distribution occurs and high values of potential are recorded on a small region, while other areas around it display relatively low potential.

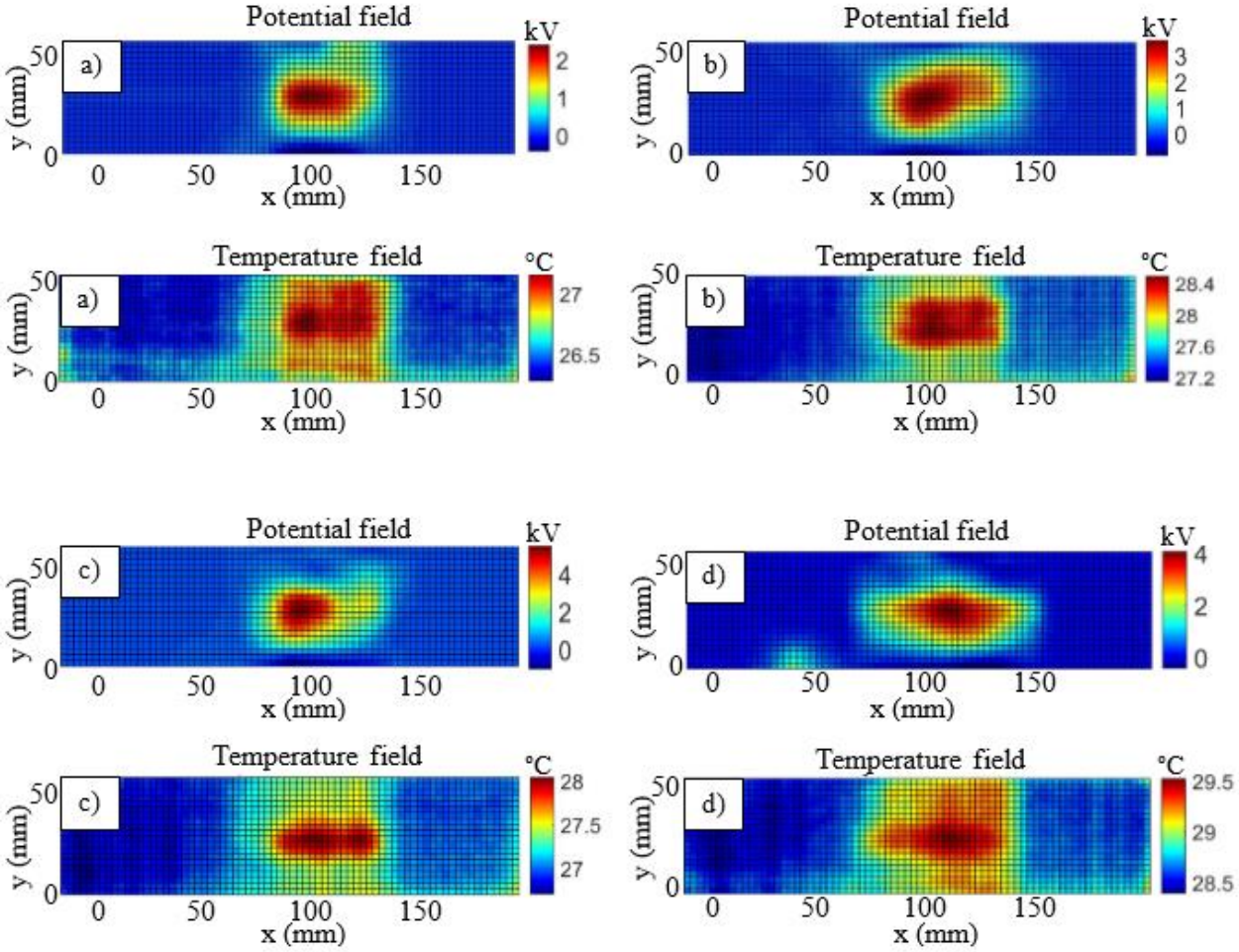

Figure III-14. Comparison between the electric potential and the temperature generated on the surface of polymer samples at applied normal force 14 N for 5 cycles and various values of the sliding speed: a) 25 mm/s, b) 50 mm/s, c) 75 mm/s, and d) 100 mm/s.

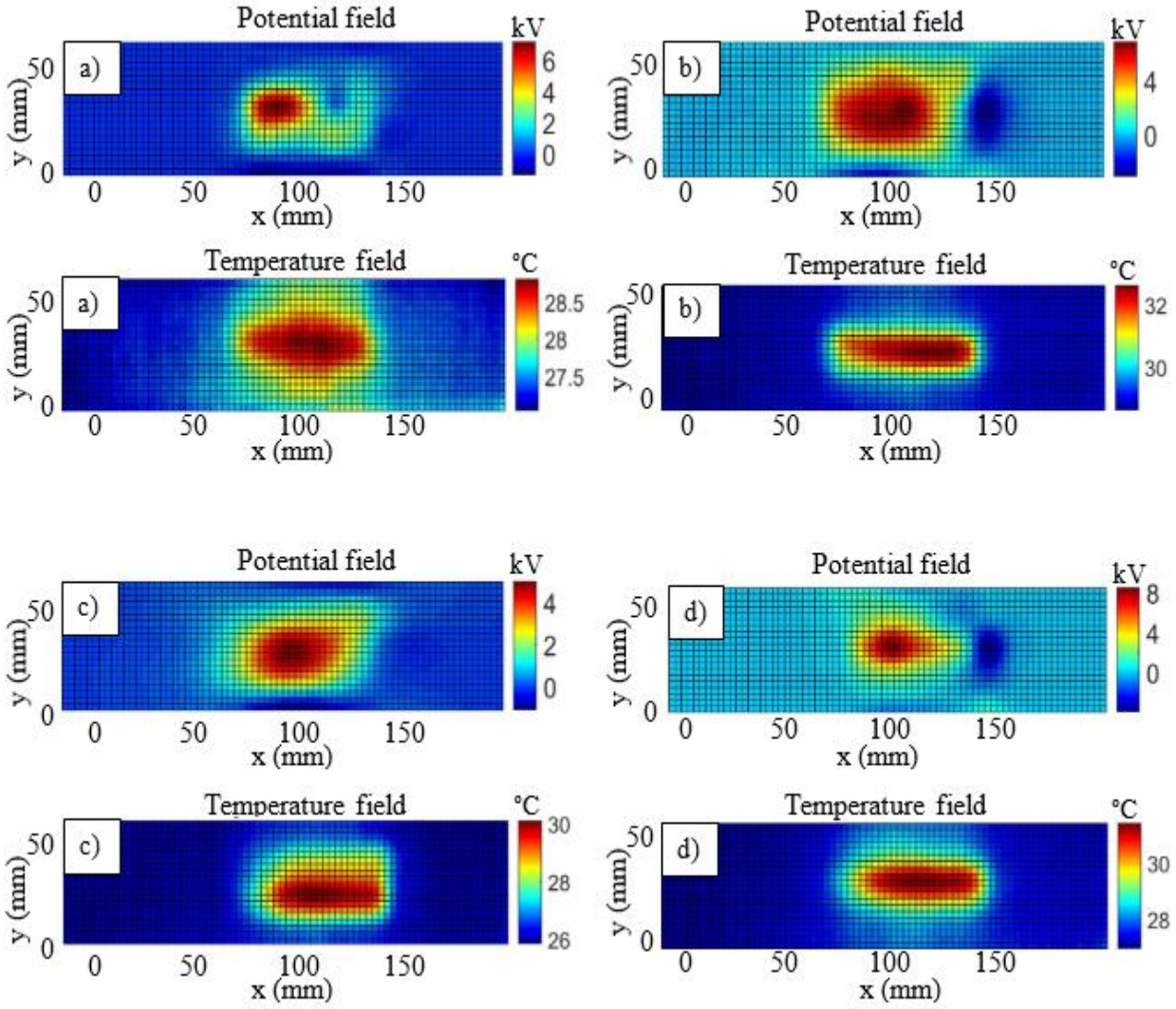

Figure III-15. Comparison between the electric potential and the temperature generated on the surface of polymer samples at applied normal force 14 N for 80 cycles, at various values of the sliding speed: a) 25 mm/s, b) 50 mm/s, c) 75 mm/s, and d) 100 mm/s.

III.1.3. *Surface geometry and texture direction*

The experiments were designed to determine the distribution of the electric potential at the surface of polymer slabs PVC and ABS of different geometries and texture direction, in frictional motion at constant pressure of 0.04 MPa, when varying the contact area, the contact position and the normal load. The bottom samples had fixed dimensions, 50 mm x 50 mm x 5 mm, and moved at 15 mm/s speed along linear rails for 20 cycles. The upper samples were stationary and characterized by different sizes of the contact area: 5 mm x 15 mm; 15 mm x 15 mm and 5 mm x 45 mm.

The ABS top sample applied a pressure of 0.04 MPa to the PVC bottom sample. Different sizes of contact area needed specific normal forces to obtain this same pressure. Thus, the samples of 5 mm x 15 mm needed an applied normal force of 3 N, while on the samples 15 mm x 15 mm and 5 mm x 45 mm the applied force was 9 N. **Figure III-16** shows the cartography of the surface electric potential in the central part of the charge area 5 mm x 15 mm (0.75 cm^2), electrostatic potential generated in the middle line of contact above 1500 V and symmetrically 200 V in the edge of top sample position of contact with bottom sample. However, high charge spotted in red scale was not distributed uniformly.

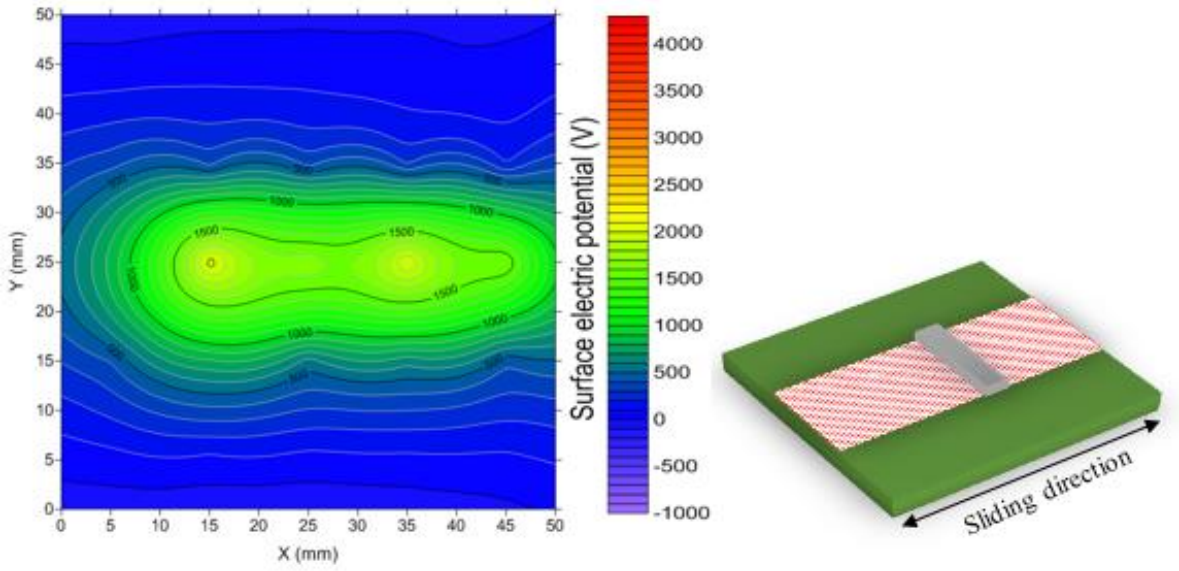

Figure III-16. Surface electric potential cartography of PVC sample after tribocharging with a 5 mm x 15 mm ABS sample.

A square type ABS sample 15 mm x 15 mm (2.25 cm^2) was rubbed against a 50 mm x 50 mm PVC surface for the second experiment (**Figure III-17a**). The recorded surface electric potential reached 4 kV and was distributed on a larger area than in the previous case. This was possible because of the increasing number of points in contact [157]. **Figure III-17 b.** shows a similar effect in another geometry: 5 mm x 45 mm (2.25 cm^2).

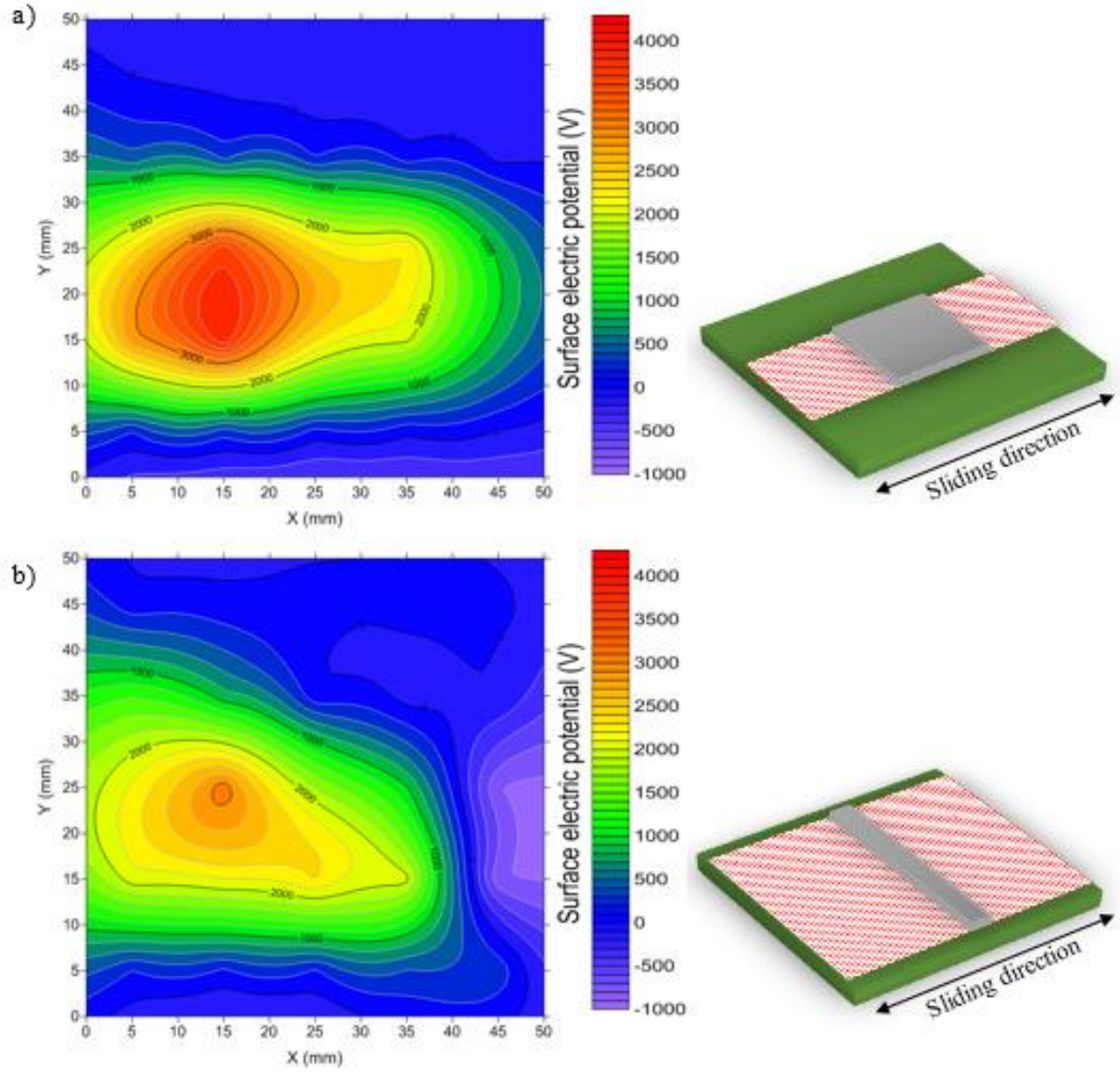

Figure III-17. Surface electrostatic potential cartography of PVC sample after tribocharging with 2.25 cm^2 surfaces of ABS sample a) 15 mm x 15 mm and b) 5 mm x 45 mm.

Comparing the results of surface electrostatic charging for two different of top sample geometry (length and width) within a similar size of the contact area, it can be seen that tribocharging with a square sample can generate relatively higher charge than using rectangular ones. This can be explained by the better sample adjustment which frictional contact in the case of the square sample.

This configuration was then used for another study related to surface texture direction, which was visually visible on PVC and ABS slabs. These textures were due to the specific manufacturing processes of the respective polymers. **Figure III-18** describes these textures for both samples. The comparison experiment was conducted for perpendicular and parallel position of the textures with respect to friction direction.

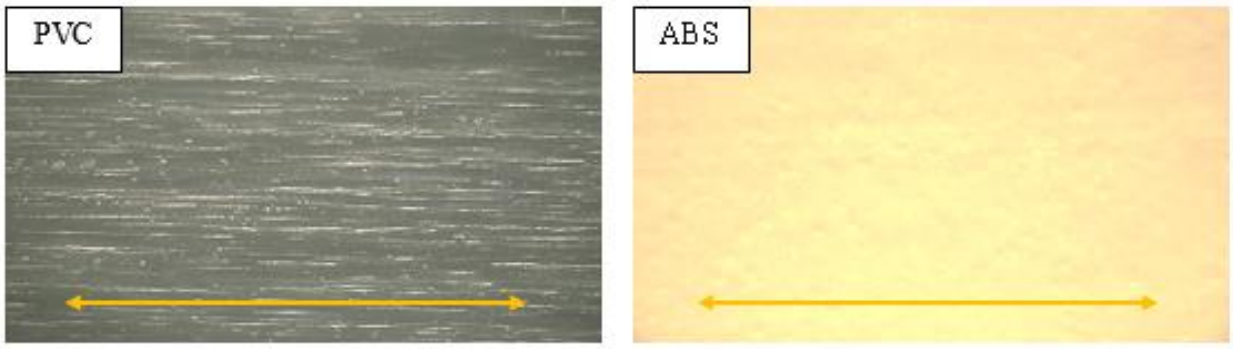

Figure III-18. Surface texture on PVC and ABS samples. The arrows indicate the direction of the texture.

The tribocharging experiment was done in four pair types of surface texture direction. The average roughness of the PVC (bottom) samples measured in directions perpendicular and parallel to the texture direction was 0.82 Ra and 0.13 Ra respectively. The ABS (top) samples were characterized by an average roughness of 0.29 Ra and 0.18 Ra in directions perpendicular and parallel to the texture, respectively. The normal force was 10 N, enough to investigate the roughness effect. The friction speed was fixed at 15 mm/s for 10 cycles, to maintain the initial surface temperature and avoid the effect of heating. Relative humidity and ambient temperature for this experiment were 32% ± 2% and ± 24° C ± 1° C respectively.

Figure III-19 shows the cartography of surface electric potential on a parallel-type PVC rubbed against parallel- and perpendicular-type ABS samples. Average potential was higher in the case when the ABS texture was perpendicular to friction direction. Surface electric potential cartography for the perpendicular texture-type PVC sample shown in the **Figure III-20** clearly shows the effect of different texture direction on charge generation. According to Menezes et al. [141,142,158] ploughing or plowing effects are related to surface texture. In the present study surface texture is proven to influence also the triboelectric effect

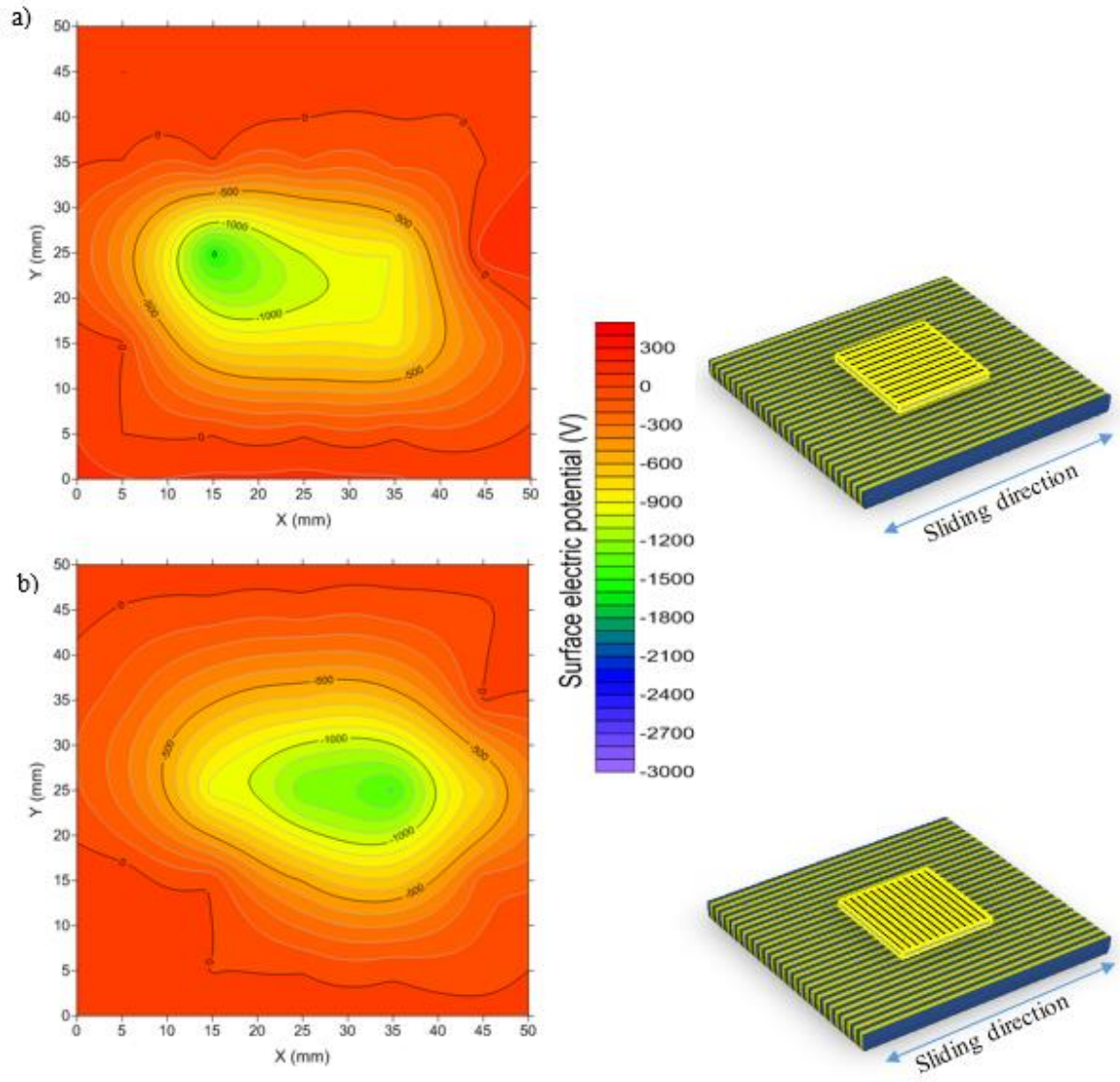

Figure III-19. Surface electrostatic potential cartography of PVC type parallel against ABS type a) parallel and b) perpendicular.

The configuration of involving two samples characterized by texture directions perpendicular to friction direction can generate higher levels of electric potential and more widely distributed electric charges than the other configurations. Therefore, the preparation of the material pair to be used in the tribocharging process should take into consideration the surface texture direction.

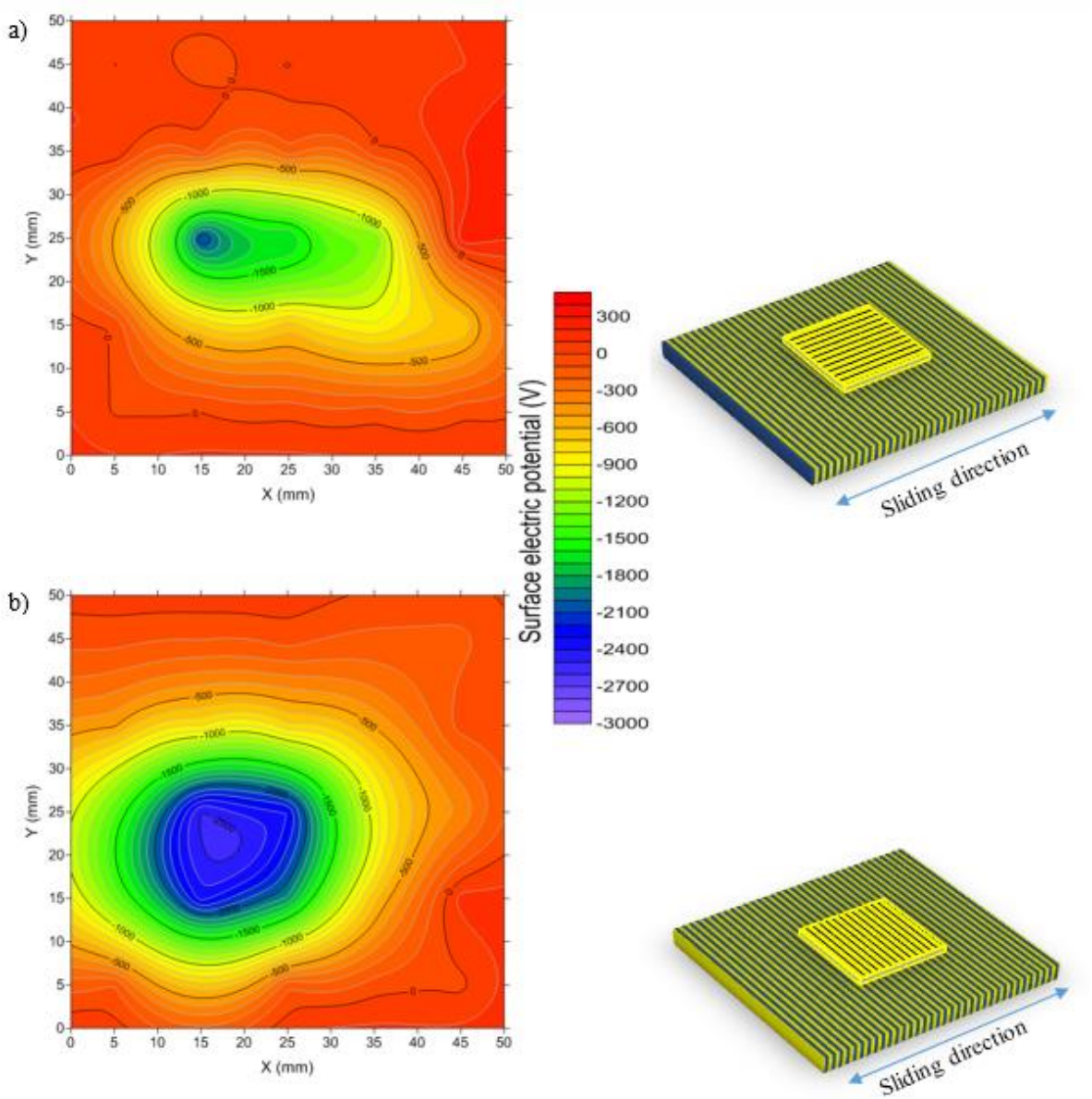

Figure III-20. Surface electric potential cartography of PVC perpendicular-type samples rubbed against ABS a) parallel- and b) perpendicular-type samples.

III.2. Surface potential decay

The tribocharging experiments were carried out with six different pairs of top and bottom samples (ABS/PP; PP/ABS; ABS/PVC; PVC/ABS; PP/PVC; PVC/PP). The effect of the misalignment of the surfaces in contact during a tribocharging experiment which can be judged by examining the results of the observations made by the thermal camera [109,159]. The image in **Figure III-21**, a) illustrates the situation when the pressure is non-uniformly applied between two samples (ABS/PP), and causes more intense friction and higher temperature (26°C) at one edge than at the other edge of the B-type sample (24°C). Consequently, the electric potential generated by the charge accumulated on the more-loaded edge is higher (about 3 kV) than at the other edge (**Figure. III-21, b**).

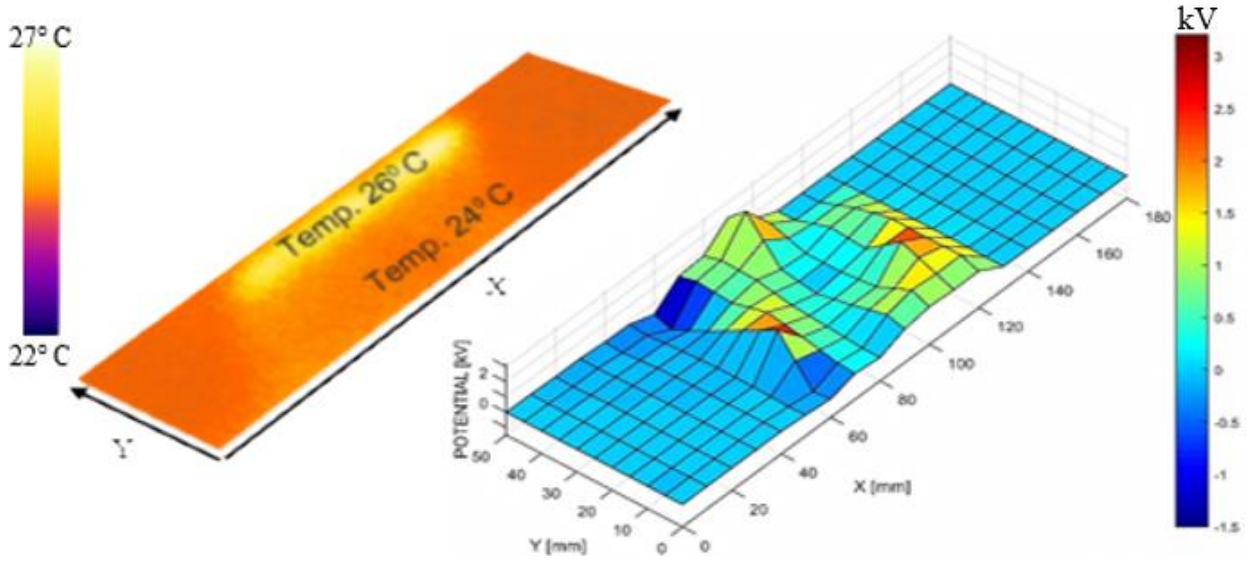

Figure III-21. Cartography of the temperature (a) and of the electric potential (b) at the surface of a non-uniformly tribo-charged B-type PP sample.

In case of a good conformal contact, during the 10 tribo-charging cycles, no significant difference in the temperature can be detected by the thermal camera (**Figure III-22, a**). The temperature due to friction is roughly the same (26°C) all over the surface. The cartography of the electric potential is also much more uniform than in the previous case (**Figure. III-22, b**).

Uniformity of surface potential charge for tribocharging depends on the quality of the conformal-contact surface and the material itself. The electric potential of ABS samples are higher than those of polypropylene and polyvinyl-chloride. Thus, the ABS samples tribocharged at a speed of 20 mm/s, normal load 10 N, for 100 cycles, display a maximum surface potential of 7.4 kV, when rubbed against PVC samples and -5.7 kV, against PP samples

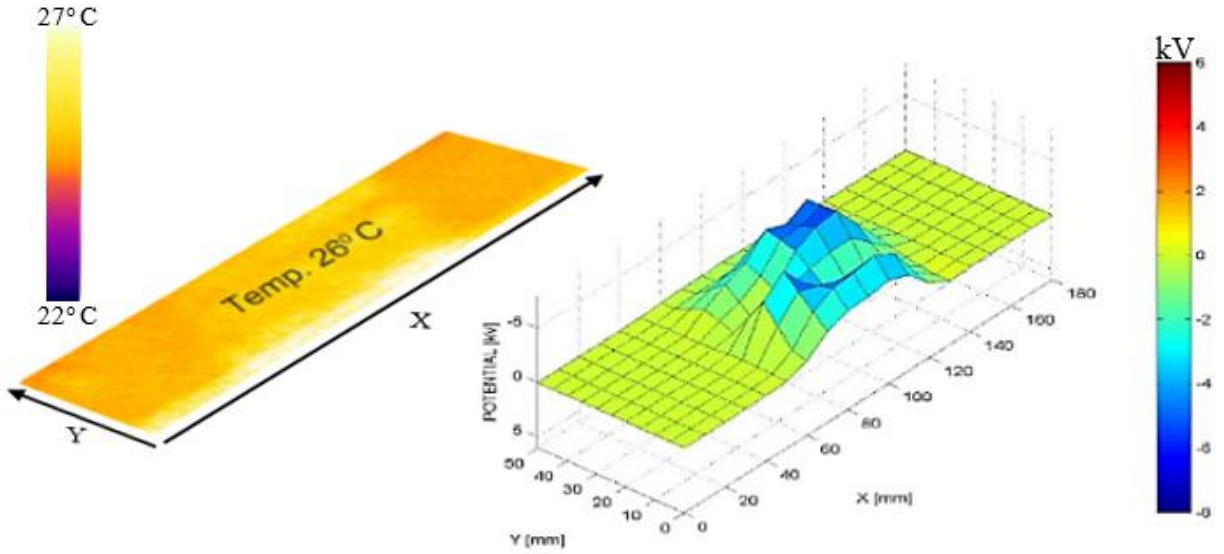

Figure III-22. Cartography of the temperature (a) and of the electric potential (b) at the surface of a uniformly tribo-charged A-type PP sample.

III.2.1. Decay of the electric potential at the surface of tribocharged polymers

The fairly-uniform contact obtained at a constant load of 10 N and a speed of 20 mm/s for 100 cycles of tribocharging generated the surface potential distributions illustrated by the cartographies in **Figures III-23** to **III-28**. In each figure, the cartography of the potential at the initial moment $t = 0$ is compared with the one recorded at $t = 30$ min, to enable a crude evaluation of the charge decay rate at the surface of the various polymer samples under investigation.

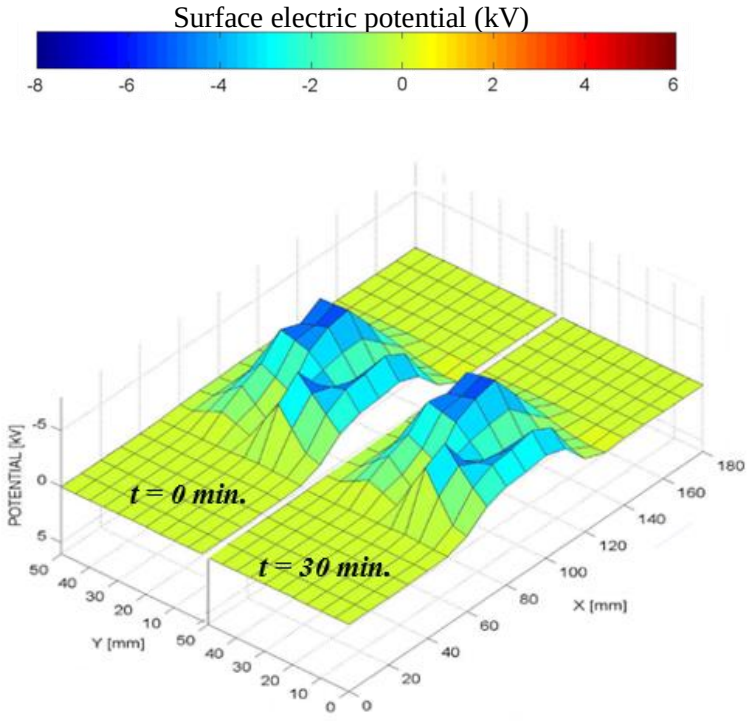

Figure III-23. Cartography of electric potential at the surface of a polypropylene (PP) sample, at t = 0 and t = 30 min after conformal-contact tribocharging with acrylonitrile-butadiene-styrene (ABS).

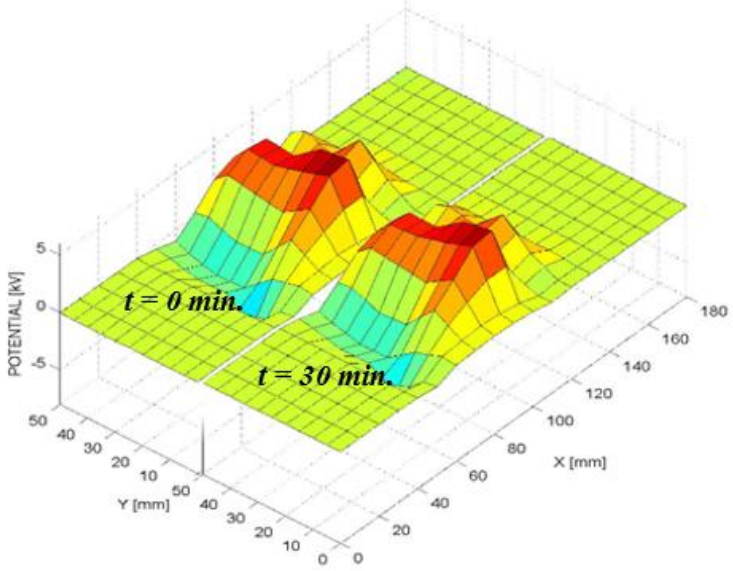

Figure III-24. Acrylonitrile-butadiene-styrene (ABS) surface potential after conformal-contact tribocharging with Polypropylene (PP).

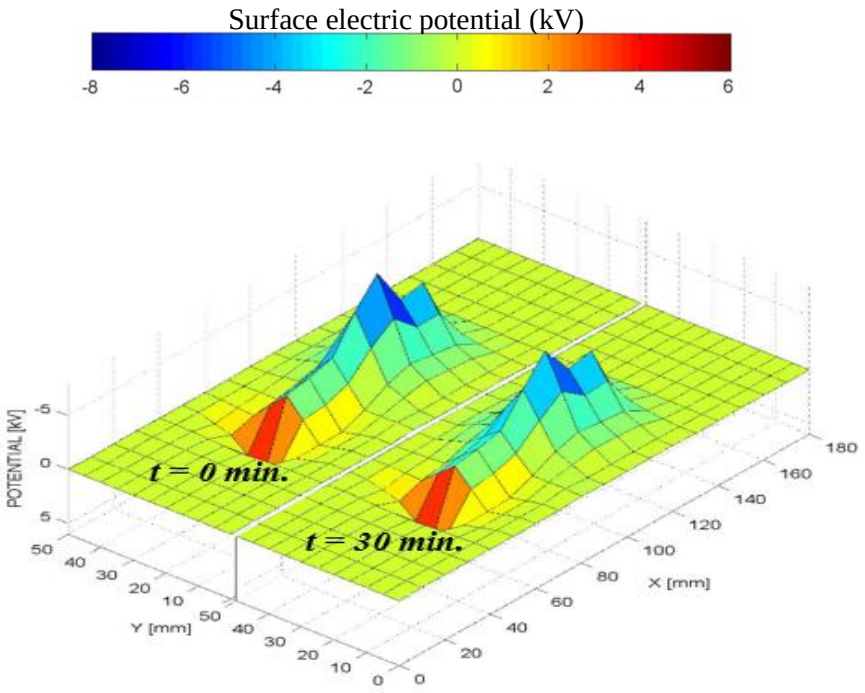

Figure III-25. Polyvinyl chloride (PVC) surface potential after conformal-contact tribocharging with acrylonitrile-butadiene-styrene (ABS).

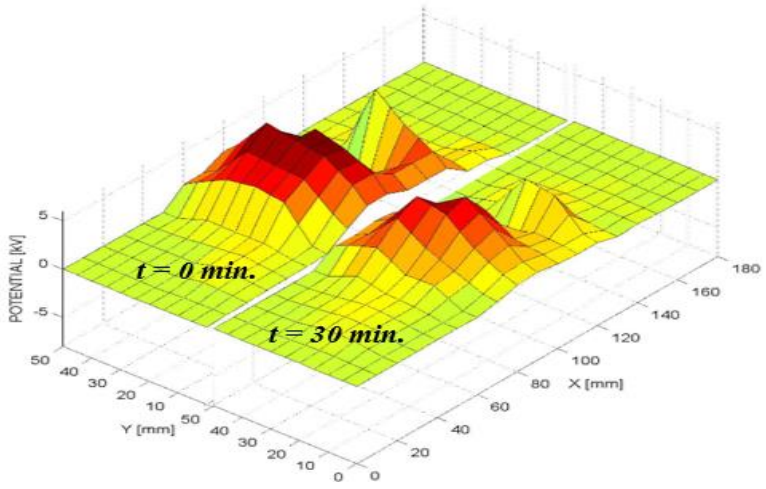

Figure III-26. Acrylonitrile butadiene styrene (ABS) surface potential after conformal-contact tribocharging with polyvinyl chloride (PVC).

Long-duration surface potential decay experiments (8 and 72 hours) confirm the fact that the materials considered in this study are very good insulators. Typical decay rates of 1% per hour are recorded for the first 8 hours after corona- or tribocharging process.

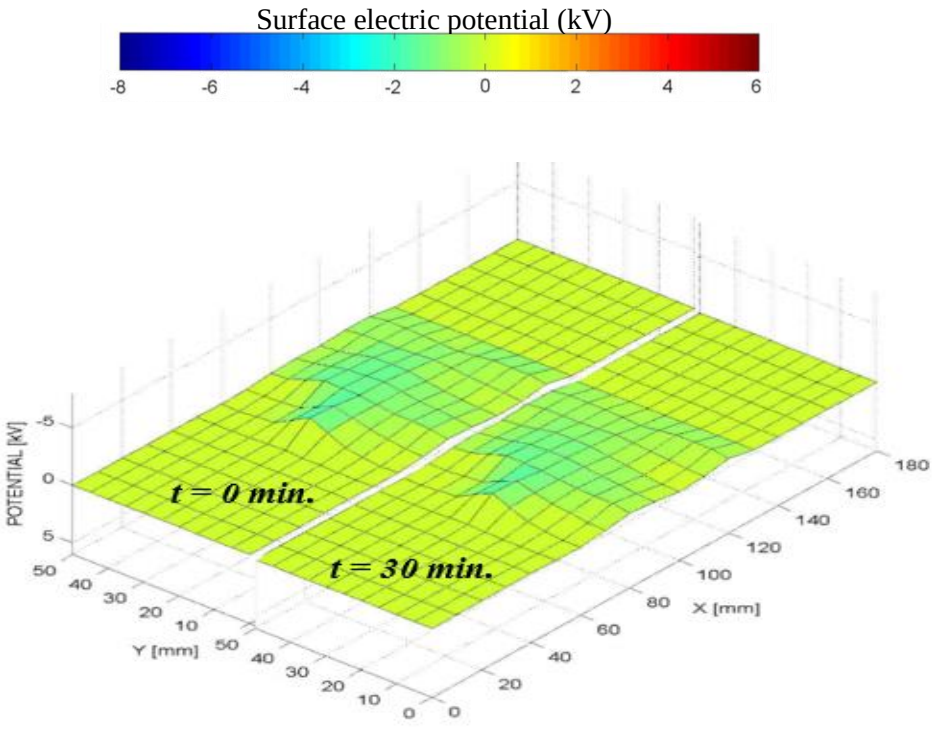

Figure III-27. Polyvinyl chloride (PVC) surface potential after conformal-contact tribocharging with polypropylene (PP).

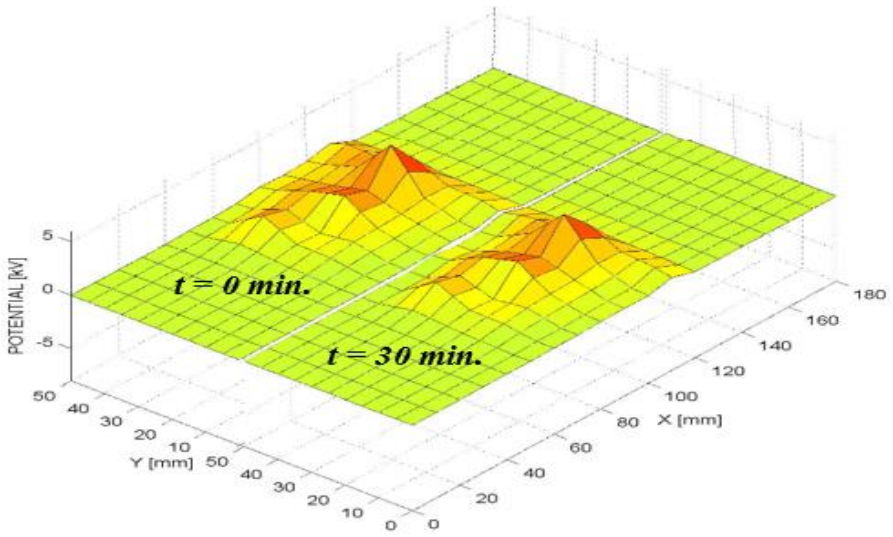

Figure III-28. Polypropylene (PP) surface potential after conformal-contact tribocharging with polyvinyl chloride (PVC).

The charging state remains practically stable after that, except for the cases when changes occurred in the ambient conditions (increase of relative humidity).

III.2.2. Decay of the electric potential at the surface of corona-charged polymers

The electric potential at the surface of corona-charged ABS, PP and PVC samples display was more uniformly distributed (**Figure III-29**) The lateral extension of the charged area was roughly 55 mm, as imposed by the grounded aluminum shield as described in **§II.2.3**.

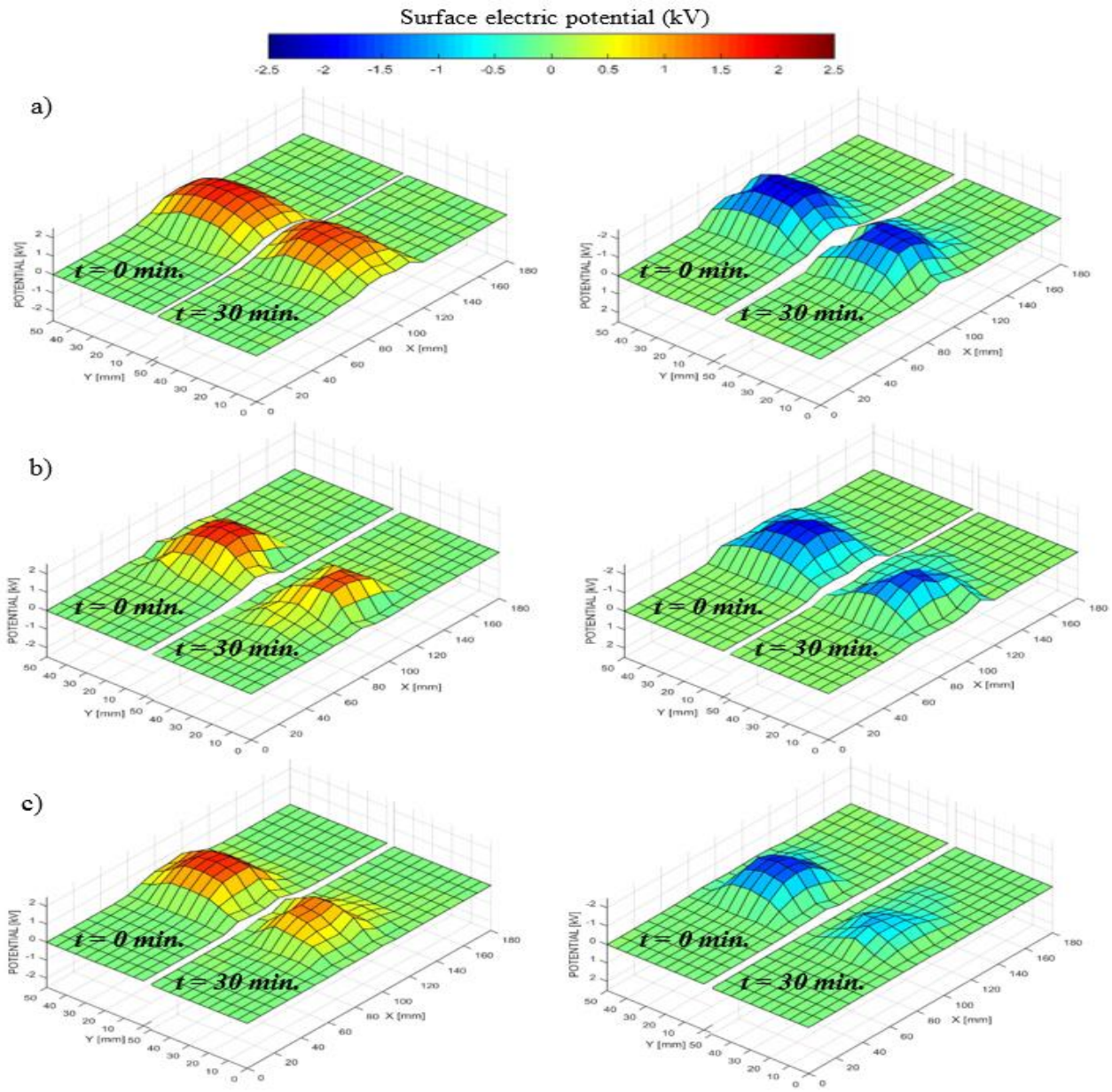

Figures III-29. Cartography of the electric potential at the surface of polymers at t = 0 s and t = 30 min after corona-charging using a 2 kV grid voltage of positive (left) and negative (right) polarity on: a) acrylonitrile-butadiene-styrene (ABS), b) Polypropylene (PP), and c) Polyvinyl chloride (PVC).

The cartographies were obtained at t = 0 and t = 30 min, after corona-charging the samples using a grid voltage of 2 kV of either positive or negative polarity.

The analysis of surface potential decay for the three polymers after tribo- or corona-charging was performed by comparing the highest, the lowest and the average values measured in the above-described experiments. (**Figures III-30 to III-33**). The curves **in Figures III-30 and III-31** show significant differences in the pattern of surface potential decay.

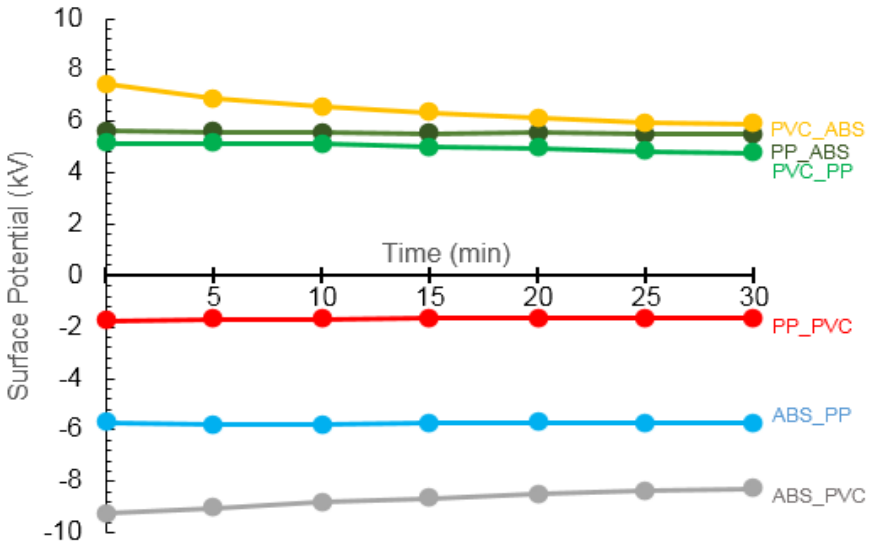

Figure III-30. Highest value potential decay, for the tribocharged polymers (the curves were recorded for the material that is listed second in the couple "top sample/bottom sample")

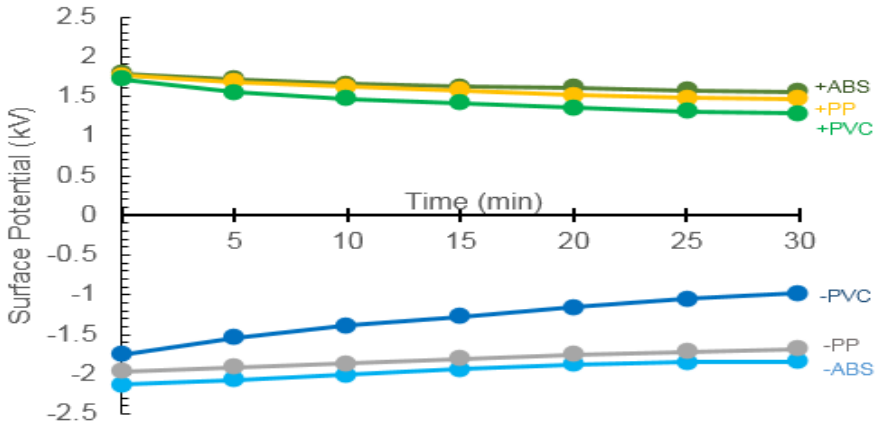

Figure III-31. Highest value potential decay at the surface of positively- or negatively-corona-charged polymers.

Thus, for the ABS sample tribocharged by rubbing against PVC, the highest value of the recorded surface potential decayed by 1.5 kV in 30 min. For PVC sample rubbed against PP, the decay is of only 0.1 kV. PP samples showed the slowest rate of surface potential decay after rubbing against ABS (0.01 kV, after 30 min) and against PVC (0.3 kV) as well after corona-charging (0.2 kV).

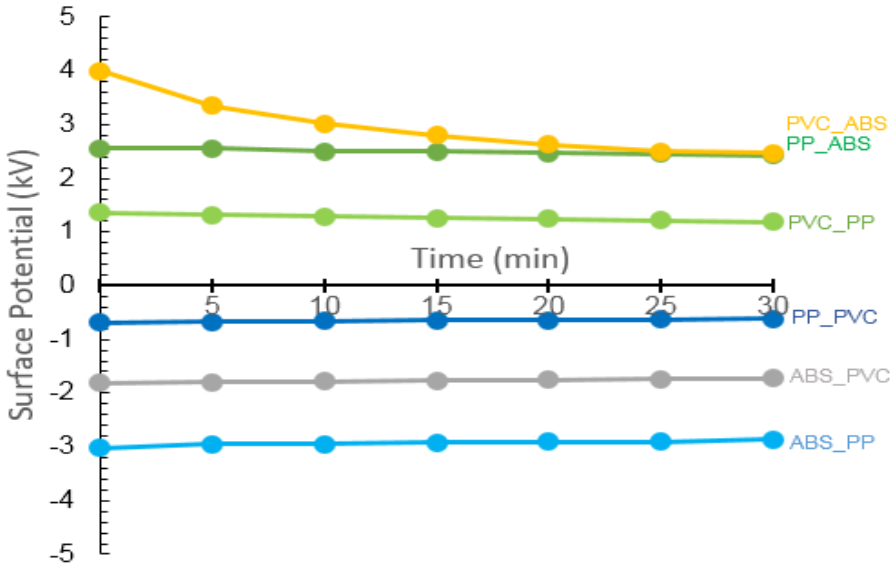

Figure III-32. Average value potential decay, for the tribocharged polymers (the curves were recorded for the material that is listed second in the couple "sample A/sample B")

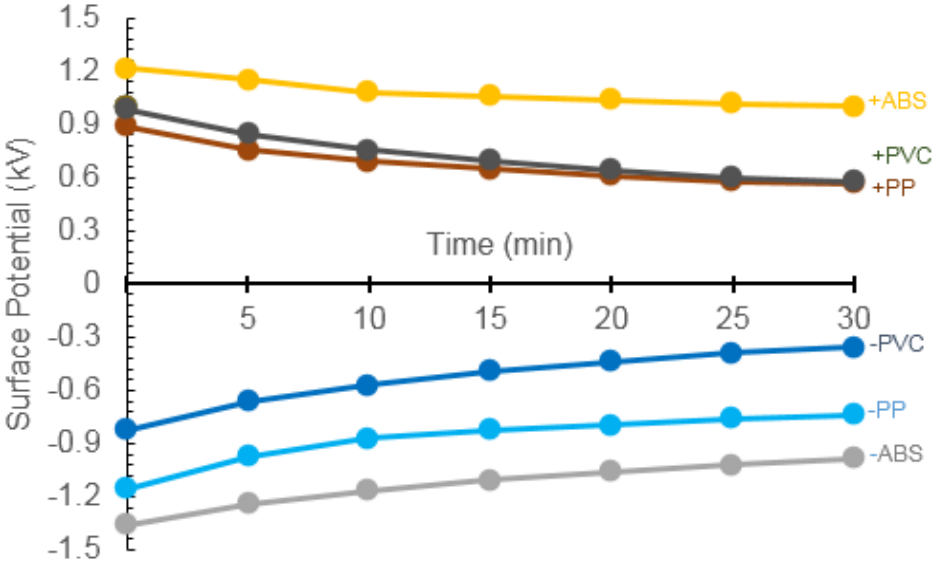

Figure III-33. Average value potential decay at the surface of positively- or negatively-corona-charged polymers

The average values of the potential measured in 25 points located in the central area of the sample are represented in **Figures III-32** and **III-33**. The values recorded for the tribocharged samples decay at a relatively slower rate than those of corona-charged similar materials. There are at least two explanations for this:

(1) The nature of charge carriers is not the same in the case of tribo-charging and positive or negative corona-charging processes. Tribocharging, which is accompanied by structure fracture of polymers chains at the surfaces in contact, may involve simultaneously electron, ion and substance transfer between the two bodies [160]. Corona- charging is produced by the different ion species generated in the electric discharge, in atmospheric air [161].

(2) The corona discharge is known to reduce the surface resistivity of polymers [162–165]. Tribocharging may also affect the surface resistivity, as the temperature rise related to friction is not negligible. However, under the conditions of these experiments, the resistivity reduction due to temperature rise seems to be less significant than that produced by the exposure to the corona discharge.

A finer analysis of the situation can be done in relation with the surface potential decay curves obtained for the 9 central points with 10 mm distance between the points indicated in **Figure III-34**. The results of several series of SPD measurements in the nine points of a tribo-charged A-type sample are given in **Figure III-35**. The initial values of the electrical potential V_0 were significantly different in each point. The SPD was steeper in points characterized by higher initial values V_0. In point (e), for which V_0 was very low, the electric potential increased in time, indicating that a redistribution of charge took place at the surface of the sample.

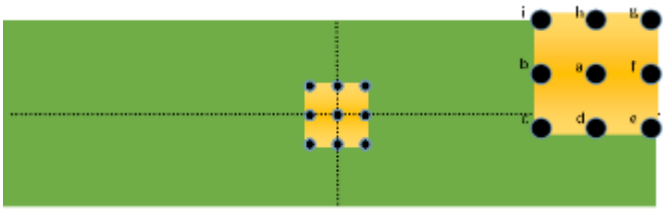

Figure III-34. Position of the 9 points in which the SPD measurements were performed for each tribo- or corona-charged B-type sample.

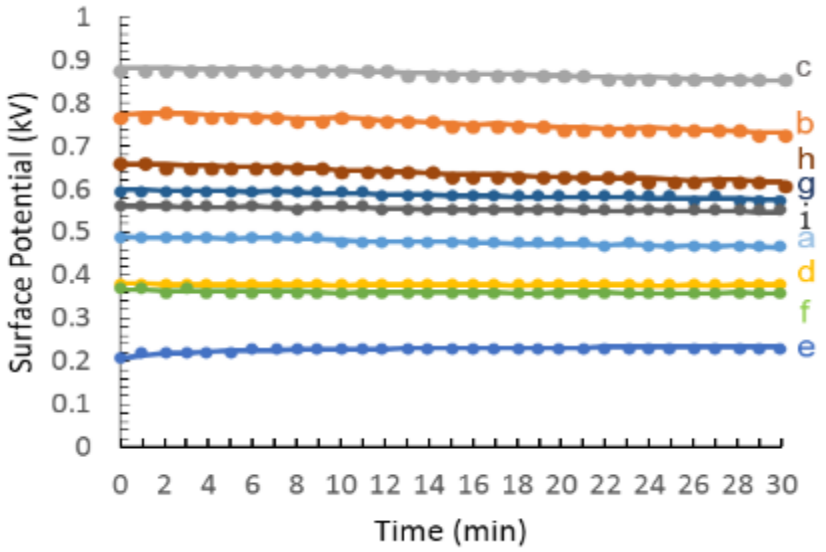

Figure III-35. SPD in 9 points at the surface of a tribo-charged B-type PVC sample.

Figure III-36 shows the SPD curves obtained for a corona-charged A-type PVC sample. The decay rate in the various points was practically the same. Corona discharge mechanism generates a much more uniform surface potential distribution, which causes a reduced charge transfer from one point to another.

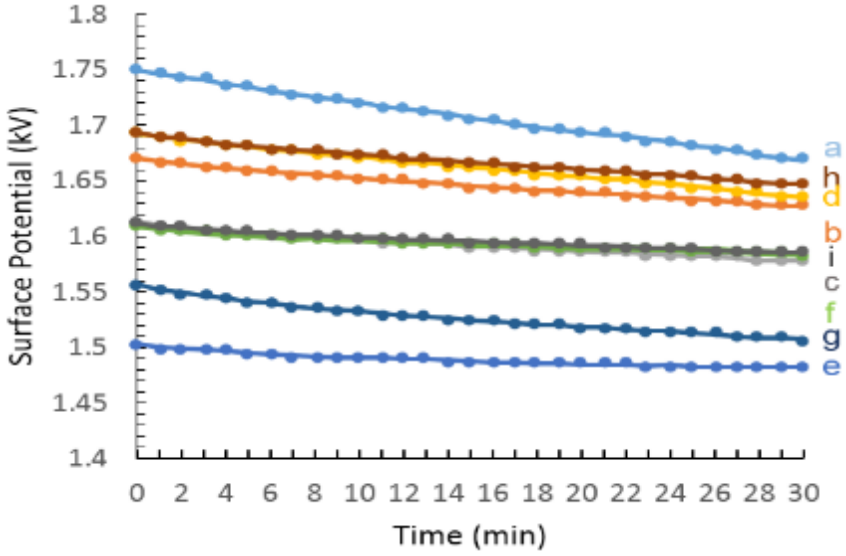

Figure III-36. SPD in 9 points at the surface of a corona-charged B-type PVC sample.

Indeed, the standard deviation of the electric potential values measured on tribocharged samples was significantly higher than that of corona-charged samples. For instance, the standard deviation of the highest electric potential value recorded for tribocharged ABS samples was 484 V, more than 10 times higher than for the respective corona-charged samples: 31 V. As for the average values of the electric potential at the surface of ABS samples, the standard deviation in the two situations under investigation, i.e. tribo- and corona-charged, was 111 V and 23 V, respectively.

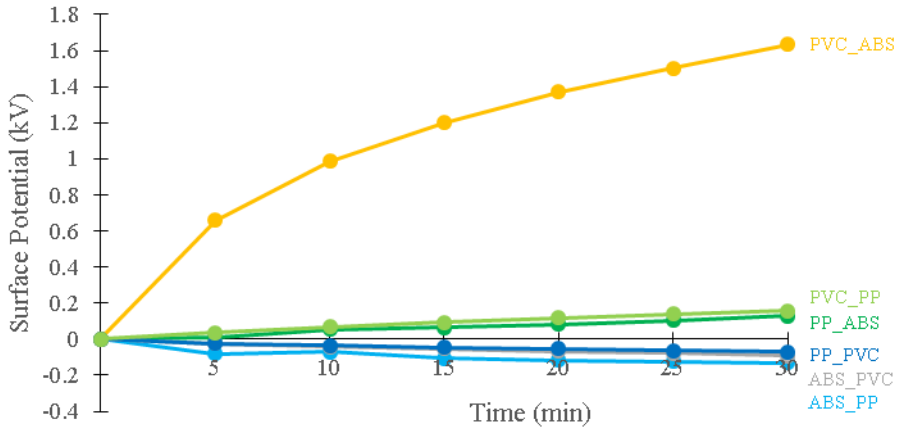

Figure III-37. SPD Relative value of average potential decay for tribocharged polymers

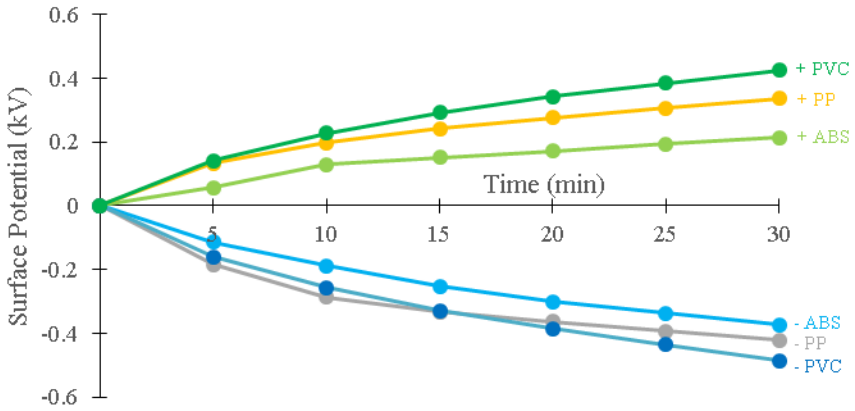

Figure III-38. SPD Relative value of average potential decay for corona charged polymers

Figure III-37 and Figure III-38 explain the relative value of average potential decay on tribocharged and corona charged samples respectively to clearly characterized the decay behavior in different polymers and processes.

III.3. Conclusions

Tribocharging properties are influenced by several factors. Thus, the materials with higher hardness and modulus of elasticity require higher normal force to achieve higher surface potential through tribocharging effect. Several process variables, such as normal force applied, the number of cycle and sliding speed, can be easily controlled, so that to provide the optimum outcome of the tribocharging process.

Both the temperature of the material and that of the environment may affect the electrostatic charging process beside its effect. Specimens with higher initial temperature acquire less triboelectric charge. Lower levels of charge are also recorded when the tribocharging process is performed at high ambient temperature and relative humidity.

As a good correlation exists between the cartographies of the electric potential and of the temperature field, it is possible to use thermal field maps as a method of identifying the contact area or wear track.

Surface texture and roughness affect the friction conditions. They can also increase the generation of electric charge by triboelectric effect. This aspect should be taken into account in the design of the machine parts or of triboelectrostatic energy harvesters.

The electric potential at the surface of tribocharged polymers is less uniform than in the case of corona-charged sample. On the other hand, the electric potential at the surface of tribocharged samples decays slower and is more stable. This comparative study indicates that the corona discharge represents a better way to electrically charge the surface of polymers than the more random and less stable in time triboelectric effect.

CHAPTER IV

OPTIMIZATION AND STATISTICAL PROCESS CONTROL OF TRIBOCHARGING PROCESS

The experiments presented in chapter III pointed out that the triboelectrification processes is affected by several factors that could be adjusted in laboratory condition, for instance the normal force applied, the number of rubbing cycles and the relative speed between the bodies in contact.

Design of experiment (DOE) methodology has been used in IV-1 to find out the optimum values of the control variables of the tribocharging process, at a minimum cost. The application of Response Surface Modelling (RSM) reduces the number of experiments needed for process optimization [166]. The results obtained from RSM were then used to carry out a series of experiments that enabled the evaluation of the capability of the tribocharging process and the set-up of appropriate control charts. These experiments are described in IV-2 and pave the way to the use of Statistical Process Control (SPC) in monitoring the operation of tribocharging devices.

IV.1. Experimental modelling and optimization

Response Surface Modelling was used to optimize the tribocharging process, after having evaluated the effects and the interactions between the control factors. Two types of samples (Top): 5 mm x 15 mm x 100 mm and (Bottom): 5 mm x 50 mm x 180 mm were employed for the tribocharging experiments. They were cut from two different polymers: Polyvinyl chloride (PVC) and Acrylonitrile butadiene styrene (ABS). The residual charge at the surface of these samples was neutralized using a commercial ionizing system. Tribocharging was done using the custom-designed experimental bench presented in **§II.2.1**, to generate the electric charge by friction between a pair of samples (top and bottom), in conformal contact. The cartography of the electric potential at the surface of the tribocharged sample, disposed on grounded plate, was recorded using an electrostatic probe connected to an electrostatic voltmeter, according to the arrangement described in **§II.2.4**.

IV.1.1. Design of experiments

Three factors were taken into account in this study: contact force, number of charging cycles and frequency of back-and-forth sliding motion. The domains of variations of the three factors were established as follows:

- Contact force (F_N): 2 - 10 N; within this range, a good contact was established between the two surfaces, which led to a measurable electrical potential without blocking the movement between the two samples;
- Number of charging cycles (cy): 10 – 100 cycles; the repetition of back-and-forth movements of the samples put into evidence the saturation of the triboelectric charge as well as the wear phenomenon;
- Frequency (f): 0.5 Hz (55 mm/s) – 2.5 Hz (275 mm/s), the lower and upper limit being fixed by the kinematic characteristics of the experimental bench.

The relative humidity and the ambient temperature were difficult to adjust but were kept keep between reasonably narrow limits: 45% to 50% and 24°C to 26°C, respectively. Surface texture and roughness were relatively the same for all samples [157].

The three responses considered in the study were: (1) the average surface potential (*Vavg*) measured in 25 points of the area of tribocharging (50 mm x 50 mm) as described in § II-2.4; (2) the relative standard deviation (*RSD*), i.e., the ratio of the standard deviation (σ) to the absolute value of average value ($\bar{x}$); (3) the difference between post- and pre-tribocharging temperature ($\Delta temp$).

The results of the 17 experiments performed according with a three-factor Central Composite Face-Centered (CCF) design are given in Table IV-1.

Table IV-1. Worksheet of CCF factorial experimental design.

Exp No.	Run Order	Cycle	Normal Force (N)	Frequency *f* (Hz)	Average Potential (V)	RSD (%)	Delta Temp (°C)
1	3	10	2	0.5	-464	48	0.3
2	9	100	2	0.5	-883	65	1.1
3	1	10	10	0.5	-1619	29	0.7
4	15	100	10	0.5	-2264	32	2.6
5	14	10	2	2.5	-903	27	0.3
6	11	100	2	2.5	-1036	56	3.4
7	17	10	10	2.5	-1316	20	1
8	6	100	10	2.5	-1674	35	5.3
9	13	10	6	1.5	-1038	42	0.8
10	16	100	6	1.5	-1427	58	3.3
11	10	55	2	1.5	-799	51	1.3
12	12	55	10	1.5	-1695	31	2.4
13	2	55	6	0.5	-1279	49	1.3
14	7	55	6	2.5	-1203	40	2.5
15	8	55	6	1.5	-1200	48	2
16	5	55	6	1.5	-1198	47	1.9
17	4	55	6	1.5	-1221	48	2

IV.1.2. Results and discussions

Figures IV-1 to **IV-3** show the cartography of electric potential at the surface of PVC sample after rubbing with ABS, for three values of the frequency of back-and-forth sliding frictional motion: 0.5 Hz, 1.5 Hz, and 2.5 Hz, respectively. These experimental data were analyzed with the MODDE 5.0 software (Umetrics, Sweden).

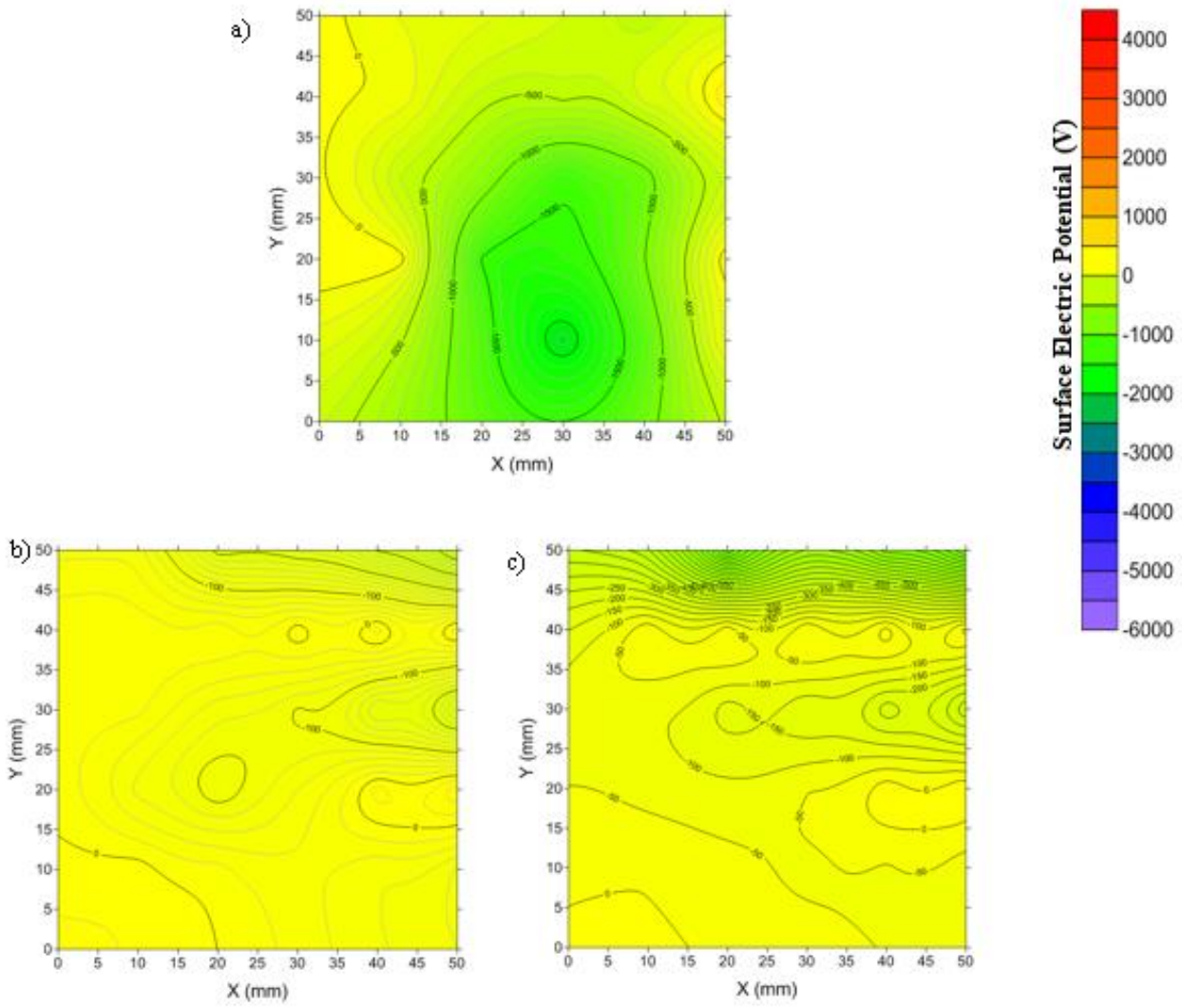

Figure IV-1. Surface electrostatic potential cartography at Frequency 0.5 Hz: a) F_N = 10 N for 10 cycles, b) F_N = 2 N for 10 cycles, and c) F_N = 2 N for 100 cycles.

Figure IV-1a shows that the electric potential generated by 10 N of normal force, after 10 cycles and at a frequency of 0.5 Hz, can reach ± 2 kV with *Vavg* = -1619 V The non-uniformity of the distribution of the surface potential indicated by RSD was 29% which was less than 48% and 65% calculated for the cases illustrated on **Figures IV-1b** and **1c**, where a normal force of 2 N had been applied for 10 cycles and 100 cycles, respectively. Moreover, the average electric potential was also relatively low that is -464 V and -883 V after respectively 10 cycles and 100 cycles, at the lowest value of the sliding speed (i.e., a frequency of 0.5 Hz).

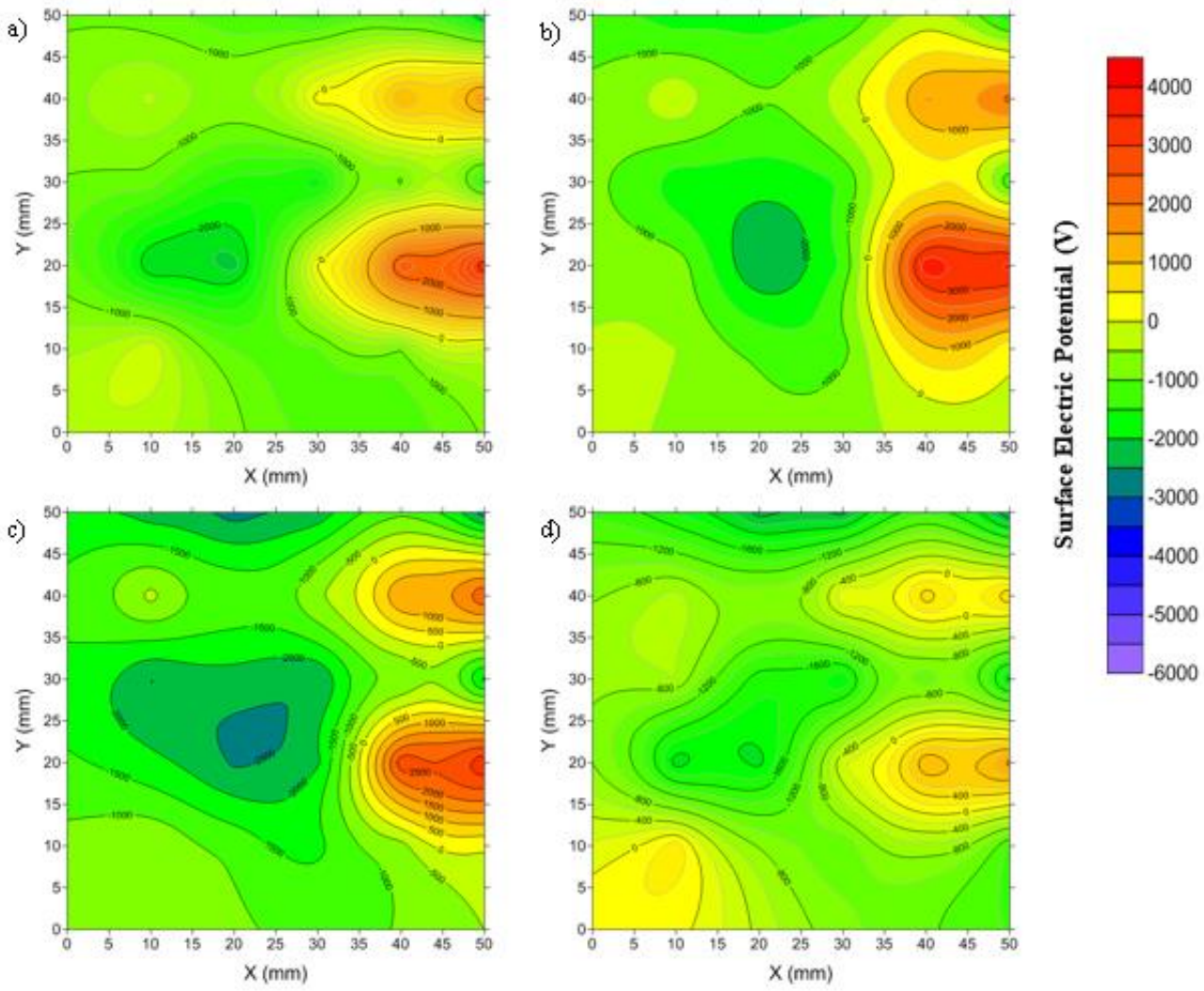

Figure IV-2. Surface electrostatic potential cartography at Frequency 1.5 Hz: a) to c) F_N = 6 N for 55 cycles, and d) F_N = 6 N for 10 cycles.

In the Central Composite Face-centered design, there are three repetitions for the central values of the control factors, i.e., at a frequency of 1.5 Hz and a normal force of 6 N, for 55 cycles. **Figure IV-2a** to **2c**. They indicate similar results for all three responses. For instance, the surface average potential was ranging between -1198 V to -1221 V, and the surface temperature rise was only of about 2°C.

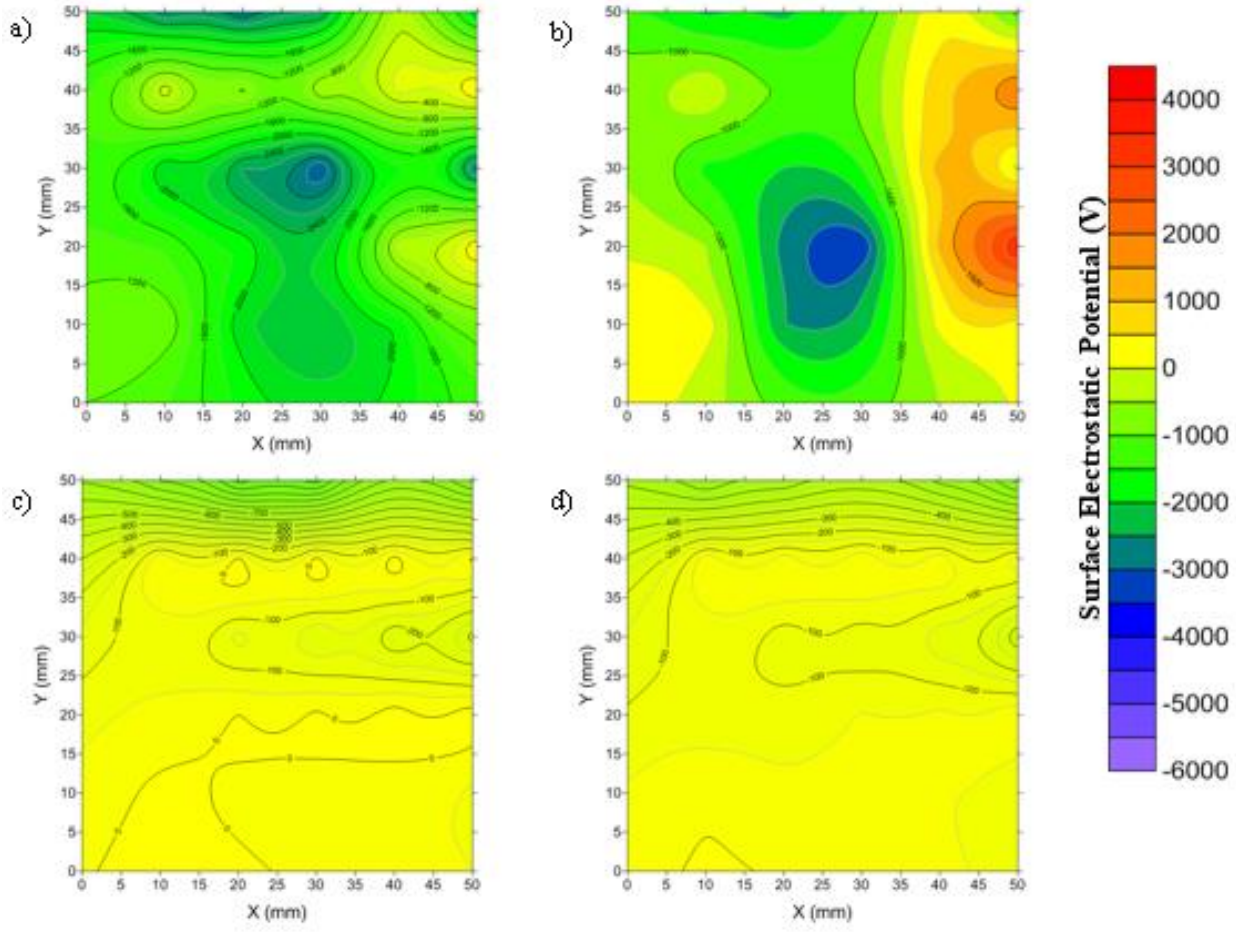

Figure IV-3. Surface electrostatic potential cartography at Frequency 2.5 Hz: a) F_N = 10 N for 10 cycles, b) F_N = 6 N for 55 cycles, c) F_N = 2 N for 100 cycles, and d) F_N = 2 N for 10 cycles.

The effect of the normal force and the number of cycles on the tribocharging process was also confirmed at high sliding speed (i.e., a frequency of 2.5 Hz). **Figures IV-3a** and **3b** show the high values of surface electric potential in the center area of contact either for 10 N of normal force at 10 cycles or 6 N of normal force at 55 cycles. In the latter case, the surface potential was of opposite polarity in the area where the specimens were in contact just before being separated at the end of the rubbing process. Much lower values of electric potential were measured at low normal force (**Figures IV-3c** and **3d**).

The regression models of the average surface potential (*Vavg*), relative standard deviation (*RSD*) and pre- and post tribocharging temperature difference (ΔT) were:

$$Vavg = -1214.89 - 153.69 * Cyc - 354.41 * Fn + 29.80 * Freq - 15.99 * Fn^2 - 12.43 * Freq^2 - 35.23 * \text{Cyc} * Fn + 44.77 * \text{Cyc} * Freq + 116.02 * Fn * Freq \quad \text{(IV-1)}$$

$$RSD = 47.85 + 6.42 * Cyc - 7.96 * Fn - 3.63182 * Freq - 3.37 * Fn^2 - 2.07 * Freq^2 - 2.22 * Cyc * Fn + 1.88 * Cyc * Freq + 1.88 * Fn * Freq \quad \text{(IV-2)}$$

$$\Delta T = 1.97 + 0.99 * Cyc + 0.44 * Fn + 0.51 * Freq - 0.06 * Fn^2 + 0.18 * Cyc * Fn + 0.37 * Cyc * Freq + 0.05 * Fn * Freq \quad \text{(IV-3)}$$

where $Cyc, Fn, Freq$ respectively are the number of cycles, the normal force and the frequency.

The coefficients R^2 for the regression models obtained with MODDE 5.0 for the average potential, the relative standard deviation and the temperature difference were close to 1 (1, 0.994 and 0.999 respectively), which means that the first order polynomials appropriately describe the triboelectric charging process. The coefficients Q^2 are also satisfactory: 0.945, 0.923 and 0.874 respectively, which means that the models have a good predictive quality.

The coefficient plots for these functions are given in **Figure IV-4**. They show that: (1) the average surface potential increases significantly with both the number of cycles and the normal force applied, but decreases with the frequency of the back-and-forth movements; (2) the relative standard deviation decreases with normal force applied and frequency, however increasing of the number of cycles will increase this percentage, which means that the surface potential is non-uniformly distributed; (3) increasing of surface temperature also increases with these three factors, especially with the number of cycles.

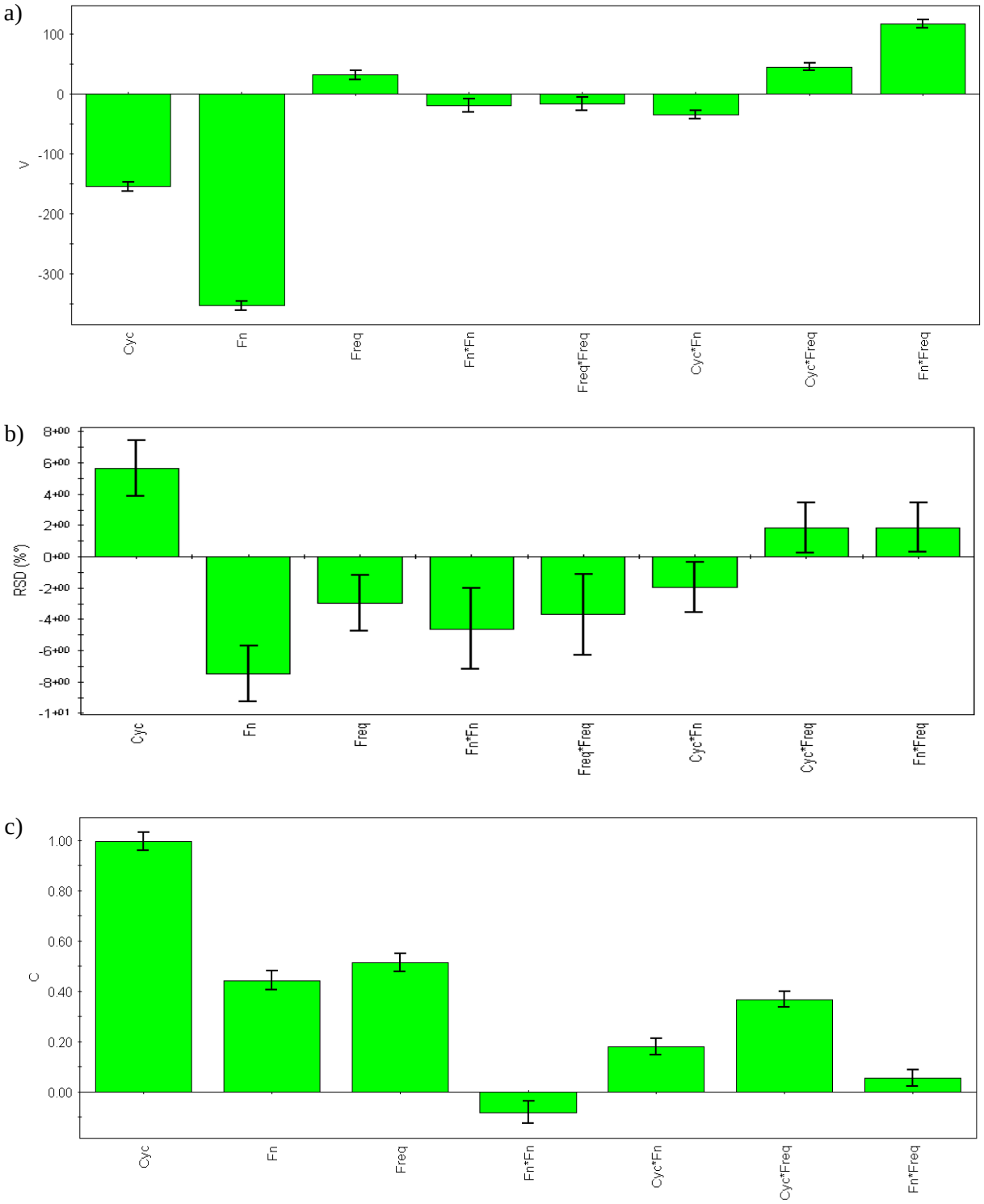

Figure IV-4. Coefficient plot of a) average surface potential, b) RSD and c) ΔT

The response contour plots in **Figures IV-5** to **IV-7** illustrate the effects of each factor and the interaction between them. **Figure IV-5** shows the effect of the number of cycles and the normal force. The generation of electrostatic charge increases with the normal force and the number of cycles for each of the three different frequencies. However at high frequency the maximum predicted surface potential is only -1600 V which, lower than the value of -2100 V expected at low frequency. This is most likely related to the shorter time of contact between two surfaces.

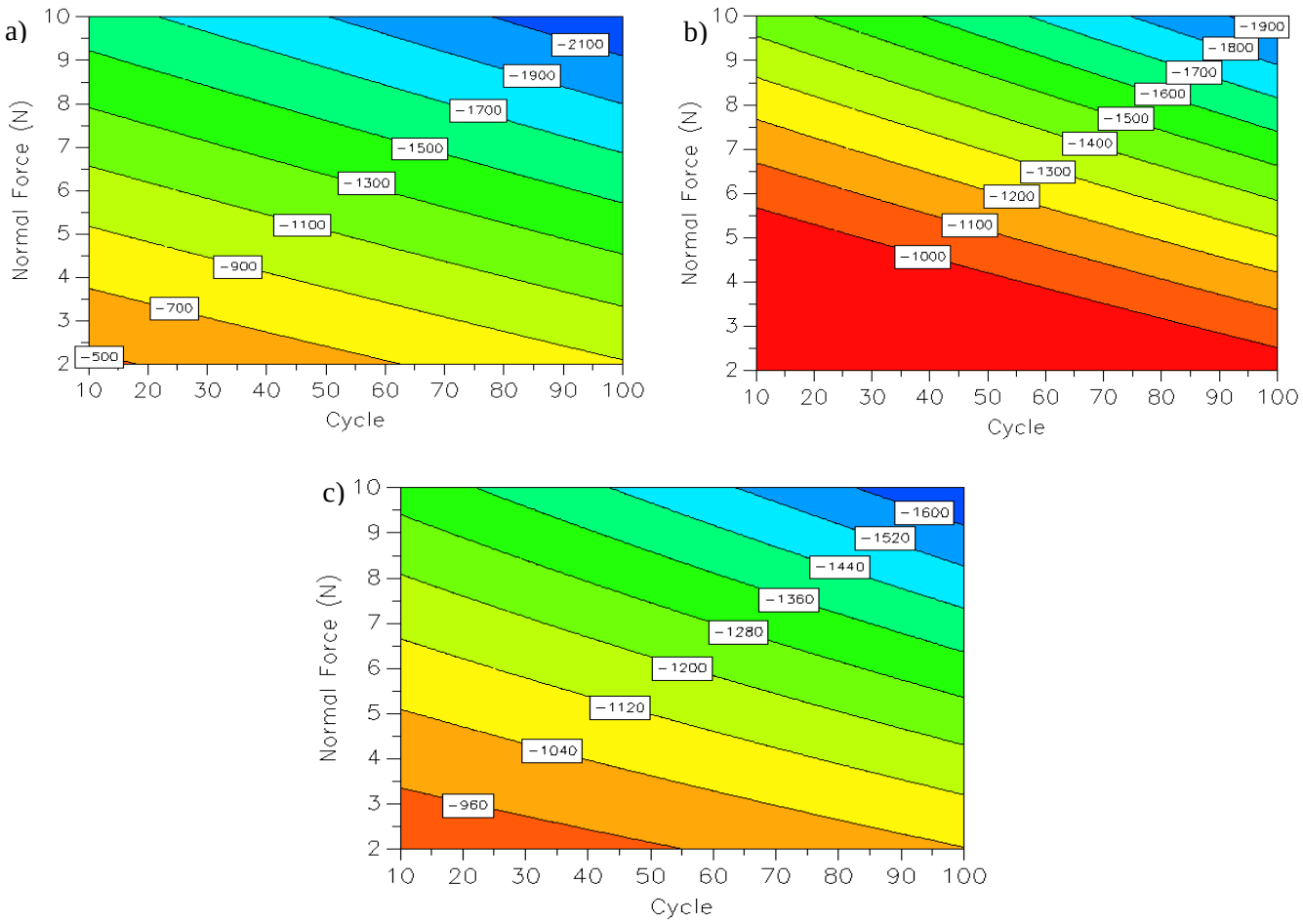

Figure IV-5. Iso-response curves predicted by MODDE 5.0, for average of surface electrostatic potential generated by triboelectric charging process at a) 0.5 Hz, b) 1.5 Hz and c) 2.5 Hz as functions of the normal force applied and the number of cycles.

Relative standard deviation (RSD) contour plot as a function of normal force and the number of cycle is shown in **Figure IV-6**. RSD which characterizes the non-uniformity of the potential distribution increases with the number of cycle at frequencies in the range of 0.5 to 2.5 Hz, however increasing of normal force applied together with sliding speed may produce typically more uniform of potential distribution. The fact that charge generated at the sample increases due the expansion of real contact area or intimate contact between two surfaces, therefore the result of quadratic model from coefficient plot indicates the complexity of the relation between the factors, which mean at some point the results of RSD may be contradictory.

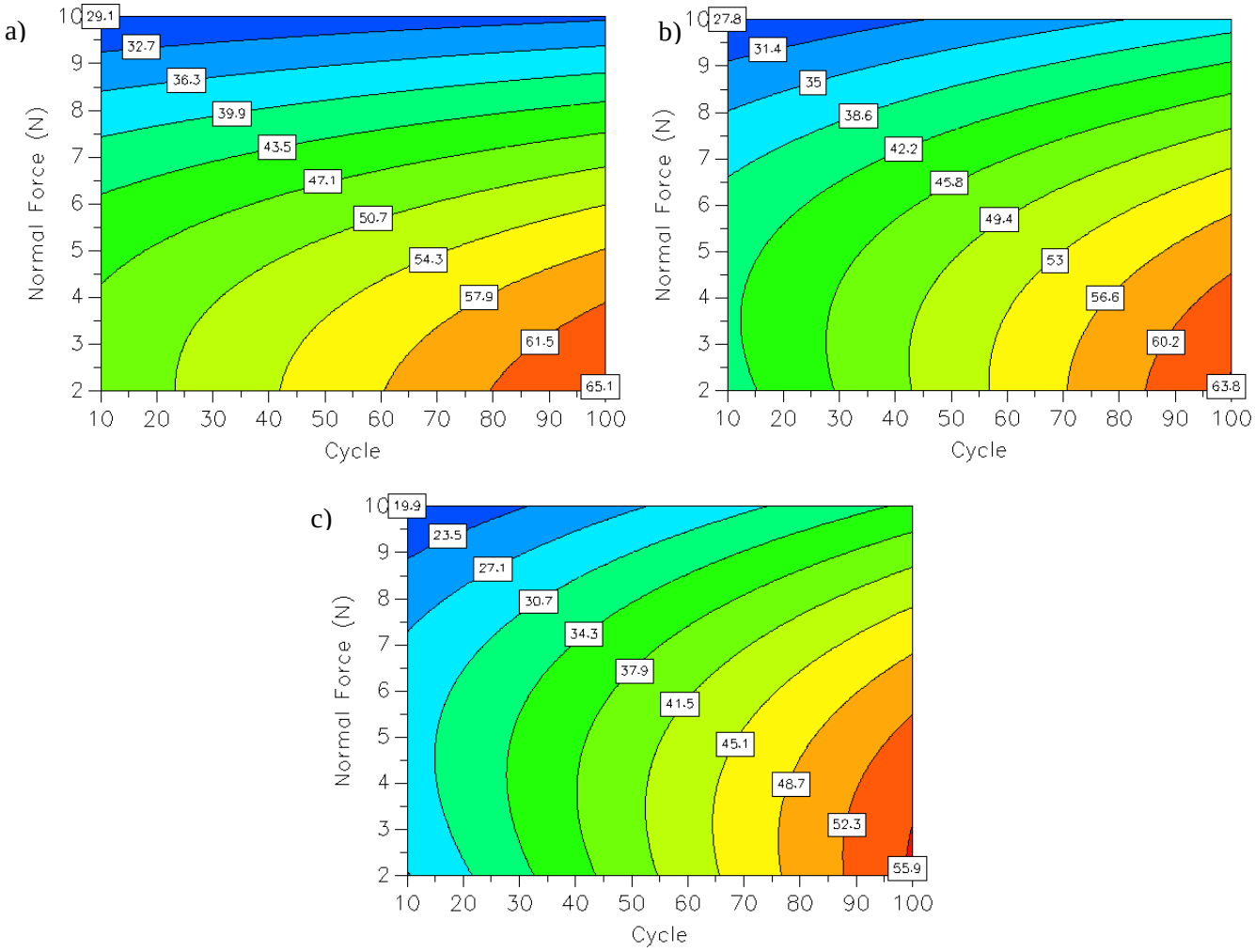

Figure IV-6. Iso-response curves predicted by MODDE 5.0, for relative standard deviation of electrostatic potential generated by triboelectric charging process at a) 0.5 Hz, b) 1.5 Hz and c) 2.5 Hz as functions of the normal force applied and the number of cycles.

Compared with other responses, surface temperature increases due tribocharging process was easier to characterize, since it increases with all the factors studied. **Figure IV-7** shows the increasing of surface temperature after tribocharging processes as function of the normal force and the number of cycles within different frequency. It defined a predicted maximum temperature rise of 4.7 °C at 2.5 Hz while at lower frequency, 0.5 Hz, this is limited at 2.4 °C.

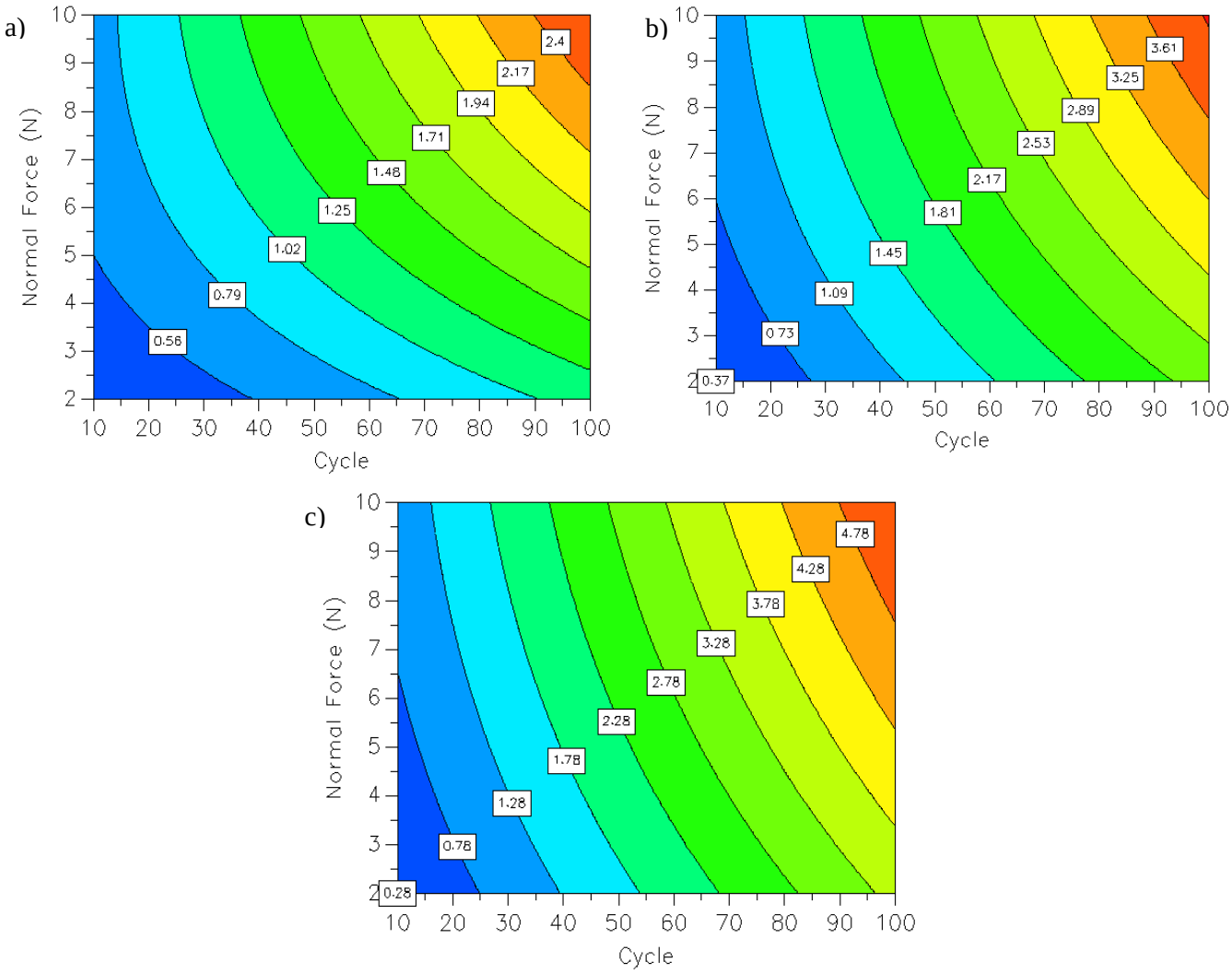

Figure IV-7. Iso-response curves predicted by MODDE 5.0, for surface temperature increase due triboelectric charging process at a) 0.5 Hz, b) 1.5 Hz and c) 2.5 Hz as functions of the normal force applied and the number of cycles.

Optimizer tool of the software MODDE 5.0 was then used to find the best values of the factors to minimize the responses (minimum average potential means maximum absolute value of charge generated). **Figure IV-8** shows this process; the result of 180 iterations is that the best tribocharging is obtained by applying 10 N of normal force for, 10 cycles at frequency 0.5 Hz,. The predicted optimal responses were -1620 V for the average surface potential, 29% for the RSD and 0.7 °C for the surface temperature rise.

a)

Iteration: 262 Iteration slider:

	1	2	3	4	5	6	7	8
	Cycle	Normal Force	Frequency	Average Potential	%RSD	DeltaTemp	iter	log(D)
1	10	2	2.5	-904.703	26.8943	0.2777	211	1.4106
2	10	10	0.5	-1620.7	29.0626	0.7015	180	1.2295
3	10	8.5481	1.2393	-1314.98	34.5997	0.8335	201	1.3783
4	48.1828	9.9603	0.5	-1876.69	30.6655	1.4915	197	1.2316
5	10.0001	9.8553	0.5008	-1597.84	29.7914	0.7017	262	1.2446
6	10.0027	2.2848	2.5	-915.879	27.3846	0.3162	237	1.4112
7	10	10	0.5	-1620.7	29.0626	0.7015	180	1.2295
8	10	2	2.5	-904.703	26.8943	0.2777	211	1.4106

b)

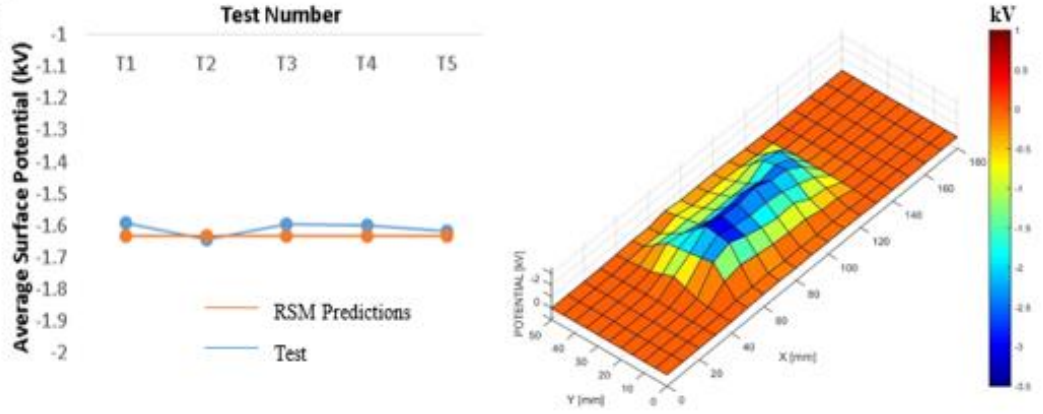

Figure IV-8. a) MODDE 5.0 Optimizer result and b) Five experiments to confirm the prediction of MODDE 5.0 optimizer and one of the surface potential mapping.

Prior to conducting an experiment to check the optimal point: number of cycle 10 times, applied normal force 10 N, and frequency 0.5 Hz, it is recommended to plot the respective response surfaces, as in **Figure IV-9**. In the center of these plots, the average surface potential is in the range -1625 V to -1756 V, relative standard deviation may vary between 29.5 V to 30.8 V and temperature difference is within the limits 1.3°C to 1.8°C.

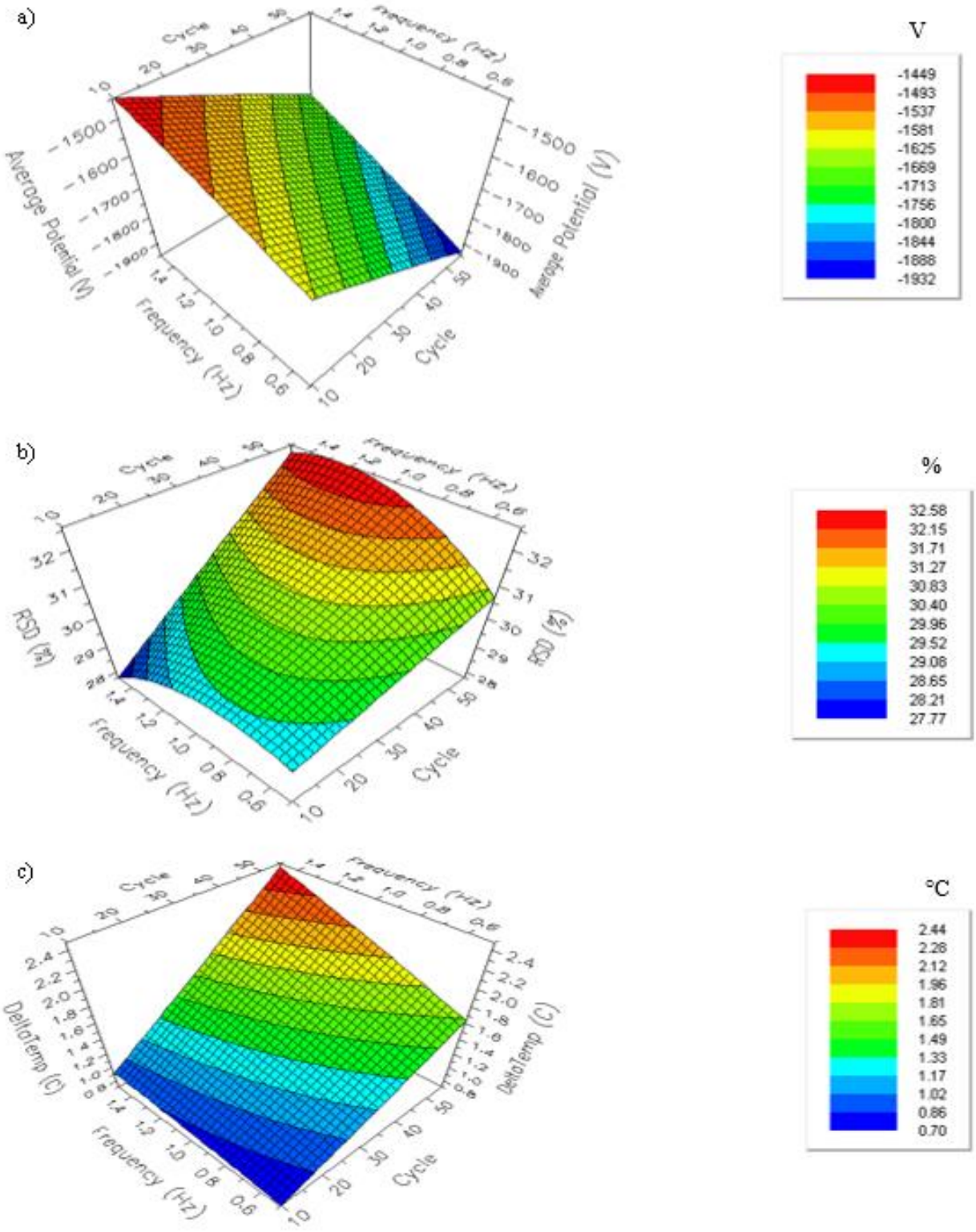

Figure IV-9. Prediction response surface plot at 6 N applied normal force for a) average potential, b) RSD and c) ΔT

IV.2. Statistical process control

SPC techniques were used to monitor the tribocharging process [167]. Thus, 30 experiments were performed for the optimal combination of control factor values. These values, which had been established using the design of experiments methodology, were the following: normal force: 10 N; sliding speed: 55 mm/s; number of sliding cycles: 10. The results of the 30 experiments were analyzed with Grubbs' test to detect the outliers. Process Capability Ratio (PCR) was expressed by several statistics, namely *Cp*, *Cpk*, and *Cpm*, which assume that the population of data values is normally distributed.

Process capability Cp and *process performance index Cpk* are unsatisfactory if their values are below 1. The capability and the performance of a process are commonly considered as low if less than 1.33, medium when their values are in the range 1.33 to 1.66, and high if beyond 1.66. Taguchi index *Cpm* is the improvement of *Cp* and *Cpk*, as it directly takes into consideration the bias from the target.

The relative dispersion of the values measured in the 25 points as described on § II-2.4 at the surface of each sample can be characterized by the coefficient of variation that is calculated as the ratio between the standard deviation S_x, and the mean value X.

IV.2.1. Measurement and data collection

An example of cartography of the electric potential at the surface of ABS sample is shown in **Figure IV-10.** The graphical representation of first, fifteenth and thirtieth test are based on the results of the measurements performed in 25 points at the surface of the sample. The non-uniformity of surface potential distribution reflects the non-uniformity of the tribocharging, most often due to the fact that the mechanical load is unevenly distributed. The values of the electric potential measured along the line L3 are several times more elevated that on L1 and L5, which means that the friction between the two samples was more intense in the center.

The results of the 30 tribocharging experiments are listed in Table IV-2. With the coefficient of confidence c = 1.28 describe on § II-3.2, Grubbs' test was performed and no erroneous data was found: the values of G calculated for both the maximum and minimum values of the 30 measurements were below G_{crit}

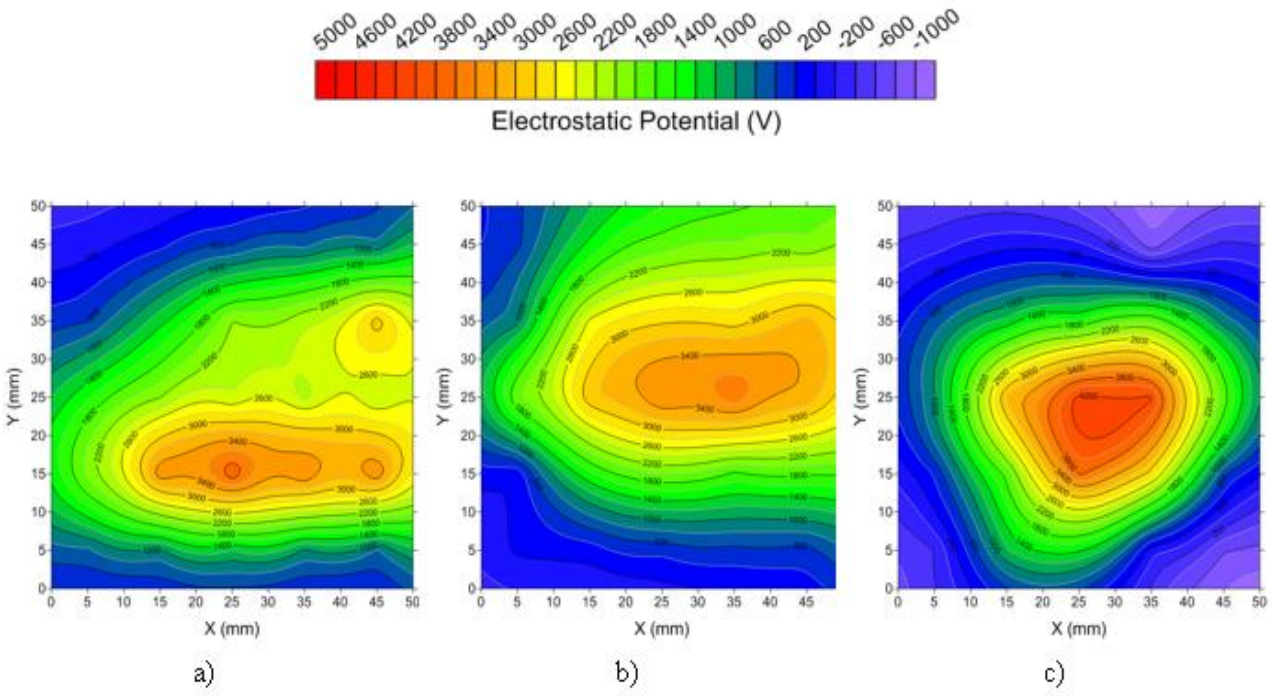

Figure IV-10. Surface electrostatic potential cartography of ABS sample after tribocharging with PVC, the test number a) first, b) fifteenth and c) thirtieth.

$$G = \frac{1690 - 1275}{1.28 \times 124} = 2.61 \qquad \text{(IV-4)}$$

$$G = \frac{1937 - 1690}{1.28 \times 124} = 1.55 \qquad \text{(IV-5)}$$

The capability indexes were then calculated as follows:

$$Cp = \frac{2400 - 1000}{6 \times 1.28 \times 124} = \frac{2400 - 1000}{6 \times 159} = 1.47 \qquad \text{(IV-6)}$$

$$Cpk = Min\left(\frac{2400 - 1690}{3 \times 159}, \frac{1690 - 1000}{3 \times 159}\right) = 1.45 \qquad \text{(IV-7)}$$

$$Cpm = \frac{2400 - 1000}{6\sqrt{159^2 + (1690 - 1700)^2}} = 1.46 \qquad \text{(IV-8)}$$

These values indicate that the process is capable and can be monitored using control charts.

Table IV-2. Experimental results.

No.	*X*[V]	*MA*[V]	S_x[V]	S_x/X	No.	*X*[V]	*MA*[V]	S_x[V]	Sx/X
1	1627		1790	110	16	1728	116	1901	113
2	1937		1321	68	17	1861	250	1395	75
3	1601	336	948	59	18	1548	313	882	57
4	1668	336	1163	70	19	1722	313	1119	65
5	1692	91	1683	100	20	1585	174	967	61
6	1710	42	1408	82	21	1747	162	1013	58
7	1793	101	1296	72	22	1868	283	1121	60
8	1649	144	1103	67	23	1701	167	1242	73
9	1760	144	1210	69	24	1738	167	1651	95
10	1666	112	739	44	25	1725	37	1863	108
11	1561	199	1288	83	26	1563	174	1500	96
12	1751	190	1734	99	27	1627	162	1790	110
13	1668	190	2202	132	28	1779	216	1156	65
14	1701	83	704	41	29	1853	226	1167	63
15	1611	89	631	39	30	1275	578	969	76

IV.2.2. Control charts

The coefficient of confidence for the 30 samples being c = 1.28, the upper and lower limits of the individual value X and moving range R control charts, were calculated as follow:

$$UCLX = 1700 + 1.772 \times 192.8 \times 1.28 = 2137 \text{ V} \quad \text{(IV-9)}$$

$$LCLX = 1700 - 1.772 \times 192.8 \times 1.28 = 1263 \text{ V} \quad \text{(IV-10)}$$

$$UCLR = 2.574 \times 192.8 \times 1.28 = 635 \text{ V} \quad \text{(IV-11)}$$

$$LCLR = 0 * 192.8 = 0 \text{ V} \quad \text{(IV-12)}$$

The two charts are represented in **Figure IV-11** and **IV-12**, with USL = 2400 V, LSL = 1000 V, and T = 1700 V, imposed by a specific industry application.

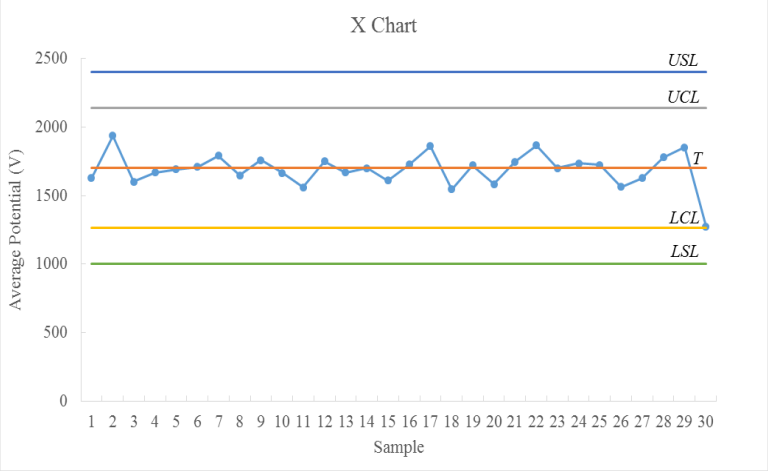

Figure IV-11. Individual values *X* control chart.

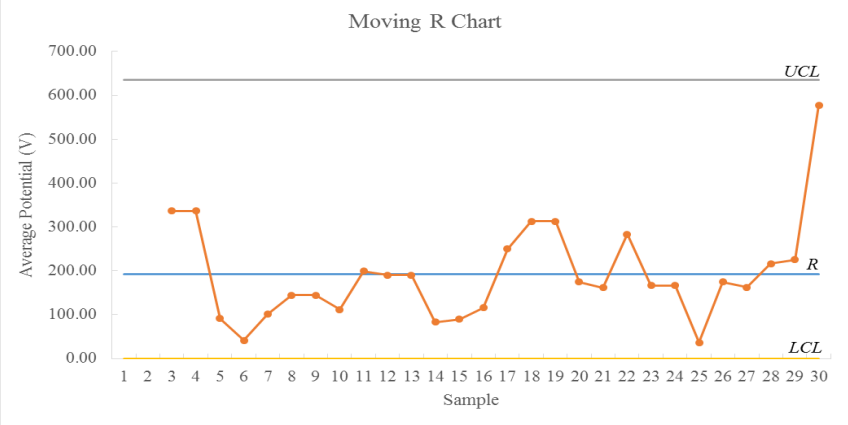

Figure IV-12. Moving range *R* control chart.

Under normal operation conditions, the friction is uniform on the surfaces in conformal contact, as demonstrated by the temperature map (an example is shown in **Figure IV-13**). However, the existing tribocharging process is characterized by a very high heterogeneity of the electric potential measured in the 25 point at the surface of the sample. The coefficient of variation *V* ranges between 39% and 132%, with an average value of 77% and a standard deviation of 23%. If the lower and upper specification limits were respectively 0% and 150% (**Figure IV-14**), the capability index of the tribocharging process would be satisfactory: 150 / (6×23) = 1.09. In case that the interval of tolerance is less than 138%, the present tribocharging process will not be able to meet the specifications.

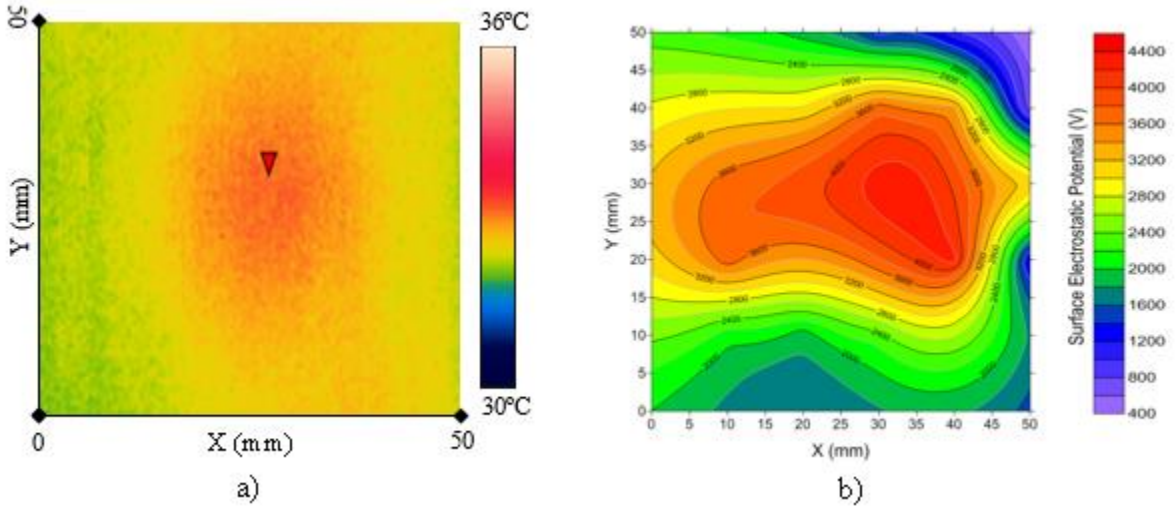

Figure IV-13. Temperature map (a) and surface potential cartography (b), in normal operation conditions.

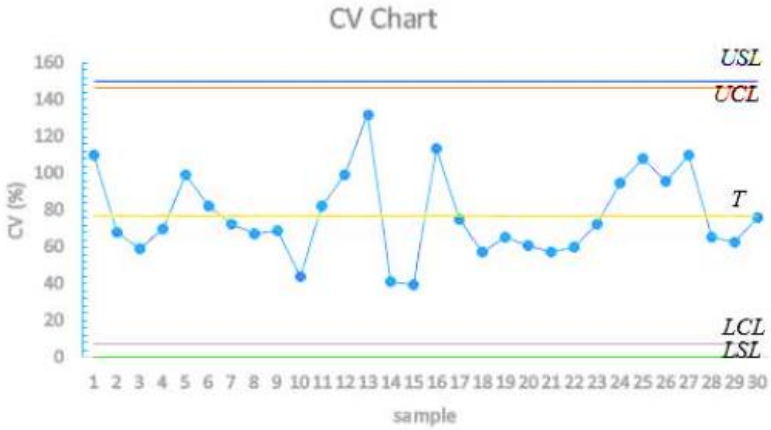

Figure IV-14. Coefficient of variation control chart.

An out-of-control situation is illustrated in **Figure IV-15**. The non-uniformity of the friction is reflected on both the temperature map (**Figure IV-15a**) and the electric potential cartography (**Figure IV-15b**). The intense friction along the L1 line modified the roughness of the sample surface and generated very high local values of the electric potential. The average value of the 25 measurements was 2252 V, which is still below the upper specification limit, but beyond the upper control limit on the individual value *X* chart (**Figure IV-16**). This out-of-control situation, due to the misalignment of the two samples, was detected as well by the moving *R* chart (**Figure IV-17**).

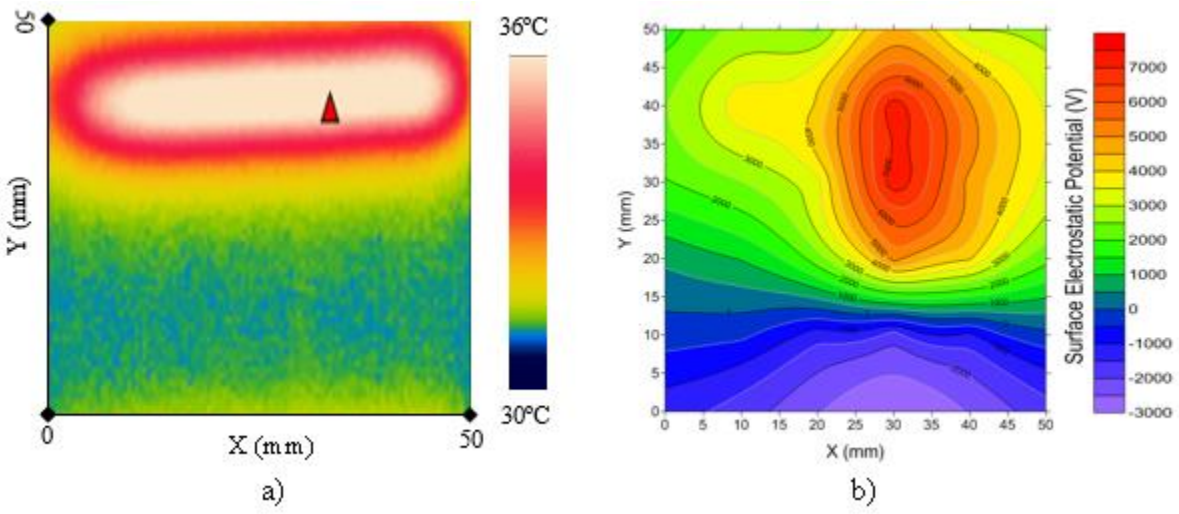

Figure IV-15. Temperature map (a) and surface potential cartography (b) of out of control sample (high surface potential).

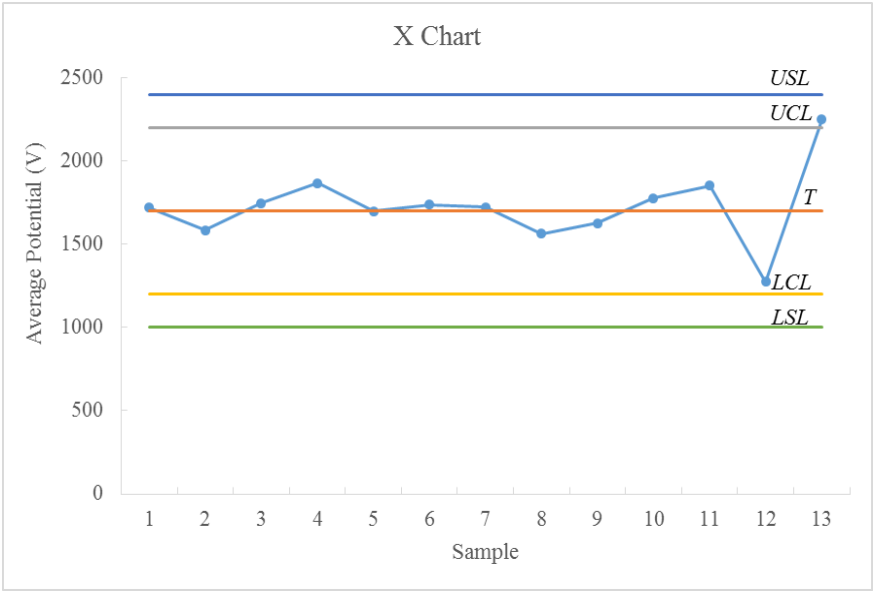

Figure IV-16. *X* control chart with simulated out of control sample (high potential)

A second out-of-control situation is illustrated in **Figure IV-18**. The mechanical device was inappropriately mounted after a maintenance operation and was not able to provide the normal force required for optimal operation and the average value of 25 measurements was 1143 V.

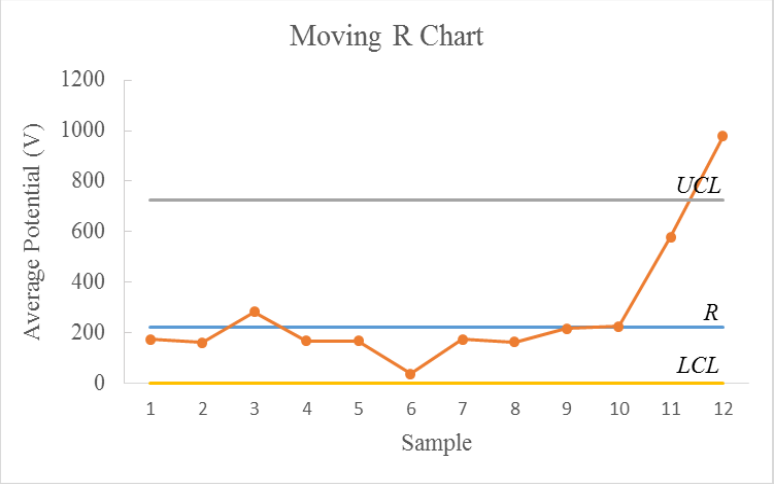

Figure IV-17. Moving $\bar{R}$ control chart with simulated out of control sample (high potential)

The low surface potential situation was detected on both the individual values X chart (**Figure IV-19**) and the moving range R chart (**Figure IV-20**). As a matter of fact, the point is below both the lower control limit and the lower specification limit of the former chart, and beyond the upper control limit of the latter chart.

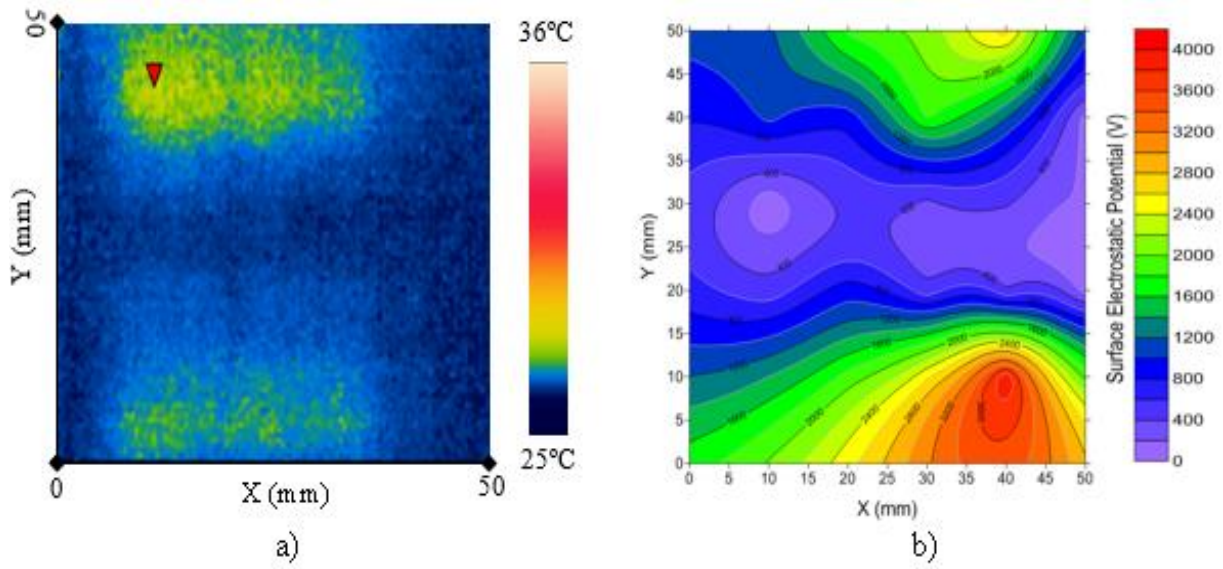

Figure IV-18. Temperature map (a) and surface potential cartography (b) of out of control sample (low surface potential).

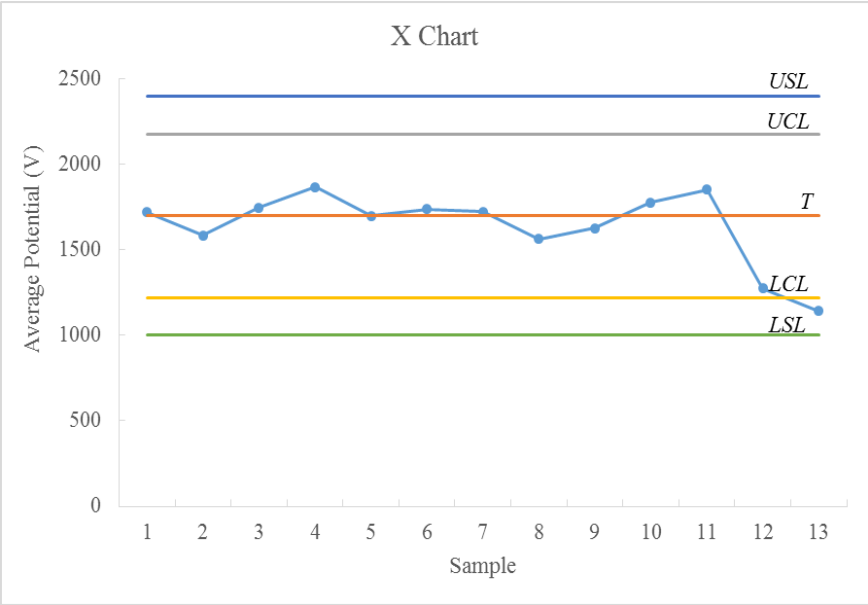

Figure IV-19. *X* control chart with simulated out of control sample (low potential)

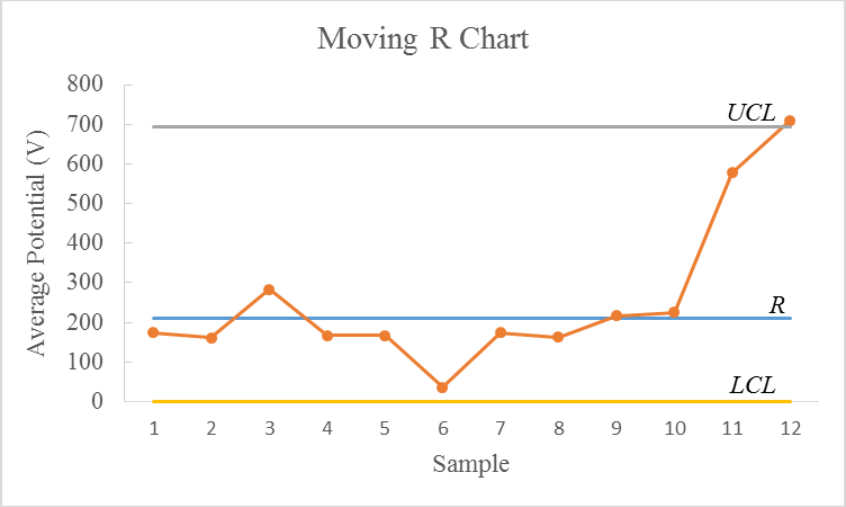

Figure IV-20. Moving $\bar{R}$ control chart with simulated out of control sample (low potential)

IV.3. Conclusions

The tribo-charging process depends on several factors, namely: the normal contact force, the charging time and the frequency of back-and-forth sliding motion. This multifactorial process can be modeled using “design of experiments” methodology.

The average electrostatic potential at the surface of PVC and ABS slabs increases with the number of cycles and normal force but decreases with the frequency of back-and-forth sliding contact. However, increasing of frequency and normal force applied provides a better charge distribution on the entire surface on contact, while the increasing the number of cycles gives opposite result.

Statistical Process Control is an effective tool for monitoring the tribocharging of polymer slabs in sliding conformal contact. The tribocharging state of such bodies can be quantified by the average value of the electric potential measured in a matrix of 5 x 5 points at the surface affected by frictional movement.

The upper and lower limits of individual value and moving range control charts can be computed from the results of 30 experiments carried out in the optimal operating conditions. The control charts can detect at least two out-of-control conditions: misalignment of the slabs in conformal contact and inappropriate mounting of the mechanical system after maintenance.

The coefficient of variation calculated for the values measured in the 25 points at the surface of each sample points out the very high heterogeneity of the electric charge generated by triboelectric effect. In case that homogeneity of the charging is required for a certain application, the present process is far from being satisfactory.

Conclusions and Perspectives

The primary objective of this work was to develop the knowledge on the triboelectric behavior of polymeric materials for dry sliding contacts. The use of various test configurations has made possible specifically targeted studies on the electrical charge generated in sliding contacts between most-frequently used polymers. For this purpose, the study first focused on the design of experimental devices capable of simultaneously measuring and controlling the sliding conditions and the generation of electric charge on the surface of specimens.

The general conclusion of this work could be formulated as follows: the generation of electric charge through polymer-on-polymer sliding contact depends on a multitude of factors and the presence of electric charge on the surfaces in contact significantly affect the conditions of friction. Multivariate optimization using response surface methodology (RSM) has proved to be a powerful tool to find the most effective combination of controllable variables of the tribocharging process. On the other hand statistical process control could be used as a technique to monitor these optimal operating conditions and to detect any out-of-control situation.

Under the conditions of the study, the following conclusions could be drawn:

1. The electric charge generated by triboelectric depends on several factors including material properties, thermal condition, surface texture direction and roughness. Several process variables, such as normal force applied, the number of cycle and sliding speed, can be easily controlled, so that to provide the optimum outcome of the tribocharging process.

2. A good correlation is found between the cartographies of the electric charge distribution and the temperature field distribution. This result suggests the possibility of using thermal field maps as a method of identifying the contact area or wear track since both phenomena are related to sliding contact between surfaces.

3. The electric charge generated by triboelectric effect is distributed in a less homogeneous way compared to that obtained by corona effect. However, the decline over time is less rapid for the triboelectrically generated charge.

4. Response surface method (RSM) using central composite face-centered (CCF) was able to find the optimal setting of tribocharging process in function of electric charge generated, distribution of this charge and surface temperature rise due to sliding. The statistical process control was successfully employed in monitoring these optimal conditions and indicates whenever out of control situations occur.

The main original contributions of the thesis are:

1. Development of a test bench for the characterization of the triboelectric behavior of polymer slabs in dry contact.

2. Better understanding of polymer-on-polymer sliding system including the evaluation of several influent factors.

3. Control of the polymer characterization bench in sliding contact using a data acquisition system.

4. The evolutions of normal force, tangential force, and position displacement have been recorded to enable the analysis of the physical phenomena.

5. Surface electric charge condition monitoring using a non-contact electrostatic probe attached on a 2D positioning system.

6. The cartographies of the electric charge distribution and the temperature field distribution for several contact conditions and materials.

7. Use of temperature field monitoring on the surface of the specimens in sliding contact to detect electrically charged areas. The method takes advantage of the correlation between the surface electric charge and the temperature field generated by friction.

8. Use of corona discharge to provide an initial charge on the specimens for study the effect of charge on the friction force.

This work has also highlighted several promising research perspectives to improve the methodology for characterizing the triboelectric properties of polymers. Following the experience gained during this PhD thesis, the future work should focus on the following aspects:

1. Study of surface anisotropy effect, since the specimens have unique surface properties which will affect the friction and charging behavior. The characterization of anisotropy should be done before and after the tribocharging test.

2. Investigation of the effect of electric charge on friction force using various charge polarities of the bodies in contact. This treatment could give different result since bodies' carrying charges of similar polarity are repelling each other, while they attract each other in the opposite case.

3. In-depth study of the effect of charge on the modification of surface properties, adhesion and self-lubrication capability, using a scanning electron microscope (SEM).

4. Experimental modeling and optimization of the electric charge generation by the triboelectric effect on other polymeric materials, also including the frictional force and wear measurement.

5. Study of the correlation between the electric charge and the temperature field generated by friction in order to acquire information related to the tribocharging mechanism

6. Comparing the charge generation process in back-and-forth and rotational tribocharging

Finally, this study may be used as reference for the application of polymers in mechanical design, and triboelectric energy harvesting.

References

[1] M.F. Ashby, K. Johnson, Materials and Design: The Art and Science of Material Selection in Product Design, Elsevier Science, 2013. doi:10.1073/pnas.0703993104.

[2] D.M. Nuruzzaman, M.A. Chowdhury, Friction and Wear of Polymer and Composites, in: N.B.T.-C. and T.P. Hu (Ed.), InTech, Rijeka, 2012: p. Ch. 14. doi:10.5772/48246.

[3] R. Chattopadhyay, Green Tribology, Green Surface Engineering, and Global Warming, ASM International, Materials Park, OH, 2014.

[4] A. Anand, M. Irfan, U. Haq, K. Vohra, A. Raina, M.F. Wani, ScienceDirect Role of Green Tribology in Sustainability of Mechanical Systems : A State of the Art Survey, Mater. Today Proc. 4 (2017) 3659–3665. doi:10.1016/j.matpr.2017.02.259.

[5] S.K. Sinha, B.J. Briscoe, Polymer Tribology, Imperial College Press, 2009. doi:10.1142/9781848162044.

[6] B.J. Briscoe, S.K. Sinha, Tribological applications of polymers and their composites – past, present and future prospects, in: Tribol. Polym. Nanocomposites, Elsevier, 2013: pp. 1–22. doi:10.1016/B978-0-444-59455-6.00001-5.

[7] G. Stachowiak, A.W. Batchelor, Experimental Methods in Tribology, Elsevier Science, 2004.

[8] B. Bhushan, Modern Tribology Handbook, Two Volume Set, CRC Press, 2000.

[9] K. Friedrich, A.K. Schlarb, Tribology of Polymeric Nanocomposites: Friction and Wear of Bulk Materials and Coatings, Elsevier Science, 2013.

[10] K. Friedrich, A. Schlarb, Tribology of Polymeric Nanocomposites, Volume 55: Friction and Wear of Bulk Materials and Coatings (Tribology and Interface Engineering), 2008.

[11] The science of self-lubrication:Debunking the Myth of "Lubed for Life". Technical notes, PBC Linear^{TM}. (2010). http://www.pbclinear.com/Download/WhitePaper/The-Science-of-Self-Lubrication.pdf (accessed January 5, 2018).

[12] R.W. Bruce, CRC Handbook of Lubrication: Theory and Practice of Tribology, Volume II: Theory and Design, CRC Press, 2010.

[13] C. Guerret-Piecourt, S. Bec, D. Treheux, Electrical charges and tribology of insulating materials, Comptes Rendus l'Academie Des Sci. - Ser. IV Physics, Astrophys. 2 (2001) 761–774. doi:10.1016/S1296-2147(01)01218-5.

[14] W.J. Bartz, History of Tribology - The bridge between the classical antiquity and the 21st Century, in: Proceeding 2nd World Tribol. Congr., Vienna, 2001: pp. 3–12.

[15] A. Fall, B. Weber, M. Pakpour, N. Lenoir, N. Shahidzadeh, J. Fiscina, C. Wagner, D. Bonn, Sliding friction on wet and dry sand, Phys. Rev. Lett. 112 (2014). doi:10.1103/PhysRevLett.112.175502.

[16] B. Bhushan, Introduction to Tribology, Second Edition, John Wiley & Sons, Ltd, The Atrium, Southern Gate, Chichester, West Sussex, PO19 8SQ, UK., 2013. doi:10.1002/9781118403259.

[17] I.M. Hutchings, Leonardo da Vinci's studies of friction, Wear. 360–361 (2016) 51–66. doi:10.1016/j.wear.2016.04.019.

[18] A.A. Pitenis, D. Dowson, W. Gregory Sawyer, Leonardo da Vinci's friction experiments: An old story acknowledged and repeated, Tribol. Lett. 56 (2014) 509–515. doi:10.1007/s11249-014-0428-7.

[19] N. Fulleringer, Contribution à l'étude des phénomènes de friction : application au matériau papier, Grenoble, 2015.

[20] V.L. Popov, Contact mechanics and friction: Physical principles and applications, Springer Berlin Heidelberg, Berlin, Heidelberg, 2010. doi:10.1007/978-3-642-10803-7.

[21] F.P. Bowden, D. Tabor, F. Palmer, The Friction and Lubrication of Solids, Am. J. Phys. 19 (1951) 428–429. doi:10.1119/1.1933017.

[22] Engineering-abc.com, History of science friction, (2005). http://www.tribology-abc.com/abc/history.htm (accessed December 10, 2017).

[23] L.C.A. van Breemen, Contact mechanics in glassy polymers, 2009. doi:10.6100/IR642891.

[24] H. Butt, M. Kappl, Surface and Interfacial Forces, Wiley-VCH, Weinheim, 2009.

[25] Q. Li, M. Lovell, On the critical interfacial friction of a two-roll CWR process, J. Mater. Process. Technol. 160 (2005) 245–256. doi:10.1016/j.jmatprotec.2004.06.022.

[26] J.C. Gerdeen, PhD, PE, R.A.L. Rorrer, Engineering Design with Polymers and Composites, Second Edition, CRC Press, Boca Raton, FL, 2011.

[27] N.K. Myshkin, M.I. Petrokovets, A. V. Kovalev, Tribology of polymers: Adhesion, friction, wear, and mass-transfer, Tribol. Int. 38 (2005) 910–921. doi:10.1016/j.triboint.2005.07.016.

[28] A. Abdelbary, Polymer tribology, in: Wear Polym. Compos., Elsevier, 2014: pp. 1–36. doi:10.1533/9781782421788.1.

[29] A. Seireg, Friction and Lubrication in Mechanical Design, 19984737 (1998) 4–7. doi:0-8247-9974-7.

[30] D.H. Cho, B. Bhushan, Friction and wear of various polymer pairs used for label and wiper in labeling machine, Tribol. Int. 98 (2016) 10–19. doi:10.1016/j.triboint.2016.02.019.

[31] I. Hutchings, P. Shipway, Tribology: Friction and Wear of Engineering Materials, 2nd ed., Butterworth-Heinemann, 2017.

[32] V.K. Shooter, D. Tabor, The Frictional Properties of Plastics, Proc. Phys. Soc. Sect. B. 65 (1952) 661–671. doi:10.1088/0370-1301/65/9/302.

[33] Z. Wang, D.G. Chetwynd, K. Mao, Friction characteristics of polymers applicable to small-scale devices, Tribol. Int. 119 (2018) 698–706. doi:10.1016/j.triboint.2017.11.036.

[34] S.F.S.P. Looijmans, P.D. Anderson, L.C.A. van Breemen, Contact mechanics of isotactic polypropylene: Effect of pre-stretch on the frictional response, Wear. 398–399 (2018) 183–190. doi:10.1016/j.wear.2017.12.002.

[35] G.M. Bartenev, V.V. Lavrentev, Friction and Wear of Polymers, Elsevier, Amsterdam, 1981. doi:10.1016/S0167-8922(08)70740-5.

[36] J. Rojsatean, P. Larpsuriyakul, N. Prakymoramas, D. Thanomjitr, S. Kaewket, T. Singsom, D. Srinun, Friction characteristics of self-lubricating ABS under different surface roughnesses and temperatures, Tribol. Int. 109 (2017) 229–237. doi:10.1016/j.triboint.2016.12.055.

[37] P. Iversen, D.J. Lacks, A life of its own: The tenuous connection between Thales of Miletus and the study of electrostatic charging, J. Electrostat. 70 (2012) 309–311. doi:10.1016/j.elstat.2012.03.002.

[38] J.F. Keithley, Story of electrical and magnetic measurements: from 500 B.C. to the 1940s, IEEE Press, New York, 1999.

[39] A.K. Chakraborty, S.C. Bhattacharya, B.G. Varma, The story of electricity, Childrens Book Trust, New Delhi, 1985.

[40] K.L. Kaiser, Electrostatic Discharge, Taylor & Francis, Boca Raton, FL, 2006.

[41] S.H. Carr, D.K. Davies, P. Fischer, Electrical of Polymers Properties, Academic Press, Orlando, FL, 1982.

[42] V.K. Jasti, Electrostatic charge generation and dissipation on woven fabrics treated with antistatic and hydrophilic surface finishes, North Carolina State University, 2012.

[43] M.D. Hogue, C.R. Buhler, C.I. Calle, T. Matsuyama, W. Luo, E.E. Groop, Insulator-insulator contact charging and its relationship to atmospheric pressure, J. Electrostat. 61 (2004) 259–268. doi:10.1016/j.elstat.2004.03.002.

[44] L.S. McCarty, G.M. Whitesides, Electrostatic charging due to separation of ions at interfaces: Contact electrification of ionic electrets, Angew. Chemie - Int. Ed. 47 (2008) 2188–2207. doi:10.1002/anie.200701812.

[45] M. Williams, What Creates Static Electricity?, Am. Sci. 100 (2012) 316. doi:10.1511/2012.97.316.

[46] C. Guerret-Piécourt, J. Vallayer, D. Tréheux, Limitation induced by electrical charges effects on micromechanisms, Wear. 254 (2003) 950–958. doi:10.1016/S0043-1648(03)00299-0.

[47] M.D. Hogue, E.R. Mucciolo, C.I. Calle, Triboelectric, corona, and induction charging of insulators as a function of pressure, J. Electrostat. 65 (2007) 274–279. doi:10.1016/j.elstat.2006.10.003.

[48] H.D. Brewster, Electrostatics, First, Oxford Book Company, Jaipur, 2009.

[49] S. Descartes, M. Renouf, N. Fillot, B. Gautier, A. Descamps, Y. Berthier, P. Demanche, A new mechanical-electrical approach to the wheel-rail contact, Wear. 265 (2008) 1408–1416. doi:10.1016/j.wear.2008.02.040.

[50] R.S. Blacker, A.W. Birley, Electrostatic charge occurrence, significance and measurement, Polym. Test. 10 (1991) 241–262. doi:10.1016/0142-9418(91)90020-X.

[51] M. Glor, Ignition hazard due to static electricity in particulate processes, Powder Technol. 135–136 (2003) 223–233. doi:10.1016/j.powtec.2003.08.017.

[52] J.N. Chubb, A Standard proposed for assessing the electrostatic suitability of materials, J. Electrostat. 65 (2007) 607–610. doi:10.1016/j.elstat.2007.01.004.

[53] B.D. Moyle, J.F. Hughes, Powder coating - corona versus tribo charging, J. Electrostat. 16 (1985) 277–286. doi:10.1016/0304-3886(85)90051-8.

[54] F.W. Peek, Dielectric Phenomena In High Voltage Engineering, (1915) 265. doi:1406783374, 9781406783377.

[55] M. Goldman, A. Goldman, R.S. Sigmond, The corona discharge, its properties and specific uses, Pure Appl. Chem. 57 (1985) 1353–1362. doi:10.1351/pac198557091353.

[56] A. Fatihou, Amélioration des performances des matériaux fibreux non-tissés chargés par décharge couronne utilisés pour la filtration de l'air, Université de Poitiers., 2016.

[57] N. Jonassen, Electrostatics, second, Springer US, Boston, MA, 2002. doi:10.1007/978-1-4615-1073-4.

[58] A. Reguig, A. Bendaoud, B. Neagoe, Y. Prawatya, L. Dascalescu, Electric potential distribution at the surface of insulating materials exposed to corona discharges from various electrode configurations, J. Electrostat. 82 (2016) 55–62. doi:10.1016/j.elstat.2016.05.006.

[59] M. Morvova, the Influence of Water Vapour and Temperature on Depletion of Carbon Monoxide in D . C . Corona Discharge, 49 (1999) 1703–1719.

[60] A. Reguig, Contribution à l'étude expérimentale et numérique de la décharge couronne dans e s différents types de configurations d'électrodes, (2017).

[61] Y. Kimura, Maintenance tribology : its significance and activity in Japan, 207 (1997) 63–66.

[62] Y. Kimura, H. Okabe, The current state of tribology in Japan, Tribol. Int. 26 (1993) 275–283. doi:10.1016/0301-679X(93)90008-O.

[63] K. Holmberg, P. Andersson, N.O. Nylund, K. Mäkelä, A. Erdemir, Global energy consumption due to friction in trucks and buses, Tribol. Int. 78 (2014) 94–114. doi:10.1016/j.triboint.2014.05.004.

[64] K. Holmberg, P. Andersson, A. Erdemir, Global energy consumption due to friction in

passenger cars, Tribol. Int. 47 (2012) 221–234. doi:10.1016/j.triboint.2011.11.022.

[65] C. Reichl, M. Schatz, G. Zsak, World Mining Data 2016, Fed. Minist. Sci. Res. Econ. Austria. 31 (2016) 1–255.

[66] K. Holmberg, P. Kivikytö-Reponen, P. Härkisaari, K. Valtonen, A. Erdemir, Global energy consumption due to friction and wear in the mining industry, Tribol. Int. 115 (2017) 116–139. doi:10.1016/j.triboint.2017.05.010.

[67] K. Holmberg, R. Siilasto, T. Laitinen, P. Andersson, A. Jäsberg, Global energy consumption due to friction in paper machines, Tribol. Int. 62 (2013) 58–77. doi:10.1016/j.triboint.2013.02.003.

[68] C. MENGUY, Électricité Statique, Tech. l'Ingénieur. (1993).

[69] J.M. Crowley, Electrostatic fundamentals, 1995. doi:10.1007/s13398-014-0173-7.2.

[70] M. Glor, Electrostatic ignition hazards in the process industry, J. Electrostat. 63 (2005) 447–453. doi:10.1016/j.elstat.2005.03.001.

[71] H.L. Walmsley, Electrostatic ignition hazards with plastic pipes at petrol stations, J. Loss Prev. Process Ind. 25 (2012) 263–273. doi:10.1016/j.jlp.2011.11.002.

[72] S. Egan, Learning lessons from five electrostatic incidents, J. Electrostat. 88 (2017) 183–189. doi:10.1016/j.elstat.2017.01.002.

[73] G. Lüttgens, N. Wilson, Electrostatic Hazards, Electrost. Hazards. (1997) 137–149. doi:10.1016/B978-075062782-5/50010-4.

[74] Z.L. Wang, Triboelectric nanogenerators as new energy technology and self-powered sensors – Principles, problems and perspectives, Faraday Discuss. 176 (2014) 447–458. doi:10.1039/C4FD00159A.

[75] Z. Li, J. Shen, I. Abdalla, J. Yu, B. Ding, Nanofibrous membrane constructed wearable triboelectric nanogenerator for high performance biomechanical energy harvesting, Nano Energy. 36 (2017) 341–348. doi:10.1016/j.nanoen.2017.04.035.

[76] W. Gong, C. Hou, Y. Guo, J. Zhou, J. Mu, Y. Li, Q. Zhang, H. Wang, A wearable, fibroid, self-powered active kinematic sensor based on stretchable sheath-core structural triboelectric fibers, Nano Energy. 39 (2017) 673–683. doi:10.1016/j.nanoen.2017.08.003.

[77] G. Zhu, P. Bai, J. Chen, Z. Lin Wang, Power-generating shoe insole based on triboelectric nanogenerators for self-powered consumer electronics, Nano Energy. 2 (2013) 688–692. doi:10.1016/j.nanoen.2013.08.002.

[78] X. Cheng, B. Meng, X. Zhang, M. Han, Z. Su, H. Zhang, Wearable electrode-free triboelectric generator for harvesting biomechanical energy, Nano Energy. 12 (2015) 19–25. doi:10.1016/j.nanoen.2014.12.009.

[79] S. Lee, W. Ko, Y. Oh, J. Lee, G. Baek, Y. Lee, J. Sohn, S. Cha, J. Kim, J. Park, J. Hong, Triboelectric energy harvester based on wearable textile platforms employing various surface morphologies, Nano Energy. 12 (2015) 410–418.

doi:10.1016/j.nanoen.2015.01.009.

[80] A. Ahmed, S.L. Zhang, I. Hassan, Z. Saadatnia, Y. Zi, J. Zu, Z.L. Wang, A washable, stretchable, and self-powered human-machine interfacing Triboelectric nanogenerator for wireless communications and soft robotics pressure sensor arrays, Extrem. Mech. Lett. 13 (2017) 25–35. doi:10.1016/j.eml.2017.01.006.

[81] T. Huang, C. Wang, H. Yu, H. Wang, Q. Zhang, M. Zhu, Human walking-driven wearable all-fiber triboelectric nanogenerator containing electrospun polyvinylidene fluoride piezoelectric nanofibers, Nano Energy. 14 (2014) 226–235. doi:10.1016/j.nanoen.2015.01.038.

[82] C. Jean-Mistral, T. Vu Cong, A. Sylvestre, Advances for dielectric elastomer generators: Replacement of high voltage supply by electret, Appl. Phys. Lett. 101 (2012). doi:10.1063/1.4761949.

[83] C. Lagomarsini, A. Sylvestre, C. Jean-Mistral, S. Monfray, Coupling of electro-active polymers for energy harvesting applications, IEEE Int. Conf. Dielectr. (2016) 443–446. doi:10.1109/ICD.2016.7547638.

[84] A. Ahmed, I. Hassan, M. Hedaya, T. Abo El-Yazid, J. Zu, Z.L. Wang, Farms of triboelectric nanogenerators for harvesting wind energy: A potential approach towards green energy, Nano Energy. 36 (2017) 21–29. doi:10.1016/j.nanoen.2017.03.046.

[85] Y. Su, G. Xie, F. Xie, T. Xie, Q. Zhang, H. Zhang, H. Du, X. Du, Y. Jiang, Segmented wind energy harvester based on contact-electrification and as a self-powered flow rate sensor, Chem. Phys. Lett. 653 (2016) 96–100. doi:10.1016/j.cplett.2016.04.080.

[86] L. biao Huang, W. Xu, G. Bai, M.C. Wong, Z. Yang, J. Hao, Wind energy and blue energy harvesting based on magnetic-assisted noncontact triboelectric nanogenerator, Nano Energy. 30 (2016) 36–42. doi:10.1016/j.nanoen.2016.09.032.

[87] M.L. Seol, J.H. Woo, S.B. Jeon, D. Kim, S.J. Park, J. Hur, Y.K. Choi, Vertically stacked thin triboelectric nanogenerator for wind energy harvesting, Nano Energy. 14 (2015) 201–208. doi:10.1016/j.nanoen.2014.11.016.

[88] Y. Xi, J. Wang, Y. Zi, X. Li, C. Han, X. Cao, C. Hu, Z. Wang, High efficient harvesting of underwater ultrasonic wave energy by triboelectric nanogenerator, Nano Energy. 38 (2017) 101–108. doi:10.1016/j.nanoen.2017.04.053.

[89] Y. Su, X. Wen, G. Zhu, J. Yang, J. Chen, P. Bai, Z. Wu, Y. Jiang, Z. Lin Wang, Hybrid triboelectric nanogenerator for harvesting water wave energy and as a self-powered distress signal emitter, Nano Energy. 9 (2014) 186–195. doi:10.1016/j.nanoen.2014.07.006.

[90] M. Taghavi, A. Sadeghi, A. Mondini, B. Mazzolai, L. Beccai, V. Mattoli, Triboelectric smart machine elements and self-powered encoder, Nano Energy. 13 (2015) 92–102. doi:10.1016/j.nanoen.2015.02.011.

[91] S. Chen, C. Gao, W. Tang, H. Zhu, Y. Han, Q. Jiang, T. Li, X. Cao, Z. Wang, Self-powered cleaning of air pollution by wind driven triboelectric nanogenerator, Nano

Energy. 14 (2014) 217–225. doi:10.1016/j.nanoen.2014.12.013.

[92] Q. Jing, G. Zhu, W. Wu, P. Bai, Y. Xie, R.P.S. Han, Z.L. Wang, Self-powered triboelectric velocity sensor for dual-mode sensing of rectified linear and rotary motions, Nano Energy. 10 (2014) 305–312. doi:10.1016/j.nanoen.2014.09.018.

[93] M. Shi, H. Wu, J. Zhang, M. Han, B. Meng, H. Zhang, Self-powered wireless smart patch for healthcare monitoring, Nano Energy. 32 (2017) 479–487. doi:10.1016/j.nanoen.2017.01.008.

[94] X.S. Meng, H.Y. Li, G. Zhu, Z.L. Wang, Fully enclosed bearing-structured self-powered rotation sensor based on electrification at rolling interfaces for multi-tasking motion measurement, Nano Energy. 12 (2015) 606–611. doi:10.1016/j.nanoen.2015.01.015.

[95] H.R. Zhu, W. Tang, C.Z. Gao, Y. Han, T. Li, X. Cao, Z.L. Wang, Self-powered metal surface anti-corrosion protection using energy harvested from rain drops and wind, Nano Energy. 14 (2014) 193–200. doi:10.1016/j.nanoen.2014.11.041.

[96] F.R. Fan, Z.Q. Tian, Z. Lin Wang, Flexible triboelectric generator, Nano Energy. 1 (2012) 328–334. doi:10.1016/j.nanoen.2012.01.004.

[97] V. Nguyen, R. Zhu, R. Yang, Environmental effects on nanogenerators, Nano Energy. 14 (2014) 49–61. doi:10.1016/j.nanoen.2014.11.049.

[98] A. Alahmadi, Influence of Triboelectrification on Friction Coefficient, Int. J. Sci. Eng. Res. 5 (2014) 22–29. https://www.ijser.org/onlineResearchPaperViewer.aspx?Influence-of-Triboelectrification-on-Friction-Coefficient.pdf.

[99] T.A.L. Burgo, C.A. Silva, L.B.S. Balestrin, F. Galembeck, Friction coefficient dependence on electrostatic tribocharging, Sci. Rep. 3 (2013) 1–8. doi:10.1038/srep02384.

[100] F. Galembeck, T. A. L. Burgo, Chemical Electrostatics, 2017. doi:10.1007/978-3-319-52374-3.

[101] R. Lewis, U. Olofsson, Wheel—rail interface handbook, Woodhead Publishing Limited, 2009. doi:10.1533/9781845696788.

[102] G. Wypych, J. Pionteck, Handbook of Antistatics, Second, ChemTec Publishing, Toronto, 2016.

[103] G.W. Poll, Life Cycle Engineering and Virtual Product Development – the Role of Tribology, Elsevier Masson SAS, 2005. doi:10.1016/S0167-8922(05)80005-7.

[104] X. Zhu, Tutorial on Hertz Contact Stress, Opti 521. (2012) 1–8.

[105] K.L. Johnson, K. Kendall, A.D. Roberts, Surface Energy and the Contact of Elastic Solids, Proc. R. Soc. A Math. Phys. Eng. Sci. 324 (1971) 301–313. doi:10.1098/rspa.1971.0141.

[106] Q.J. Wang, Encyclopedia of Tribology, 2013. doi:10.1007/978-0-387-92897-5.

[107] University of Leeds. Institute of Tribology., Institut national des sciences appliquées de Lyon., Tribological Research and Design for Engineering Systems, Proceedings of the

29th Leeds-Lyon Symposium on Tribology, Elsevier, 2003. doi:10.1016/S0167-8922(03)X8112-2.

[108] K. Hiratsuka, K. Hosotani, Effects of friction type and humidity on triboelectrification and triboluminescence among eight kinds of polymers, Tribol. Int. 55 (2012) 87–99. doi:10.1016/j.triboint.2012.05.017.

[109] Y.E. Prawatya, M.B. Neagoe, T. Zeghloul, L. Dascalescu, Surface-Electric-Potential Characteristics of Tribo- and Corona-Charged Polymers: A Comparative Study, IEEE Trans. Ind. Appl. 53 (2017) 2423–2431. doi:10.1109/TIA.2017.2650145.

[110] H.T. Baytekin, A.Z. Patashinski, M. Branicki, B. Baytekin, S. Soh, B.A. Grzybowski, The mosaic of surface charge in contact electrification, Science (80-.). 333 (2011) 308–312. doi:10.1126/science.1201512.

[111] T.A.L. Burgo, T.R.D. Ducati, K.R. Francisco, K.J. Clinckspoor, F. Galembeck, S.E. Galembeck, Triboelectricity: Macroscopic charge patterns formed by self-arraying ions on polymer surfaces, Langmuir. 28 (2012) 7407–7416. doi:10.1021/la301228j.

[112] J. Sun, R.J.K. Wood, L. Wang, I. Care, H.E.G. Powrie, Wear monitoring of bearing steel using electrostatic and acoustic emission techniques, Wear. 259 (2005) 1482–1489. doi:10.1016/j.wear.2005.02.021.

[113] L. Wang, R.J.K. Wood, T.J. Harvey, S. Morris, H.E.G. Powrie, I. Care, Wear performance of oil lubricated silicon nitride sliding against various bearing steels, Wear. 255 (2003) 657–668. doi:10.1016/S0043-1648(03)00045-0.

[114] L. Liu, A.M. Seyam, W. Oxenham, Frictional electrification on polymeric flat surfaces, J. Eng. Fiber. Fabr. 8 (2013) 126–136. http://www.jeffjournal.org/papers/Volume8/JEFF8-01-15.A.Seyam.pdf%0Ahttps://www.scopus.com/inward/record.uri?eid=2-s2.0-84875394479&partnerID=40&md5=b8af10d1b698bed066e5bca5bc550dea.

[115] J.N. Chubb, Comments on methods for charge decay measurement, 62 (2004) 73–80. doi:10.1016/j.elstat.2004.04.004.

[116] J. Chubb, How should the electrostatic suitability of materials be assessed ?, J. Electrostat. 77 (2015) 163–165. doi:10.1016/j.elstat.2015.08.010.

[117] G. Raju, Dielectrics in Electric Fields, 2003. doi:10.1201/9780203912270.

[118] W. Kaialy, A review of factors affecting electrostatic charging of pharmaceuticals and adhesive mixtures for inhalation, Int. J. Pharm. 503 (2016) 262–276. doi:10.1016/j.ijpharm.2016.01.076.

[119] P. Molinié, Recherches en {Electrostatique} - {Actualité} d'une science ancienne et applications à la caractérisation des matériaux, (2010). http://tel.archives-ouvertes.fr/docs/00/54/07/37/PDF/Philippe_Molinie_Electrostatique_memoire_hdr.pdf.

[120] Y. Onogi, N. Sugiura, Y. Nakaoka, Dissipation of Triboelectric Charge into Air from Textile Surfaces, Text. Res. J. 66 (1996) 337–342. doi:10.1177/004051759606600508.

[121] D.C. Montgomery, D.C. Montgomery, G.C. Runger, N.F. Hubele, W.W. Hines, D.M. Goldsman, C.M. Borror, E.A. Peck, G.G. Vining, Introduction to Statistical Quality Control, 2013.

[122] R.H. Myers, D.C. Montgomery, C.M. Anderson-Cook, Response surface methodology. Process and product optimization using designed experiments, John Wiley Sons, Inc. (2009) 1–1247. doi:10.1007/s13398-014-0173-7.2.

[123] Y.E. Prawatya, M.B. Neagoe, T. Zeghloul, L. Dascalescu, Optimization of continuous triboelectrification process for polymeric materials in dry contact, in: IOP Conf. Ser. Mater. Sci. Eng., 2017. doi:10.1088/1757-899X/174/1/012067.

[124] H. Mellouki, L. Herous, Y. Prawatya, B. Neagoe, L. Dascalescu, Tribo and corona charging and charge decay on polymers plates, in: 2017 5th Int. Conf. Electr. Eng. - Boumerdes, IEEE, 2017: pp. 1–5. doi:10.1109/ICEE-B.2017.8192161.

[125] G. Xiao, Z. Zhu, Friction materials development by using DOE/RSM and artificial neural network, Tribol. Int. 43 (2010) 218–227. doi:10.1016/j.triboint.2009.05.019.

[126] B. Peng Chang, H. Md Akil, R. Bt Nasir, A. Khan, Optimization on wear performance of UHMWPE composites using response surface methodology, Tribol. Int. 88 (2015) 252–262. doi:10.1016/j.triboint.2015.03.028.

[127] B. Rashid, Z. Leman, M. Jawaid, M.J. Ghazali, M.R. Ishak, M.A. Abdelgnei, Dry sliding wear behavior of untreated and treated sugar palm fiber filled phenolic composites using factorial technique, Wear. 380–381 (2017) 26–35. doi:10.1016/j.wear.2017.03.011.

[128] L. Dascalescu, A. Urs, S. Bente, M. Huzau, A. Samuila, Charging of mm-size insulating particles in vibratory devices, J. Electrostat. 63 (2005) 705–710. doi:10.1016/j.elstat.2005.03.042.

[129] L. Dascalescu, K. Medles, S. Das, M. Younes, L. Caliap, A. Mihalcioiu, Using design of experiments and virtual instrumentation to evaluate the tribocharging of pulverulent materials in compressed-air devices, IEEE Trans. Ind. Appl. 44 (2008) 3–8. doi:10.1109/TIA.2007.912801.

[130] M. Rezzouga, A. Tilmatine, R. Gouri, K. Medles, L. Dascalescu, Experimental modeling of high-voltage corona discharge using design of experiments, Front. Electr. Electron. Eng. China. 2 (2007) 139–143. doi:10.1007/s11460-007-0026-7.

[131] K. Medles, K. Senouci, A. Tilmatine, A. Bendaoud, A. Mihalcioiu, L. Dascalescu, Capability Evaluation and Statistical Control of Electrostatic Separation Processes, IEEE Trans. Ind. Appl. 45 (2009) 1086–1094. doi:10.1109/TIA.2009.2018903.

[132] K. Senouci, A. Bendaoud, K. Medles, A. Tilmatine, L. Dascalescu, Statistical Control of Electrostatic Separation Processes, IEEE Ind. Appl. Mag. 16 (2010) 22–27. doi:10.1109/MIAS.2010.936973.

[133] K. Senouci, K. Medles, S. Messal, L. Dascalescu, Multivariate control for three variables of an industrial roll-type electrostatic separator, IEEE Trans. Ind. Appl. 51 (2015) 4752–4758. doi:10.1109/TIA.2015.2448052.

[134] G. Buda, A. Samuila, M. Bilici, L. Dascalescu, Premises for statistic control of a tribocharging process for granular materials, Part. Sci. Technol. 32 (2014) 138–143. doi:10.1080/02726351.2013.840346.

[135] T. Zeghloul, A. Mekhalef, G. Richard, K. Medles, L. Dascalescu, Effect of particle size on the tribo-aero-electrostatic separation of plastics, J. Electrostat. 88 (2017) 24–28. doi:10.1016/j.elstat.2016.12.003.

[136] Association of Plastics Manufacturers in Europe, European Association of Plastics Recycling and Recovery Organisations, Plastics – the Facts 2016, (2016). doi:10.1016/j.marpolbul.2013.01.015.

[137] P. Cartwright, S. Singh, A.G. Bailey, L.J. Rose, Electrostatic Charging Characteristics of Polyethylene Powder During Pneumatic Conveying, IEEE Trans. Ind. Appl. IA-21 (1985) 541–546. doi:10.1109/TIA.1985.349702.

[138] R. Mukherjee, V. Gupta, S. Naik, S. Sarkar, V. Sharma, P. Peri, B. Chaudhuri, Effects of particle size on the triboelectrification phenomenon in pharmaceutical excipients : Experiments and multi-scale modeling, Asian J. Pharm. Sci. 11 (2016) 603–617. doi:10.1016/j.ajps.2016.04.006.

[139] K.W. Biegaj, M.G. Rowland, T.M. Lukas, J.Y.Y. Heng, Surface Chemistry and Humidity in Powder Electrostatics: A Comparative Study between Tribocharging and Corona Discharge, ACS Omega. 2 (2017) 1576–1582. doi:10.1021/acsomega.7b00125.

[140] D. Zenebe, P. Hwang, Tribology International Friction control by multi-shape textured surface under pin-on-disc test, Tribiology Int. 91 (2015) 111–117. doi:10.1016/j.triboint.2015.06.028.

[141] P.L. Menezes, S.V. Kailas, Role of surface texture and roughness parameters on friction and transfer film formation when UHMWPE sliding against steel, Biosurface and Biotribology. 2 (2016) 1–10. doi:10.1016/j.bsbt.2016.02.001.

[142] P.L. Menezes, Kishore, S. V. Kailas, M.R. Lovell, Role of surface texture, roughness, and hardness on friction during unidirectional sliding, Tribol. Lett. 41 (2011) 1–15. doi:10.1007/s11249-010-9676-3.

[143] S. Karner, M. Maier, E. Littringer, N.A. Urbanetz, Surface roughness effects on the tribo-charging and mixing homogeneity of adhesive mixtures used in dry powder inhalers, Powder Technol. 264 (2014) 544–549. doi:10.1016/j.powtec.2014.03.040.

[144] D.S. B. IVKOVIC, M. DJUKDJANOVIC, The Influence of the Contact Surface Roughness on the Static Friction Coefficient*, Tribol. Ind. 22 (2000) 41–44. http://www.tribology.fink.rs/journals/2000/3-4/1.pdf.

[145] M.F. Ashby, Materials and the Environment:Eco-informed Material Choice (Second Edition), Butterworth-Heinemann, Amsterdam, 2013.

[146] B. Neagoe, Y. Prawatya, T. Zeghloul, D. Souchet, L. Dascalescu, Laboratory bench for the characterization of triboelectric properties of polymers, J. Phys. Conf. Ser. 646 (2015) 12058. doi:10.1088/1742-6596/646/1/012058.

[147] T. Zeghloul, M.B. Neagoe, Y.E. Prawatya, L. Dascalescu, Triboelectrical charge generated by frictional sliding contact between polymeric materials, in: IOP Conf. Ser. Mater. Sci. Eng., 2017. doi:10.1088/1757-899X/174/1/012002.

[148] B. Neagoe, H.-N. Teodorescu, Y. Prawatya, L. Dascalescu, T. Zeghloul, Experimental bench for studying the relation between the dynamic characteristics of the frictional motion and the electric potential at the surface of polymer slabs in sliding conformal contact, Tribol. Int. 111 (2017). doi:10.1016/j.triboint.2017.03.006.

[149] T. Zeghloul, L. Dascalescu, K. Rouagdia, A. Fatihou, P. Renoux, D. Souchet, Tribocharging phenomena in sliding contacts between polymeric materials, in: 2014 IEEE Ind. Appl. Soc. Annu. Meet., IEEE, 2014: pp. 1–4. doi:10.1109/IAS.2014.6978340.

[150] T. Zeghloul, L. Dascalescu, K. Rouagdia, A. Fatihou, P. Renoux, D. Souchet, Sliding Conformal Contact Tribocharging of Polystyrene and Polyvinyl Chloride, IEEE Trans. Ind. Appl. 52 (2016) 1808–1813. doi:10.1109/TIA.2015.2493065.

[151] M.B. Neagoe, Y.E. Prawatya, T. Zeghloul, L. Dascalescu, Electric-potential-measurement-based methodology for estimation of electric charge density at the surface of tribocharged insulating slabs, J. Electrostat. 90 (2017) 123–130. doi:10.1016/j.elstat.2017.10.007.

[152] C. Gao, D. Kuhlmann-Wilsdorf, D.D. Makel, Fundamentals of stick-slip, Wear. 162–164 (1993) 1139–1149. doi:10.1016/0043-1648(93)90133-7.

[153] S.W. Yoon, M.W. Shin, W.G. Lee, H. Jang, Effect of surface contact conditions on the stick-slip behavior of brake friction material, Wear. 294–295 (2012) 305–312. doi:10.1016/j.wear.2012.07.011.

[154] J.S. Park, S.M. Lee, B.S. Joo, H. Jang, The effect of material properties on the stick–slip behavior of polymers: A case study with PMMA, PC, PTFE, and PVC, Wear. 378–379 (2017) 11–16. doi:10.1016/j.wear.2017.01.097.

[155] S.M. Lee, M.W. Shin, W.K. Lee, H. Jang, The correlation between contact stiffness and stick-slip of brake friction materials, Wear. 302 (2013) 1414–1420. doi:10.1016/j.wear.2012.12.017.

[156] L. Lee, S. Descartes, R.R. Chromik, Comparison of fretting behaviour of electrodeposited Zn-Ni and Cd coatings, Tribol. Int. 120 (2018) 535–546. doi:10.1016/j.triboint.2018.01.021.

[157] M.B. Neagoe, Y.E. Prawatya, T. Zeghloul, L. Dascalescu, Influence of surface roughness on the tribo-electric process for a sliding contact between polymeric plate materials, in: IOP Conf. Ser. Mater. Sci. Eng., 2017. doi:10.1088/1757-899X/174/1/012003.

[158] P.L. Menezes, M. Schimjith, S. V. Kailas, Influence of Surface Texturing on Friction and Transfer Layer Formation in Mg-8Al Alloy/Steel Tribo-system, Indian Jouranl Tribol. 2 (2007) 46–54.

[159] Y. Prawatya, B. Neagoe, T. Zeghloul, L. Dascalescu, Comparison between the surface-electric-potential characteristics of tribo- and corona-charged polymers, in: IEEE Ind. Appl. Soc. - 51st Annu. Meet. IAS 2015, Conf. Rec., 2015.

doi:10.1109/IAS.2015.7356756.

[160] G.S.P. Castle, Contact charging between insulators, J. Electrostat. 40–41 (1997) 13–20. doi:10.1016/S0304-3886(97)00009-0.

[161] L.B. Loeb, Electrical Coronas, Their Basic Physical Mechanisms, University of California Press, Berkeley, CA, 1965. https://books.google.fr/books?id=xdJEAAAAIAAJ.

[162] A. Crisci, B. Gosse, J.-P. Gosse, V. Ollier-Duréault, Surface-potential decay due to surface conduction, Eur. Phys. J. Appl. Phys. 4 (1998) 107–116. doi:10.1051/epjap:1998249.

[163] H. Lim, Y. Lee, S. Han, Y. Kim, J. Cho, K. Kim, Reduction in surface resistivity of polymers by plasma source ion implantation, Surf. Coatings Technol. 160 (2002) 158–164. doi:10.1016/S0257-8972(02)00365-1.

[164] A. Bulletti, L. Capineri, M. Materassi, B.D. Dunn, Surface Resistivity Characterization of New Printed Circuit Board Materials for Use in Spacecraft Electronics, IEEE Trans. Electron. Packag. Manuf. 30 (2007) 115–122. doi:10.1109/TEPM.2007.899075.

[165] T. Sugimoto, H. Ishii, Y. Higashiyama, Corona Charging and Current Measurement Using Phi-Type Corona Electrodes, IEEE Trans. Ind. Appl. 46 (2010) 1175–1180. doi:10.1109/TIA.2010.2045330.

[166] R.F. Gunst, Response Surface Methodology: Process and Product Optimization Using Designed Experiments, Technometrics. 38 (1996) 284–286. doi:10.1080/00401706.1996.10484509.

[167] Y. Prawatya, K. Senouci, T. Zeghloul, B. Neagoe, L. Dascalescu, K. Medles, Statistical process control of the tribocharging of polymer slabs in frictional sliding contact, in: 2017 IEEE Ind. Appl. Soc. Annu. Meet., IEEE, 2017: pp. 1–6. doi:10.1109/IAS.2017.8101698.

MULTIVARIATE OPTIMISATION AND STATISTICAL PROCESS CONTROL OF POLYMER TRIBOELECTRIC CHARGING

The main objective of the thesis was to study the triboelectric behavior of dry sliding contacts between polymeric materials (ABS, PE, PP, PS and two types of PVC), including the possibility to control and optimize the results in terms of either surface charge generated or wear. A linear tribometer with tribocharging capabilities was designed and built, to enable the study of the sliding contact between solids and to allow the adjustment of main tribocharging control variables: normal force, sliding speed, time and stroke. This device also provided measurement data to characterize the friction condition: the variations of the normal and tangential forces, as well as the relative displacement between the specimens. Furthermore, the electric charge generated and temperature raise due to rubbing on the surface of the polymer were measured, so that to investigate the relationship between the tribological properties. The experiments showed that the level and distribution of the charge generated by dry friction depends on the normal force applied, friction time (cycle), sliding speed, material mechanical properties and surface roughness or texture. Corona discharge may be used to provide initial charge on the surfaces before sliding. Modelling of tribocharging processes was done using the design of experiments methodology. The models can be used to predict and optimize the tribocharging. Control charts were used to monitor the process and detect the special causes of variation in the charge generated by triboelectric effect. .

Key words: Triboelectrification, Polymeric materials, Dry friction, Surface electric potential, Modelling and optimization, Statistical process control

OPTIMISATION MULTI-VARIABLES ET CONTROLE STATISTIQUE DES PROCESSUS DE CHARGE TRIBOÉLECTRIQUE DES POLYMERES

L'objectif principal de la thèse a été d'étudier le comportement triboélectrique des contacts glissants à sec entre matériaux polymères (ABS, PE, PP, PS et deux types de PVC), incluant la possibilité de contrôler et d'optimiser les résultats générés, en termes de charge électrique et d'usure. Un tribomètre linéaire a été conçu et construit, afin de permettre le réglage des principales variables de contrôle du processus de charge triboélectrique : force normale, vitesse de glissement, durée et course. Ce dispositif facilite la mesure de certaines grandeurs physiques caractérisant les conditions de frottement: les variations des forces normale et tangentielle, ainsi que le déplacement relatif entre les éprouvettes. De plus, la charge électrique générée et l'augmentation de la température à la surface du polymère ont été aussi été mesurées et mise en relation avec les propriétés tribologiques. Les expériences ont montré que le niveau et la distribution de la charge générée par le frottement sec dépendent de la force normale appliquée, du temps de frottement (le nombre de cycles), de la vitesse de glissement, des propriétés mécaniques des matériaux et de la rugosité ou de la texture des surfaces en contact. La décharge couronne peut être utilisée pour déposer une charge initiale sur les surfaces avant le glissement. La modélisation du processus de charge triboélectrique a été faite avec la méthodologie des plans d'expériences. Les résultats peuvent alors être utilisés pour prédire et optimiser la charge triboélectrique. Des cartes de contrôle peuvent assurer le monitoring du processus et la détection de variations non-maîtrisés de la charge générée par effet triboélectrique.

Mots clés: Effet triboélectrique, Polymères, Frottement sec, Potentiel électrique de surface, Modélisation et optimisation, Contrôle statistique de processus